To who believed in me

Synopsis

We live, as defined by prof. Chua [1], in the age of complexity, whose ubiquity is the reason of the increasing interest in the scientific community.

Many of the systems that surround us are complex. The goal of understanding their properties motivates many researchers. Universal laws and phenomena are essential to inquiry and to understand and all scientific endeavor is based on the existence of universality, which manifests itself in diverse ways. The study of complex systems as a new effort seeks to increase the ability to understand the universality that arises when systems are highly complex.

A complex system may be thinked as a system formed out of many components whose behavior is emergent, meaning that the behavior of the system cannot be simply inferred from the behavior of its components. In fact, it is not possible to describe the whole without describing each part, and each part must be described in relation to other parts to understand the behavior of a complex system. The amount of information necessary to describe the behavior of such a system is a measure of its complexity.

Usually, the behavior of a complex system is investigated considering how the simple units communicate. Thus, a complex system can be defined by its network of interactions and studied according to graph theory.

The aim of this PhD Thesis is to provide new tools and strategies for the analysis and modeling of complex systems. The designed tools will be then applied to two particular classes of complex systems: complex networks and cellular automata.

In particular, several fundamental topics of complex networks have been faced in this work. Starting from the key issue of data analysis in networks, which due to the large availability of data has now become a fundamental aspect of the research in complex networks, we found that existing models do not adequately reproduce the characteristics, often uniques, of the social networks analysed and introduced a new model of growing network based on an attachment to communities instead of sparse nodes. We have then considered one of the major applications of complex networks, i.e., power grids. While most of the approaches existing in literature are static ones and focuse on the network topology, we considered a model which explicitely takes into account the oscillatory dynamics of power grid nodes. Our results revealed different qualitative scenarios to the network failure. Finally, the Thesis focuses on a hardware tool for the emulation of a nearest-neighbor coupled network, which, despite its simple topology, is able to generate many complex phenomena and for a set of parameters is equivalent to a Turing machine.

The Thesis is organized as follow: in Chapter 1 complex systems and in particular complex networks will be introduced; Chapter 2 and 3 will describe the results obtained on social networks and power grids; Chapter 4 will introduce a new stand-alone complex system hardware emulator; in the conclusive Chapter the conclusions will be drawn.

Contents

1

What is Complex

In this Chapter a brief introduction on complex systems is given and in particular complex networks are taken into account. Starting from the historical roots of the complex networks analysis some definitions are given and models for generation of these networks are introduced.

1.1 Complex Systems

One of the most wide and interesting research field is the study of complex systems. Researchers studying complex systems include physicists, ecologists, economists, engineers of all kinds, entomologists, computer scientists, linguists, sociologists, and political scientists. The field of complex systems seeks to explain and uncover common laws for the emergent, self-organizing behavior seen in complex systems across disciplines.

A complex system may be imagined as a collection of numerous components and interconnections, interactions or interdependencies that are difficult to describe, understand, predict, manage, design, and/or change. Alternatively, a complex system may be considered as a large network of simple components with no central control, in which emergent complex behavior is exhibited.

In the framework of complex systems a very interesting field is the analysis of complex networks. Under this consideration, a complex system is well-defined by knowing the complex network underlying the interactions and by analyzing the topological properties, because information sharing between the parts occurs through links connecting them.

Many real systems, in fact, may be represented in the form of networks of nodes joined together by links. Well-known examples are communication networks such as the Internet or the telephone network, transportation networks such as airline routes or roads, distribution networks such as the movements of delivery trucks or the blood vessels of the body, biological networks such as the metabolic networks or food chain [2]. A very interesting area of complex networks is composed by social networks where people, as individuals, with different kinds of social relationship (friendship, kinship, status, sexual, business or political) are the units of several networks. This brief list shows how complex networks are all around us being tangible objects in the Euclidian space or entities defined in an abstract space.

1.2 Complex Networks

Historically, the analysis of networks has been the domain of discrete mathematics and in particularly of graph theory. The "conception" of the theory is universally attributed to Euler with his solution, in 1736, to the Königsberg bridge puzzle shown in Figure 1.1.

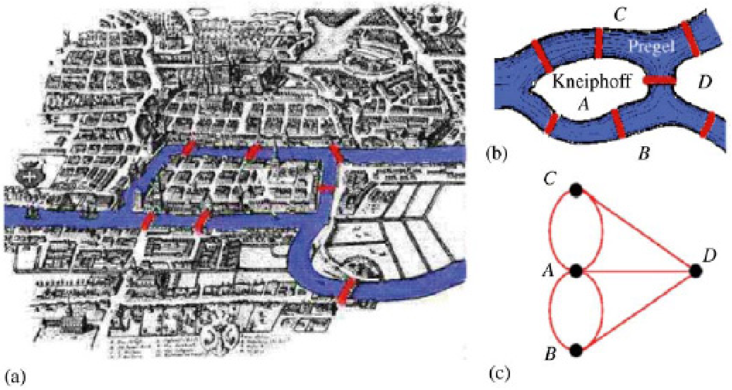

Fig. 1.1. The Königsberg bridge puzzle. (a) The town of Königsberg, now Kaliningrad, Russia, with seven bridges. (b) Schematic representation of the area with the bridges. (c) Eulers representation of the problem.

As stated in Euler's manuscript: "In the town of Königsberg in Prussia there is an island, called "Kneiphoff", with the two branches of the river (Pregel) flowing around it. There are seven bridges, a, b, c, d, e, f, and g, crossing the two branches. The question is whether a person can plan a walk in such a way that he will cross each of these bridges once but not more than once." Euler noticed that physical distance is of no importance in this problem and represented the topological constraints of the problem in the form of a graph of nodes and links connecting pairs of nodes. Euler divided the nodes into odd and even based on the parity of their degree, that is, the number of links directly connected to the node.

He demonstrated that the sum of degrees of the nodes of a graph is even and every graph must have an even number of odd nodes. Basing on these results he obtained that to have walk between two arbitrary nodes for which every link in the graph appears exactly once, the so called Euler walk, the number of odd nodes can't be greater than 2. Therefore, since all four nodes in the Königsberg bridge problem are odd, Euler demonstrated that there was no solution.

The development of network theory is due in great part to Erdös.

Erdös interest on network theory is linked to a social puzzle: What is the structure of social networks? This problem was formalized by Kochen and Pool in the 1950s, leading them to the definition of random graphs [3]: i.e., graphs in which a link between any pair of nodes exists with probability p. Erdös, in collaboration with Rènyi, pursued the theoretical analysis of the properties of random graphs obtaining a number of important results [4].

In 1960s Milgram brought a series of experiments to estimate the number of steps in a chain of acquaintances discovering a new property that many real networks show: the small world effect. In these networks, in fact, there is a relatively short path between any two nodes, despite of their often large size [5].

In the last years there has been within the scientific community a renewed and increasing interest in the study of complex networks because it is possible to describe, using a common paradigm, different kinds of systems.

Watts and Strogatz in 1998 [6] proposed a minimal model for the emergence of the small-world phenomenon in simple networks. In their model, small-world networks emerge as the result of randomly rewiring a fraction p of the links in a d-dimensional lattice.

In the late nineties, Barabàsi and Albert [7] founded that a number of real-world networks have a scale-free degree distribution with tails that decay as a power law. So they defined a new model suggesting that scale-free networks emerge in the context of growing network in which new nodes connect preferentially to the most connected nodes already in the network.

After that a plenty of new models and results related to topological properties, networks models, static and dynamic robustness, epidemic and rumor spreading, synchronization and collective dynamics, algorithms for finding community structures has been produced within the scientific community [2].

1.3 Some definitions

In this Section some definitions and notations will be introduced and the basic quantities used to describe the topology of a network will be discussed.

A network is a collection of vertices or nodes, that are the fundamental units, and edges connecting two vertices. Edge may be directed or undirected. An edge is directed if it runs in only one direction, and undirected if it runs in both directions. A network is directed if all of its edges are directed.

It is often useful to consider a matricial representation of a network. A network of N nodes connected by L links can be completely described by giving the adjacency (or connectivity) matrix A, a $N \times N$ square matrix whose entry a_{ij} $(i, j = 1, ..., N)$ is equal to 1 when the link l_{ij} exists, and zero otherwise. The diagonal of the adjacency matrix contains zeros. For undirected graphs the adjacency matrix is symmetric.

1.3.1 Node degree and degree distribution

The degree (or connectivity) k_i of a node i is the number of edges incident with the node [2], and is defined in terms of the adjacency matrix A as:

$$k_i = \sum_{j \epsilon N} a_{ij}. \tag{1.1}$$

If the graph is directed, the degree of the node has two components: the number of outgoing links $k_i^{out} = \sum_j a_{ij}$, and the number of ingoing links $k_i^{in} = \sum_j a_{ji}$. The total degree is then defined as $k_i = k_i^{out} + k_i^{in}$.

The most basic topological characterization of a network can be obtained in terms of the degree distribution $P(k)$, defined as the probability that a node chosen uniformly at random has degree k or, equivalently, as the fraction of nodes in the graph having degree k. In the case of directed networks one needs to consider two distributions, $P(k_{in})$ and $P(k_{out})$.

1.3.2 Shortest path lengths, diameter and betweenness

An interesting parameter with an important role in the characterization of the internal structure of a graph is the shortest path. It may be defined as the path that connects two nodes with the minimum cost, and it is possible to have more than one shortest path between two vertices.

It is useful to represent all the shortest path lengths of a network as a matrix D in which the entry d_{ij} is the length of the path from node i to node j. The maximum value of d_{ij} is called the diameter of the graph.

A measure of the typical separation between two nodes in the graph is given by the average shortest path length, also known as characteristic path length, defined as the mean of shortest paths over all couples of nodes [8]:

$$L = \frac{1}{N(N-1)} \sum_{i,j\epsilon N, i\neq j} d_{ij}. \tag{1.2}$$

A measure of the relevance of a given node can be obtained by counting the number of shortest paths going through it, and defining the so-called *node betweenness* [2]. The betweenness, togheter with the degree of a node, is one of the standard measures of node centrality, originally introduced to quantify the importance of an individual in a social network. Mathematically the betweenness b_i of a node i is defined as:

$$b_i = \sum_{i,j\epsilon N, i\neq j} \frac{n_{jk}(i)}{n_{jk}}, \tag{1.3}$$

where n_{jk} is the number of shortest paths connecting j and k, while $n_{jk}(i)$ is the number of shortest paths connecting j and k and passing through i.

The concept of betweenness can be extended also to edges. The edge betweenness is defined as the number of shortest paths between pairs of nodes that run through that edge.

1.3.3 Clustering

Clustering, also known as transitivity, is a typical property of acquaintance networks, where two individuals with a common friend are likely to know each other [9]. In terms of network topology, transitivity means the presence of a heightened number of triangles in the network, i.e., sets of three vertices each of which is connected to each of the others. It can be quantified by the clustering coefficient C defined as:

$$C = \frac{3 \times \textit{number of triangles in the network}}{\textit{number of connected triples of vertices}}, \tag{1.4}$$

where a “connected triple” means a single vertex with edges running to an unordered pair of others. The factor of three in the numerator accounts for the fact that each triangle contributes to three triples and ensures that C lies in the range $0 \leq C \leq 1$. An alternative definition of the clustering coefficient, also widely used, has been given by Watts and Strogatz [6]. A quantity c_i (the local clustering coefficient of node i) is first introduced, expressing how likely $a_{jm} = 1$ for two neighbors j and m of node i. Its value is obtained by counting the actual number of edges (denoted by e_i) in the subnetwork of neighbors of i. The local clustering coefficient is defined as the ratio between e_i and $k_i(k_i-1)/2$, i.e., the maximum possible number of edges in the subnetwork:

$$c_i = \frac{2e_i}{k_i(k_i-1)}. \tag{1.5}$$

The clustering coefficient of the network is then given by the average of c_i over all the nodes:

$$C = \langle c \rangle = \frac{1}{N}\sum_i c_i. \tag{1.6}$$

1.4 Complex Network Models

Measuring some basic properties of a complex network, such as the average path length L, the clustering coefficient C, and the degree distribution $P(k)$, is the first step toward understanding its structure. The next step is to develop a mathematical model with a topology of similar statistical properties, thereby obtaining a platform on which mathematical analysis is possible.

1.4.1 Regular Coupled Networks

The first very simple model that we discuss is a network in which each node is connected to all the other ones of the network. This is called all-to-all network or globally coupled network.

An all-to-all network is characterized by the smallest average path length and the largest clustering coefficient. Although the globally coupled network model captures the small-world and large-clustering properties of many real networks, there are many limitations. In fact, real networks are not fully connected and their number of edges is generally of order N rather than N^2 like for fully connected networks.

A widely studied, sparse, and regular network model is the nearest-neighbor coupled network (a lattice), which is a regular graph in which every node is joined only by a few of its neighbors [9]. A nearest-neighbor lattice with a periodic boundary condition consists of N nodes arranged in a ring, where each node i is adjacent to its neighboring nodes, $i = 1, 2, \ldots, K/2$, with K being an even integer. The nearest-neighbor coupled network is not a small-world network. On the contrary, its average path length is quite large and tends to infinity as $N \rightarrow \infty$. An example of regular network that is sparse and clustered, but has a small average path length is a star-shaped coupled network, in which there is a center node and each of the other $N - 1$ nodes only connects to this center but not among themselves. For this kind of network, the average path length tends to 2 and its clustering coefficient tends to 1, as $N \rightarrow \infty$. The star-shaped network model captures the sparse, clustering, small-world, as well as some other interesting properties of many real-world networks and, in this sense, it is better than the regular lattice as a model of many well-known real networks.

1.4.2 Random Networks

At the opposite end of the spectrum from a completely regular network is a network characterized by the disordered nature of links arrangement between different nodes. First studies on this model were conducted by Erdös and Rènyi [4], that proposed a model to generate random graphs with N nodes and K links. Starting with N disconnected nodes, ER random networks are generated by connecting couples of randomly selected nodes, prohibiting multiple connections, until the number of edges equals K. An alternative model for ER random graphs consists in connecting each couple of nodes with a probability $0 \leq p \leq 1$. The result is a network with N nodes and about $pN(N-1)/2$ edges.

A central problem of the random graph theory is to determine at what connection probability p a particular property of a graph will most likely arise. ER showed that, if the probability p is greater than a certain threshold $p_c \sim (lnN)/N$, then almost every random graph is connected.

The average degree of the random network is $\langle k \rangle = p(N-1) \sim= pN$. For large N, and fixed $\langle k \rangle$, the degree distribution is well approximated by a Poisson distribution, since all nodes are statistically equivalent.

The average shortest path length L has the same behavior as a function of N, $L \sim lnN/ln\langle k \rangle$. This logarithmic increase in average path length with the size of the network is a typical small-world effect.

The clustering coefficient of these networks is equal to $C = p = \langle k \rangle/N$. This means that a large-scale random network does not show clustering.

1.4.3 Small-World Models

As discussed in the previous Sections, regular lattices are clustered, but do not exhibit the small-world effect while random graphs show the small-world effect, but do not show clustering. In view of this, the regular lattice model and the ER random model are not appropriate to reproduce some important features of many real networks.

Aiming to describe a transition from a regular lattice to a random graph, Watts and Strogatz [6] introduced an interesting small-world network model, referred to as WS small-world model.

The model is based on a rewiring procedure of the edges implemented with a probability p. The starting point is a N nodes ring, in which each node is symmetrically connected to its $2m$ nearest neighbors for a total of $K = mN$ edges. Then, for every node, each link is rewired to a randomly chosen node with a probability p, and preserved with a probability $1 - p$. Limit cases are $p = 0$ and $p = 1$ in which a regular lattice and a random network are obtained respectively. For intermediate values of p the procedure generates networks with the small-world property and a non-trivial clustering coefficient, where clustering coefficient and average path length are function of the rewiring probability p.

For a small probability of rewiring, when the local properties of the network are still nearly the same as those for the original regular network, and when the clustering coefficient does not differ subsequently from its initial value, the average path length drops rapidly and is in the same order as the one for random networks. It is sufficient to make several random rewirings to decrease the average path length significantly but several rewired links cannot crucially change the local clustering property of the network.

A typical variant of the WS-model is the one proposed by Newman and Watts [10]. In this model, there is no rewiring of any connection between neighbors, but, instead, with probability p a connection between a pair of nodes is added. With $p = 0$, the NW model reduces to the original nearest-neighbor coupled network, and if $p = 1$ it becomes a globally coupled network. The NW model is easier to analyze than the original WS model because it does not lead to the formation of isolated clusters. For sufficiently small p and sufficiently large N, the NW model is essentially equivalent to the WS model.

The small-world models are able to reproduce some characteristics of social networks.

1.4.4 Scale-Free Models

To explain the origin of power-law degree distribution of many real networks, such as the Internet and WWW, Barabàsi and Albert (BA) proposed another network model [7]. They argued that many existing models fail to take into account two important attributes of most real networks: real networks are open and dynamically formed by continuous addition of new nodes to the network, and new nodes are preferentially attached to existing nodes with large numbers of connections (the so called rich get richer effect). So the BA model is based on the concepts of growth and preferential attachment.

Starting with m_0 isolated nodes, at each time step $t = 1, 2, 3, ..., N - m_0$ a new node j with $m \leq m_0$ links is added to the network. The probability that a link j will connect to an existing node i is linearly proportional to the actual degree of i: $\prod_{j \to i} = \frac{k_i}{\sum_l k_l}$.

After t time steps, this algorithm results in a network with $N = t + m_0$ nodes and mt edges. Growing according to this model, the network evolves into a scale-invariant state: the shape of the degree distribution does not change over time. The corresponding degree distribution is described by a power law with exponent -3, so the probability of finding a node with k edges is proportional to k^{-3}. In comparison with a random graph with the same size and the same average degree, the average path length of the scale-free model is smaller and the clustering coefficient is higher.

To account for more realistic models of real networks, preferential attachment has been modified and generalized in several ways [11]. Node initial attractiveness [12], nonlinear attachment probability [13], accelerating growth [14] or preferential attachment applied only to the neighborhood of the newly added nodes [15] are a few examples of the factors that have been included in the model. In general, preferential attachment has been shown to be very important for the growth of social networks [7, 16].

2

A New Model for Growing Social Networks

In this Chapter real social networks extracted from the popular on-line social network Facebook are analyzed and a new model is introduced. The main characteristic of this model is an attachment mechanism based on the existence of network communities, a key feature of real social networks. This model shares with real networks several peculiarities (such as high levels of clustering, low values of the characteristic path length and node betweenness, division into communities and heterogeneous degree distribution), not captured in other network models.

At the end of this Chapter another issue of these networks is shown. A time-series is obtained taken into account the number of on-line friends of a given user to study its determinism.

2.1 On-line social networks

Among complex networks, social ones have a primary role for several reasons. On one hand, today, they provide a large amount of data that can be analyzed to test the hypothesis from which new models are derived. On the other hand, in an historically perspective, social networks analysis started very early (in the 1920s), focusing on relationships among social entities that are subject of research in various disciplines as sociology, applied anthropology, social psychology, physics and statistics [17], and often pushed and motivated the research on complex networks and the definition of new network models.

Nowadays, there is an explosion of on-line social networks, which, thanks also to the large dataset they constitute, often offer interesting case studies. Among these, Facebook, originally developed for students of U.S. colleges, is one of the most popular on-line social networks that today put in relation people from many countries of the whole world. Users may share pictures, video, music, add friends and talk with them with private or public messages, add applications or games, update their personal profile, join groups and networks organized by city, workplace, school, region, interest. It is available in more than 65 languages, and at present there are about 500 millions of active users in the world with an average number of friends for user of about 130 persons [18].

An important characteristic of on-line social networks is that users tend to form groups, called communities, where the connections between nodes of the same community are more dense than between nodes of different communities [19]. These communities represent the different groups a user belongs to, for instance, schools, works, etc. The presence of communities is not limited to on-line social networks, and the problem of *community detection* in complex networks has now become an important topic. In particular, several algorithms for community detection have been developed. Among these, there are algorithms based on spectral graph partitioning, hierarchical clustering, centrality and modularity optimization [2, 20], as well as on other techniques [21, 22] such as the method proposed by Wu and Huberman [23] and based on voltage drops across the network.

2.2 Analysis of the dataset

Analysis on a dataset of on-line social networks from Facebook has been conducted.

On the basis of 100 volunteer participants (18-60 years of age), developing an appropriate application, for each user the so-called *friends network* has been extracted: for a given user A, the nodes of his friends network represent the users to which he is connected to, i.e., the friends, while the links are the connections existing between his friends. Therefore, each of the networks analyzed in this work represents the subnetwork of first neighbors of the user A extracted from the entire Facebook network.

An example of such network is reported in Figure 2.1 where a network with 79 nodes and 338 edges is shown. The graphic user interface of the developed application is also shown. It allows the user to extract the main component of the network [2] and to measure the most important network characteristics like characteristic path length, clustering and so on.

The number of nodes of the networks in the dataset varies from 62 to 694, while the number of links varies from 634 to 29731. The average number of friends is about 130 persons for user. When the main component of the network is considered, removing isolated nodes and secondary components, completely connected networks with a number of nodes ranging from 53 to 592 and a number of links ranging from 372 to 24909 are obtained.

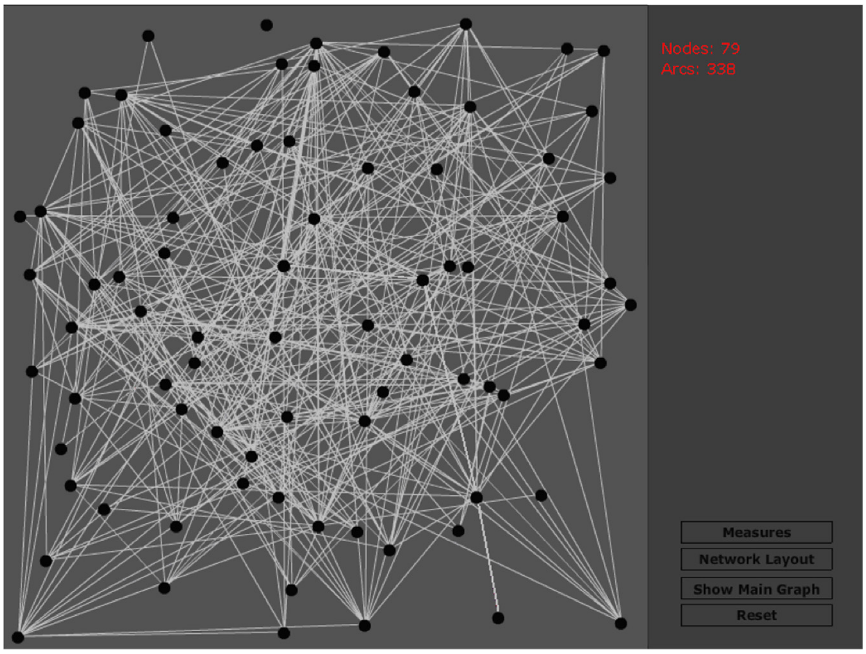

Nodes: 79
Arcs: 338

Fig. 2.1. An example of the network of the used dataset and the graphic user interface of the developed application.

The analysis of the topological characteristics of the friends networks of our dataset revealed a great heterogeneity. Common characteristics of these networks are an high clustering coefficient, a low characteristic path length and a low node betweenness compared to that of random networks with the same number of nodes and links. Furthermore, such networks are characterized by a significant presence of communities of different sizes, that point out the peculiarity of having friends belonging to different contexts. The analysis carried out has been focused on the following topological features [2]: number of nodes N, characteristic path length L, average degree $\langle k \rangle$, clustering coefficient C, node betweenness B, number of communities N_C and type of degree distribution $P(k)$. Table 2.1 reports several examples of these parameters measured for the networks in our dataset. Interestingly, our results [24] reach the same conclusions on high clustering coefficient and low characteristic path length of [25, 26] which have access to a much larger database of Facebook data.

As concerns the degree distribution, different types of distributions have been found. To characterize such variability of the degree distribution a statistical analysis has been carried out. Consequently, it has been found that, on the basis of their degree distribution, the networks under analysis can be grouped in two main classes: networks with a log-logistic–like degree distribution (an example is shown in Figure 2.2) and networks with a normal–like degree distribution (Figure 2.3). This classification has been performed by carrying on a χ-squared test [27] on the network probability density function with a significance level $\alpha = 0.05$.

These networks have been compared with ER and BA models. In particular, ER and BA networks have been generated in such a way

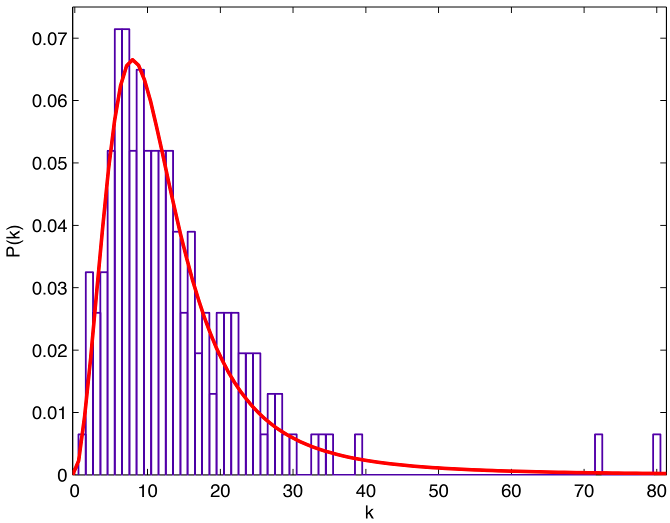

Fig. 2.2. Degree distribution $P(k)$ of a real network of 154 nodes. The continuous line represents a log-logistic fitting.

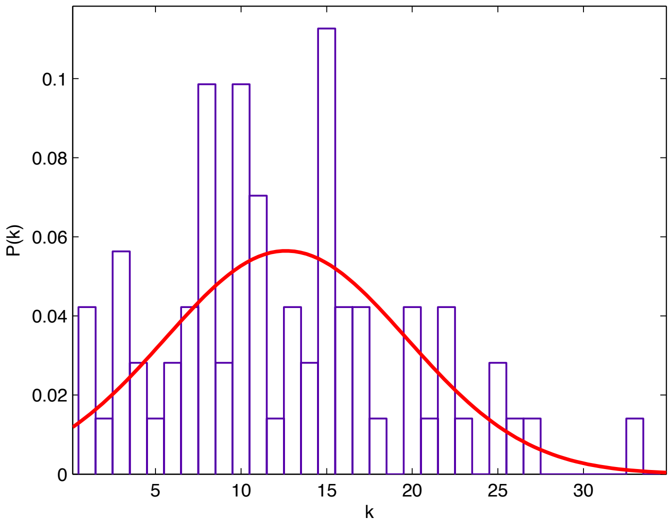

Fig. 2.3. Degree distribution $P(k)$ of a real network of 71 nodes. The continuous line represents a normal fitting.

	Real networks					
N	L	<k>	C	B	N_C	type of $P(k)$
58	2.275	10.724	0.726	0.057	6	log-logistic
59	2.285	12.576	0.735	0.080	7	log-logistic
71	2.172	12.628	0.538	0.039	6	normal
89	2.671	11.303	0.692	0.079	12	log-logistic
91	2.488	9.538	0.675	0.050	10	log-logistic
102	2.910	7.784	0.560	0.050	11	log-logistic
105	2.301	10.666	0.609	0.033	4	log-logistic
129	2.449	18.108	0.653	0.032	4	normal
138	2.733	8.811	0.621	0.037	15	log-logistic
140	2.829	10.085	0.601	0.033	14	normal
146	2.643	20.739	0.655	0.032	6	log-logistic
154	2.566	13.751	0.592	0.025	11	log-logistic
163	2.162	34.687	0.566	0.016	9	normal
209	2.612	12.665	0.516	0.018	20	log-logistic
234	2.195	28.393	0.578	0.011	9	log-logistic
242	2.190	29.900	0.572	0.011	9	log-logistic
266	2.690	19.015	0.539	0.014	13	log-logistic
340	2.338	28.214	0.400	0.008	8	log-logistic
592	2.419	46.947	0.467	0.005	13	log-logistic

Table 2.1. Topological measures for some examples in our dataset of friends networks.

that they have the same number of nodes and the same average degree of the real networks of Table 2.1, so that they can be compared to real networks with respect to the other topological parameters such as L, C, B, N_C and type of $P(k)$. Table 2.2 and Table 2.3 report the topological parameters obtained for ER networks and for BA networks, respectively. The comparison revealed that, in general, real networks have an higher clustering coefficient and a lower characteristic path length with respect to ER and BA models and a different degree distribution.

This has been considered as an indication of the fact that in the real networks links are established in a different way with respect to BA and ER models. In fact, neither with the preferential attachment of BA model, where there are some high-degree nodes that acquire new links at higher rates than low-degree ones, nor with random linking mechanism of ER model, the topological features observed in the real networks, including also the low number of communities (indicating a strong tendency to form communities) and the type of degree distribution, have been obtained.

For these reasons, a new model able to account for the variability of the observed degree distributions as a function of its parameters and able to reproduce the other characteristics of friends networks has been developed.

2.3 The FA model

Growing network models are characterized by the way in which new nodes attach to the others. The most important model of growing networks is the BA model [7], introduced in the previous Chapter, but the existing models are not able to reproduce all the characteristics of the real on-line social networks analysed.

In fact, in the real networks derived from Facebook, it can be observed a strong tendency of new nodes (i.e., new Facebook users) to

	ER networks					
N	L	<k>	C	B	N_C	type of $P(k)$
58	1.907	11.103	0.197	0.031	11	normal
59	1.856	12.102	0.225	0.029	8	normal
71	1.872	13.239	0.181	0.024	7	normal
89	2.094	11.011	0.133	0.024	10	normal
91	2.200	9.890	0.115	0.026	8	normal
102	2.434	8.059	0.079	0.028	22	normal
105	2.177	10.952	0.107	0.022	13	normal
129	1.922	18.140	0.138	0.014	12	normal
138	2.455	9.159	0.073	0.021	25	normal
140	2.353	10.343	0.073	0.019	16	normal
146	1.900	20.918	0.143	0.012	13	normal
154	2.223	12.935	0.080	0.016	16	normal
163	1.791	33.939	0.209	0.010	12	normal
209	2.413	12.115	0.057	0.013	19	normal
234	1.914	27.812	0.122	0.008	16	normal
242	1.898	29.835	0.121	0.007	14	normal
266	2.170	18.992	0.072	0.009	32	normal
340	2.013	27.759	0.083	0.006	17	normal
592	1.944	46.659	0.079	0.003	18	normal

Table 2.2. Topological measures for ER networks.

link to nodes belonging to a community. To make an example, in such networks, often a community representing the high school classmates of the given user is present. It may happen that a classmate makes a search for known people and, once he/she founds the given user, he/she connects not only to the given user, but also to several of the individuals belonging to the high school classmate community. Therefore, when a new user links to an existing one, it happens often that, since he/she

	BA networks					
N	L	<k>	C	B	N_C	type of $P(k)$
58	1.961	10.897	0.470	0.045	9	power law
59	1.942	12.068	0.476	0.044	10	power law
71	1.950	12.789	0.512	0.041	8	power law
89	2.186	11.169	0.390	0.032	17	power law
91	2.192	9.495	0.377	0.043	18	power law
102	2.515	7.255	0.219	0.039	22	power law
105	2.212	10.648	0.427	0.035	20	power law
129	2.055	18.806	0.476	0.023	15	power law
138	2.535	7.855	0.156	0.028	29	power law
140	2.367	9.800	0.275	0.024	30	power law
146	2.055	19.507	0.364	0.017	11	power law
154	2.186	13.610	0.346	0.019	20	power law
163	1.848	35.975	0.534	0.013	11	power law
209	2.333	13.627	0.301	0.015	33	power law
234	2.030	28.171	0.452	0.012	11	power law
242	2.016	29.636	0.454	0.012	12	power law
266	2.143	20.383	0.371	0.012	23	power law
340	2.098	29.741	0.367	0.008	16	power law
592	2.097	46.716	0.373	0.005	14	power law

Table 2.3. Topological measures for BA networks.

also knows other ‘friends’ of the user, he/she links with several nodes; at this points two possibilities arise: 1) the ‘friends’ belong to a community to which the new user has some relations; 2) the ‘friends’ don’t belong to a community. These two possibilities represent two different kinds of social relations with the given user: a relation involving a community shared by the new and the given user or a relation just involving some sparse common friends (not forming a community). In the first case, the community of the user is enforced as result of the new connections.

These considerations motivated the idea underlying the model, referred to as *friend attachment* (FA) model, where a new attachment mechanism has been implemented. In particular, the attachment can occur either with nodes belonging to a community or with nodes picked at random in the whole network. More in details, the growth of the FA model is ruled by the following algorithm. The algorithm starts from a fully connected network of three nodes. Then, at each time step:

1. the communities $C_1, C_2, \ldots, C_h$ in which the network is divided are calculated;
2. a new node is added;
3. the attachment mechanism is selected: with probability p *random attachment* is selected; with probability $1-p$ *community attachment* is selected;
4. in case of random attachment, the new node is linked with nodes picked at random (uniform distribution) from the entire network; in particular, m_p new links are generated, with m_p chosen with uniform distribution probability in the interval $[1, n_p]$;
5. in case of community attachment one of the communities $C_1, C_2, \ldots,$ C_h is chosen (with uniform distribution probability). Let us indicate this community as C_j: the new node is linked with nodes picked at random (uniform distribution) from C_j; in particular, m_{1-p} new links are generated, with m_{1-p} chosen with uniform distribution probability in the interval $[1, n_{1-p}]$.

The model introduced contains several parameters which can be here summarized: the threshold parameter p (ruling at each time step if random or community attachment has to be chosen); n_p, i.e., the maximum number of connections made to existing network nodes in case of random attachment; n_{1-p}, i.e., the maximum number of connections made to existing nodes of a network community in case of community attachment.

These parameters make the model quite general and able to account for the great variability of real social networks previously shown. The threshold parameter p allows to obtain networks with different characteristics, ranging from a completely random network ($p = 1$) to a single community network ($p = 0$). When not differently specified, n_p is set to the number of existing nodes in the network and n_{1-p} is set to the size of the chosen community. Finally, it is worth remarking that at each time step the communities of the network are recalculated and that the initial network configuration is not divided into communities. For community detection the so-called Louvain Method [28] has been used.

The FA model exhibits the small-world effect and it is characterized by a great variety of possible degree distributions. These distributions have been classified according to the results of a χ-squared tests on their probability density functions with significance level $\alpha = 0.05$. Varying the threshold p, in fact, different degree distributions can be obtained: log-logistic–like distributions (two examples are shown in Figure 2.4 and Figure 2.5 obtained with $p = 0.5$), and normal–like distributions

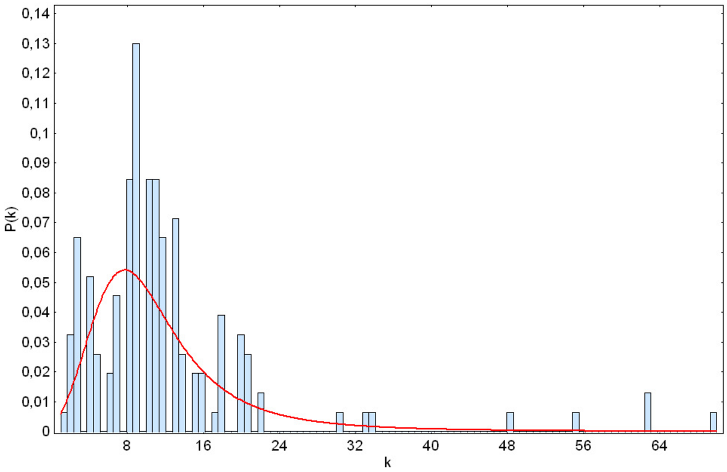

Fig. 2.4. Degree distribution $P(k)$ for a FA network. The number of nodes is 154. The continuous line represents a log-logistic fitting.

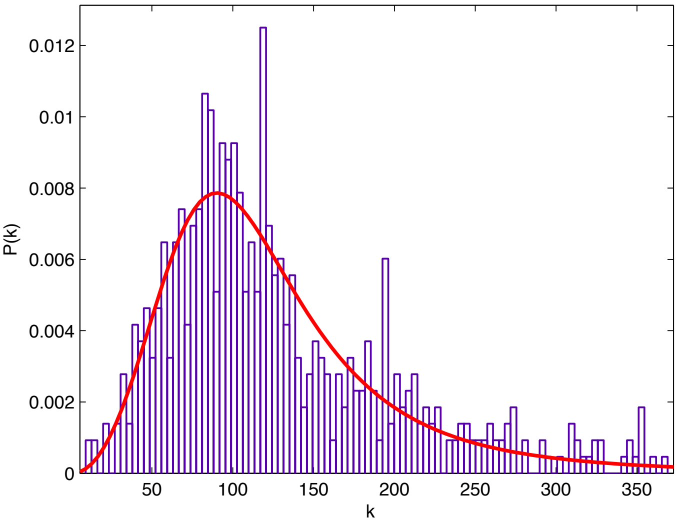

Fig. 2.5. Degree distribution $P(k)$ for a FA network. The number of nodes is 600. The continuous line represents a log-logistic fitting.

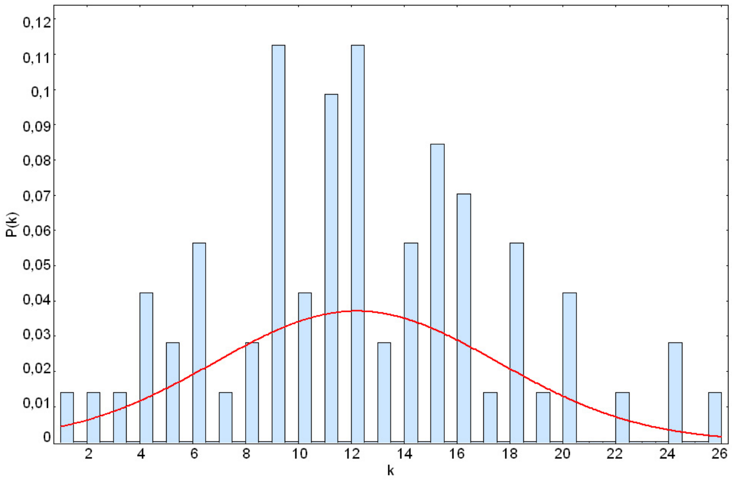

Fig. 2.6. Degree distribution $P(k)$ for a FA network. The number of nodes is 71. The continuous line represents a normal fitting.

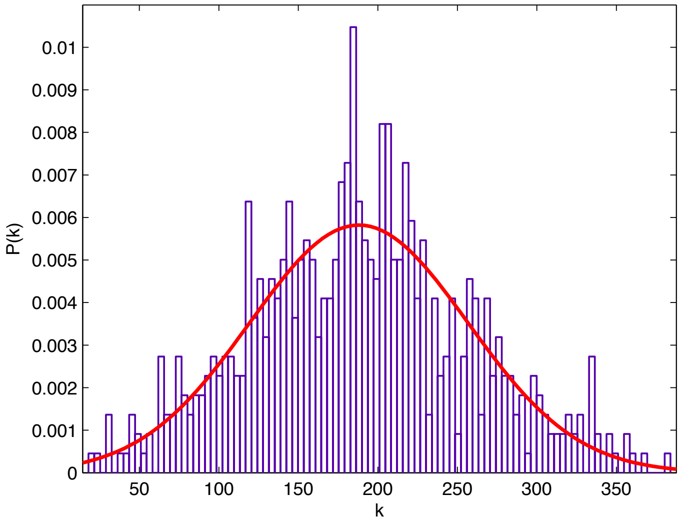

Fig. 2.7. Degree distribution $P(k)$ for a FA network. The number of nodes is 600. The continuous line represents a normal fitting.

(as shown in Figure 2.6 and Figure 2.7, obtained with $p = 0.8$). Varying these parameters it is also possible to obtain networks with power law degree distribution, as shown in Figure 2.8.

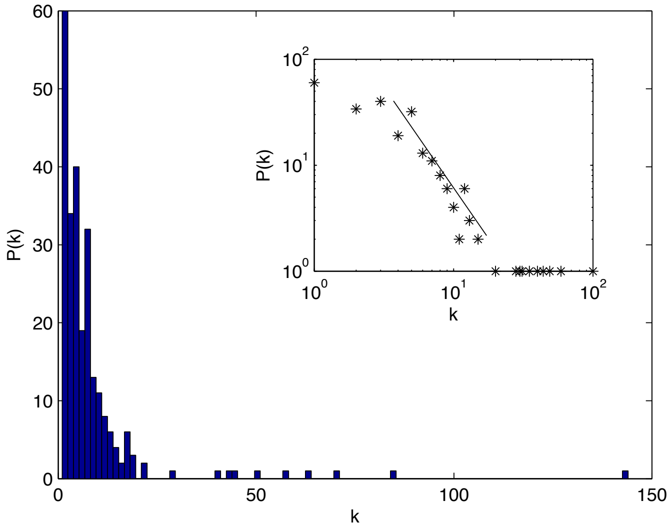

Fig. 2.8. Degree distribution $P(k)$ for a network obtained with FA model. The number of nodes is 250 and $p = 0.05$, $n_p = 2$.

The comparison between FA model and the real social networks analyzed has been performed in terms of characteristic path length L, clustering coefficient C, node betweenness B, number of communities N_C and type of degree distribution $P(k)$. In Table 2.4 some examples of networks generated by the introduced model are reported. Networks with the same number of nodes of the real networks in Table 2.1 have been generated, so that they can be directly compared. The other parameters of the model (p, n_p and n_{1-p}) have been fixed by trial and error in order to obtain approximatively the same average degree $\langle k \rangle$ of the real network. Then, the topological features (L, C, B, N_c and type of $P(k)$) have been extracted so that they can be compared with those of the real networks. As it can be observed the matching of L, C, and B is quite good. Furthermore, the model may account for different degree distributions (the type of degree distribution also matches with that of the real networks). Finally, in many cases the number of communities is similar to that really observed in networks with the same number of nodes. More precisely, if the mean square error (MSE) between the number of communities in the model and in the real case is calculated for ER networks (Table 2.2), BA networks (Table 2.3) and FA networks (Table 2.4), one obtains $MSE_{ER} = 28.8$, $MSE_{BA} = 55.9$ and $MSE_{FA} = 5.4$. FA networks thus predict the number of communities more accurately than ER and BA networks. As an example, in Figures 2.9 and 2.10 a real network and a FA network generated with the same number of nodes ($N = 154$) are shown, respectively. The number of communities is quite similar (11 for the real network, 12 for the FA network).

The results discussed above refer to networks obtained by assuming as initial network configuration a fully connected network of three nodes and that the communities are detected by using the Louvain method [28]. As initial configuration, the different topologies shown in Figure 2.11 have been considered, with the aim to study if these hypotheses affect the behaviour of the FA model: a fully connected network of three or five nodes (Figure 2.11(a) and (c)); an array of five

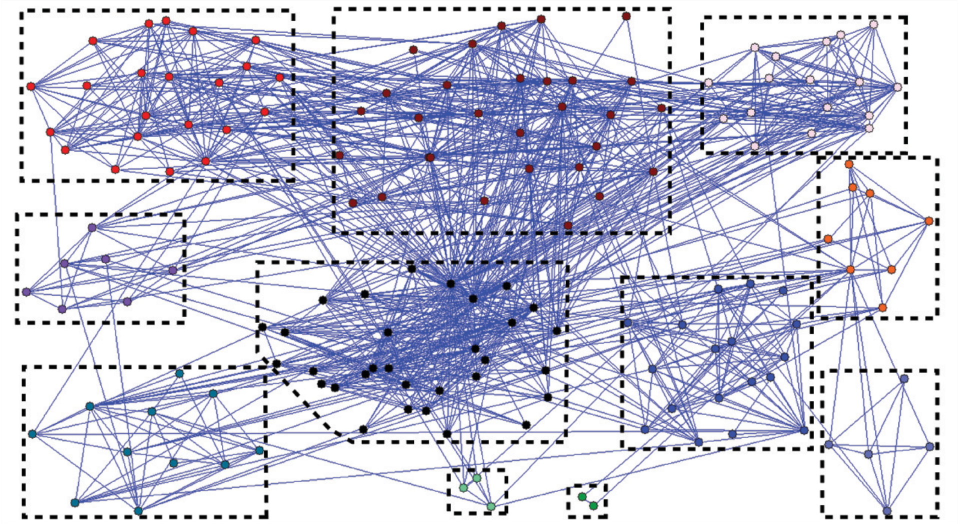

Fig. 2.9. A real network with 154 nodes. The network is divided in 11 communities.

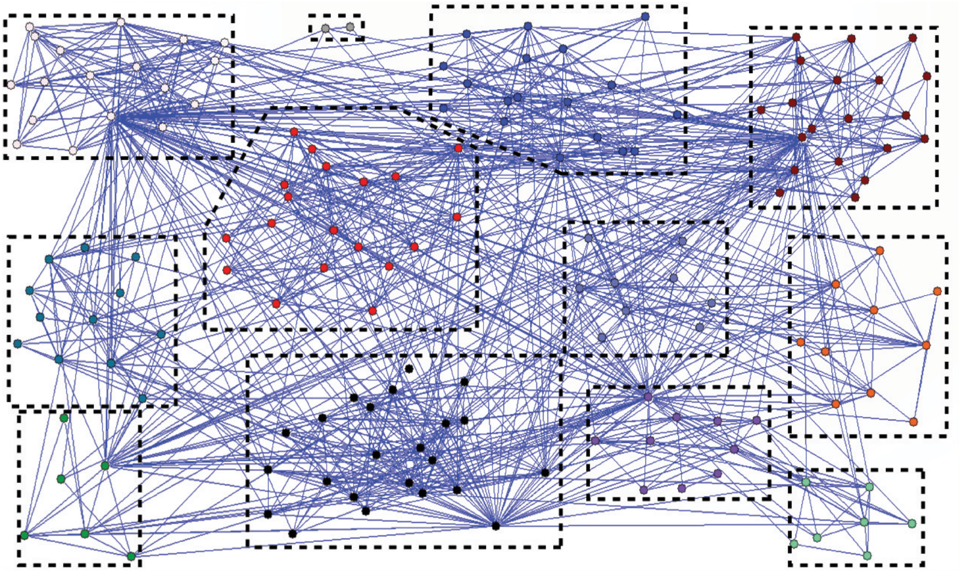

Fig. 2.10. A FA network with 154 nodes. The network is divided in 12 communities.

	FA model						
N	L	<k>	C	B	N_C	model parameters	type of $P(k)$
58	2.804	10.413	0.725	0.106	4	p=0.35, n_p=45, n_{1-p}=21	log-logistic
59	2.401	12.610	0.758	0.087	4	p=0.3, n_p=65, n_{1-p}=21	log-logistic
71	2.127	12.197	0.449	0.033	5	p=0.3, n_p=20, n_{1-p}=20	normal
89	3.471	10.921	0.674	0.081	5	p=0.3, n_p=60, n_{1-p}=2	log-logistic
91	2.810	9.560	0.606	0.043	9	p=0.4, n_p=60, n_{1-p}=5	log-logistic
102	3.607	7.156	0.525	0.063	9	p=0.1, n_p=12, n_{1-p}=2	log-logistic
105	2.736	10.209	0.578	0.039	7	p=0.05, n_p=19, n_{1-p}=1	log-logistic
129	2.9230	18.186	0.578	0.035	3	p=0.2, n_p=45, n_{1-p}=1	normal
138	3.428	7.913	0.526	0.042	16	p=0.5, n_p=60, n_{1-p}=4	log-logistic
140	3.293	11.500	0.590	0.038	7	p=0.1, n_p=24, n_{1-p}=1	normal
146	2.270	20.095	0.510	0.018	6	p=0.4, n_p=130, n_{1-p}=10	log-logistic
154	2.303	12.194	0.416	0.018	12	p=0.1	log-logistic
163	2.232	30.023	0.526	0.016	9	p=0.1, n_p=60, n_{1-p}=15	normal
209	3.074	11.428	0.514	0.021	13	p=0.5, n_p=52, n_{1-p}=6	log-logistic
234	2.899	20.357	0.481	0.016	5	p=0.1, n_p=40, n_{1-p}=2	log-logistic
242	2.518	27.301	0.435	0.013	6	p=0.01, n_p=40, n_{1-p}=40	log-logistic
266	3.071	18.105	0.528	0.016	8	p=0.3, n_p=60, n_{1-p}=5	log-logistic
340	2.040	27.741	0.394	0.009	10	p=0.25, n_p=1	log-logistic
592	1.941	59.003	0.341	0.003	5	p=0.2, n_p=30	log-logistic

Table 2.4. Topological measures for FA networks.

nodes (Figure 2.11(b)); a star network with five nodes (Figure 2.11(d)); and several others (Figure 2.11(e)-(g)). The numerical simulations performed have shown that the results discussed above do not depend on the initial configuration used. The application of different algorithms for community detection (and, in particular, spectral graph partitioning, hierarchical clustering and the algorithm by Girvan and Newman [2, 20]) has led to the same conclusion.

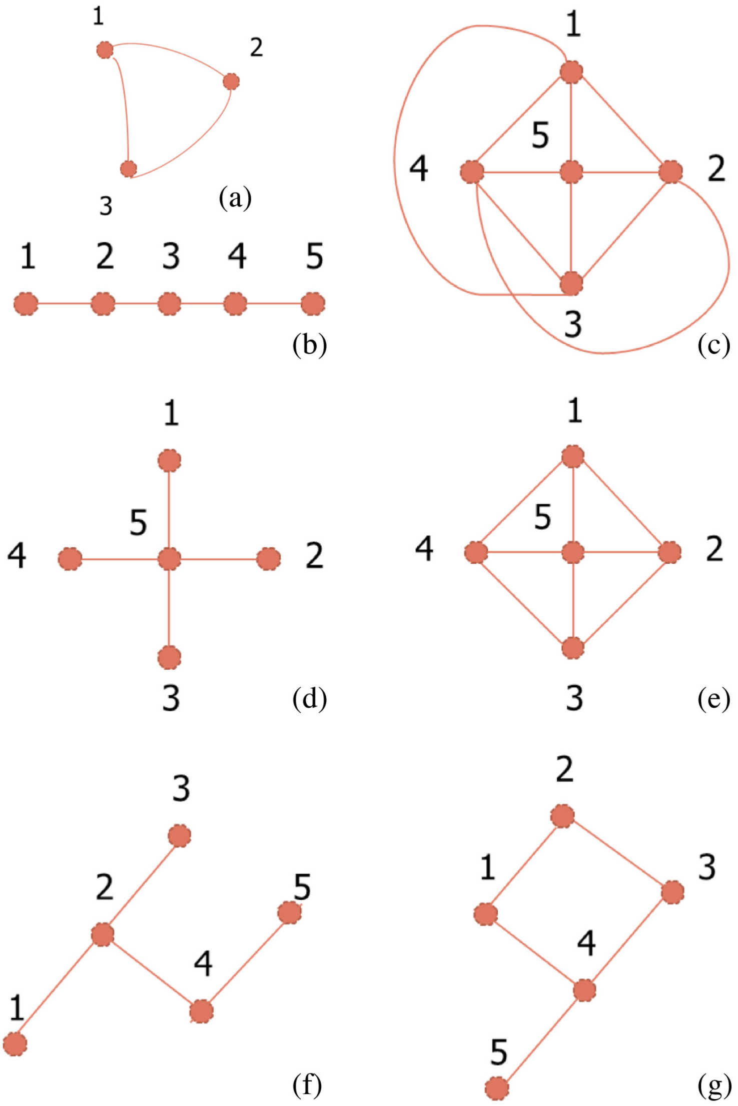

Fig. 2.11. Initial configurations used for the FA model.

2.4 Analysis of the determinism of time-series extracted from social systems

Another interesting issue that has been studied on the networks of our dataset is the observation of the time evolution of the number of the on-line friends [29]. For this analysis an appropriate application has been developed and the number of on-line friends of a Facebook user with about 300 friends has been monitored. The number of friends is constant during this analysis to avoid erroneous measurements and the application has been used for a week with sampling frequency of 5 minutes, obtaining the trend shown in Figure 2.12 where the maximum is 27 while the minimum is 2.

To correctly study this trend the time series has been filtered to eliminate the sinusoidal component that represents the day and night cycle. To obtain this the power spectrum of the time series has been analyzed to know at which frequency to apply a filter. So a second order Butterworth high pass filter with cutoff frequency of 0.2 Hz has been applied, obtaining the signal shown in Figure 2.13.

The Kaplan test [30] has been applied to detect determinism in this time series. The results of this analysis are shown in Figure 2.14, where the trend of L_n parameter for the Kaplan test of the filtered time series is shown. If this parameter is high, and remains high as n is varied, this can be considered an indication of the presence of determinism in the time-series.

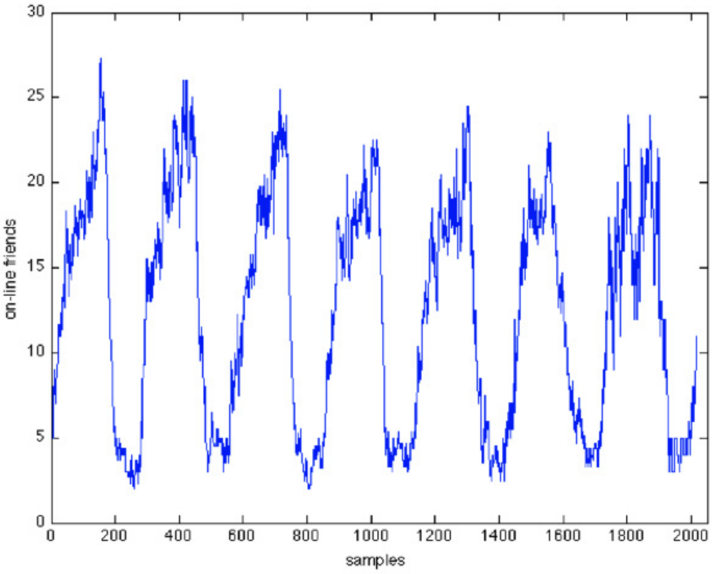

Fig. 2.12. Trend of the number of on-line friends of a Facebook user for a week, sampled with frequency f=5 min.

For comparison Figure 2.15 shows the trend of the L_n parameter for the Kaplan test for a surrogate signal with the same mean and variance of the filtered signal.

A deterministic component in the time series obtained starting from on-line Facebook users is evident: in fact the trend of L_n parameter in the first case is totally different than in the second one.

We remark that often the lack of data availability and of adequate analysis tools makes impossible or very difficult the analysis of a network under the point of view of its time evolution, so that in most of the cases the links are considered static. However, as this example shows, links may evolve in time and, for instance, be active at different

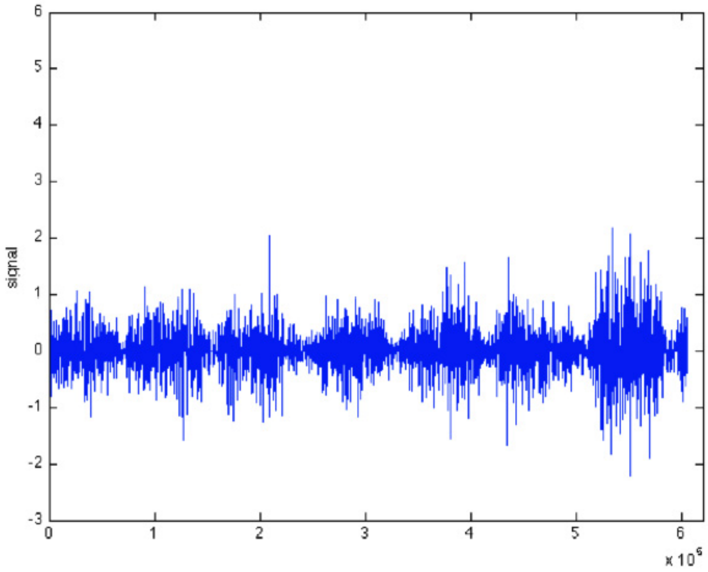

Fig. 2.13. Signal obtained applying the Butterworth high-pass filter.

times. Such analysis is one of the most interesting open problems now faced in complex network theory.

2.5 Conclusions

In this Chapter, starting from the analysis of a dataset of on-line social networks, i.e., friends networks extracted from Facebook on the basis of a volunteer participation to the project, a new model of growing complex networks has been introduced. The idea underlying this model is based on a possible mechanism explaining the growth of the friends networks analyzed. In such networks, in fact, communities play a fundamental role, being eventually also involved in the growing process of the network itself. In particular, when a new node attaches to

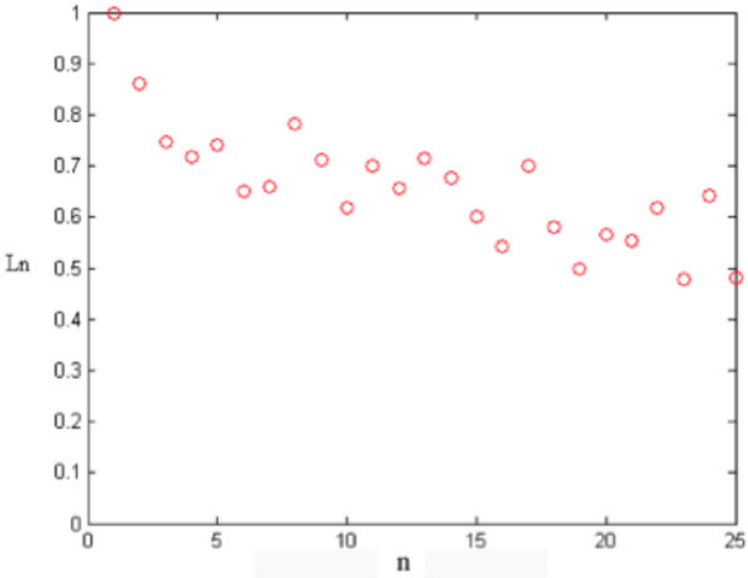

Fig. 2.14. Trend of the L_n parameter for the Kaplan test of the filtered time series.

the existing ones, due to the strong social interactions in the networks analyzed, it may happen that the selected nodes are not uncorrelated, but belong to the same community. This mechanism has been explicitly incorporated in the model, leading to a new attachment rule. It has been then shown that this model is able to reproduce the main features observed in the networks of the dataset, such as high clustering coefficient, low characteristic path length, low node betweenness, strong division in communities and variability of degree distributions.

The topological features of the introduced model (including the degree distribution type) are obviously influenced by the model parameters in a way not simple to be characterized. The comparison between real networks and those generated with the model has been carried

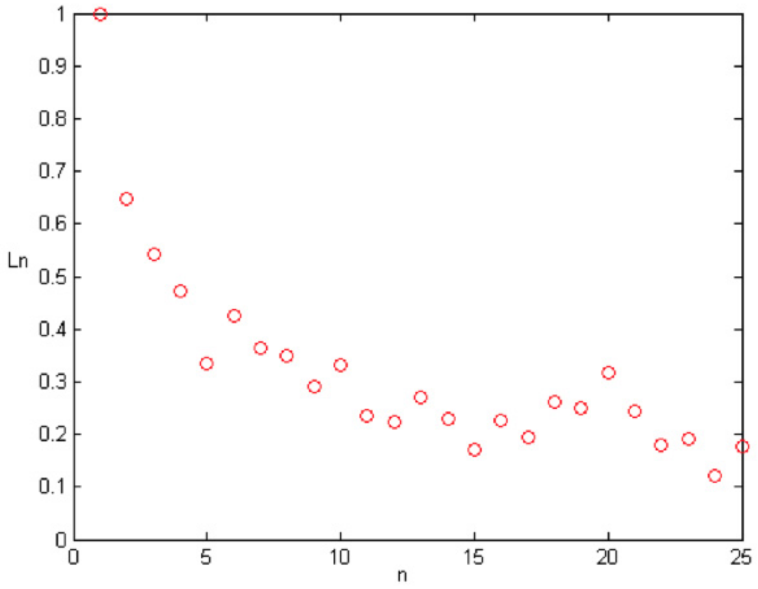

Fig. 2.15. Trend of the L_n parameter for the Kaplan test of a random signal with with the same mean and variance of the filtered signal.

out by fixing the model parameters to match only the node number and the average degree of the real network, so that the similarity of the other topological features can be considered in favor of the capability of the model to capture the real attachment mechanism of the social networks investigated. This could imply that, depending on the relationship involved in the formation of the social network, a richer-get-richer principle or other attachment mechanisms could be at the basis of the network growth.

Another aspect of the analysis of real social networks has been shown in the last Section where the number of on-line friends using a Facebook account has been analyzed showing the presence of a deterministic component. Including the time-dependence in complex networks makes the analysis more difficult, but at the same time may reveal new interesting features.

3

Dynamical Analysis of the Italian High-Voltage Power Grid

In this Chapter, the tools from complex networks theory are used for the analysis of the Italian high-voltage (380 kV) power grid. The topological properties of the network are investigated and, using a dynamical model based on Kuramoto-like oscillators, the synchronization of nodes is analyzed. Synchronization in the network represents the normal working operating regime, after which the effect of perturbations has been studied to investigate the dynamical robustness of the network to faults, then the relationship between threshold and topological properties and the time to obtain complete loss of synchronization is investigated. The analysis allows to define several dynamical parameters whose relationship with the topological ones is not-trivial. The results obtained are then compared with those obtained on a surrogate random network.

3.1 Topological analysis of power grids

The rapid development of complex network theory provides new research tools for complex power grids e. g. to analyze error and attack resilience of both artificially generated topologies and real world networks where nodes are generators, substations and transformers and edges are high-voltage (220-380-400 kV) transmission lines.

Power grids are one of the most attractive case studies of complex networks, together with social networks, so that many works [31, 32] focused on them, although often without considering the specific nature and characteristics of nodes and links, but working on a higher level of abstraction.

The analysis of the topology of power grids of the major European countries carried out in [33] and [34] allows to reveal some common characteristics of these networks: (a) most of them are small world; (b) they are very sparse; (c) the link distribution is exponential; (d) these networks are weakly or not correlated.

Another interesting topic, specially when the analysis of blackouts is dealt with, is identification of critical lines and modeling of cascading failures [31, 32, 34, 35]. Such phenomena are often explained by focusing on the topological properties of the network. In fact, in most of the above mentioned works, the approach is essentially static, and the dynamical characteristics of the nodes are not considered. However, recent works [36, 37, 38], have removed this hypothesis by applying to the power grids analysis the Kuramoto model of coupled oscillators [39] and studied the power grid behavior in terms of synchronization.

Power systems depend on synchronous machines for electricity generation and so the synchronism of the machines that form the system is a necessary condition for the whole network to operate in a proper way. The concept of stability of a power system is therefore closely linked to that of synchronism. An important form of stability for an electrical network is the so-called transient stability [37], which is the ability of the network to maintain synchronism when it is subjected to transient disturbances such as faults in transmission systems or problems with generators or heavy loads. If the perturbations cause a limited angular separation between the components of the system, the system maintains synchronism.

The response of the system to these perturbations involves large ranges of machine rotor angles values, power flows, voltages at the nodes, and other variables of the system. In this case it is possible that the automatic security devices of the nodes isolate parts of the system to prevent damages. For example, the Italian blackout of 2003 was caused by the fault on a line and caused a series of failures that led to loss of synchronism of the Italian power system with respect to the rest of Europe [40].

3.2 Kuramoto-like model of generators and substations

Following [36], a Kuramoto-like second-order model of electric systems can be obtained using a power balance equation to describe each generator or machine. A generator converts some source of energy into electrical power, while the reverse is true for a machine. The turbine of the generic generator i produces electrical power with a frequency that is close to the standard frequency $\mathit{\Omega}$ of the electric system (50 or 60 Hz):

$$\theta_i = \mathit{\Omega} t + \tilde{\theta}_i, \tag{3.1}$$

where θ_i is the phase angle at the output generator i and $\tilde{\theta}_i$ is the deviation from the uniform rotation. During the rotation the turbine dissipates energy at a rate proportional to the square of the angular velocity $\dot{\theta}_i$:

$$P_{diss} = K_D \dot{\theta}_i^{\,2} \tag{3.2}$$

or it accumulates kinetic energy

$$P_{acc} = \frac{1}{2} I \frac{d}{dt} (\dot{\theta}_i)^2, \tag{3.3}$$

where I is the moment of inertia.

The condition for the power transmission is that devices do not operate in phase, being the mismatch between the rotators of two of them (devices i and j) indicated by:

$$\mathit{\Delta}\theta = \theta_j - \theta_i = \tilde{\theta}_j - \tilde{\theta}_i, \tag{3.4}$$

considering that all the oscillators share the same common frequency Ω. As a function of this phase difference a power is transmitted:

$$P_{transmitted} = -P^{MAX} \sin \Delta\theta. \tag{3.5}$$

Each generator or machine is described by a power balance equation of the type:

$$P_{source} = P_{diss} + P_{acc} + P_{transmitted}. \tag{3.6}$$

Substituting expressions (3.2), (3.3) and (3.5) in equation (3.6) and assuming that dissipation is the same for all sources, it is possible to obtain a Kuramoto-like equation for the node i:

$$\ddot{\tilde{\theta}}_i = -\alpha\dot{\tilde{\theta}}_i + P_i + P^{MAX} \sum_{j \neq i} a_{j,i} \sin(\tilde{\theta}_j - \tilde{\theta}_i), \tag{3.7}$$

where α is the dissipation parameter, P_i is the power generated or absorbed and contains informations on the nature of the device and it is positive for a generator that is a source of power while negative for an absorbing machine, $a_{j,i}$ is the element of the adjacency matrix and accounts for the topology of the power grid.

The Italian high-voltage (380 kV) power grid is taken into account in this Chapter. It counts 127 nodes, divided into 34 sources (hydroelectric and thermal power stations) and 93 substations, and 342 edges. Informations on the location of generating plants and substations have been obtained from the UCTE map [41] and the data used in [31, 32, 42] and have been used to obtain the elements of the adjacency matrix.

For this network some significant topological parameters such as degree distribution, clustering and betweenness have been calculated. Av-

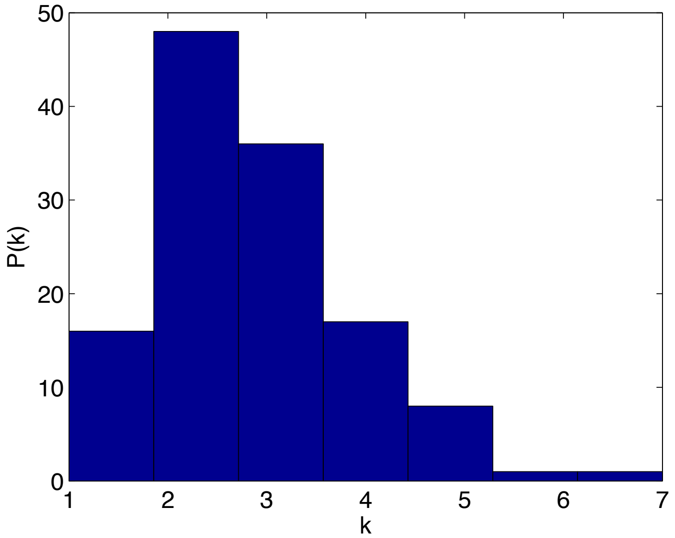

Fig. 3.1. Degree distribution of the high-voltage Italian power grid network.

erage values for these three parameters are $\langle k \rangle = 2.6850$, $\langle c \rangle = 0.1561$, $\langle b \rangle = 0.2032$. In Fig. 3.1 and Fig. 3.2 the degree and betweenness distributions are shown respectively. It is possible to observe that there are a lot of nodes characterized by a low degree and a low betweenness, a characteristic of the Italian power grid network that it is possible to correlate to the streched shape of the Italian peninsula (and consequently on the related power grid). In [38] the topological vulnerability and improvability of the Italian high-voltage (380 kV) power grid have been analyzed. The removal of a single edge, as the line connecting Laino and Rossano, is sufficient to isolate seven nodes from the rest of the network and Italian power grid, compared with Spanish and French ones, is the most vulnerable but also the most improvable network.

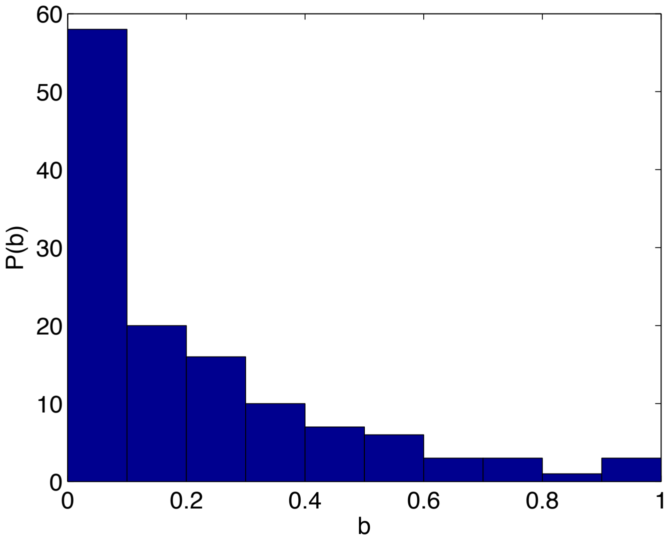

Fig. 3.2. Betweenness distribution of the high-voltage Italian power grid network.

3.3 Analysis of the Italian high-voltage power grid

In the Italian high-voltage (380 kV) power grid two are the kinds of network nodes: generators and substations [43]. The system has been simulated using equal parameters for all the nodes and links. It has been considered unitary absorbed power for substations (1 pu) and, in order to respect the equality between generated and absorbed power, the power supplied by generators are all been put equal to 2.7353 pu. The dissipation parameter α is the same for all the nodes and its value is $\alpha = 0.1$. Concerning the coupling parameter P^{MAX}, numerical simulations were carried out to find the value that allows to obtain complete synchronization. It was found that for values less than 5 it is not possible to obtain complete synchronization. In fact, the difference between two phases is subjected to fluctuations that persist over time. For values greater or equal to 5, the network reaches synchronism: differences between two phases, apart from the initial transient, stabilize at a value that remains constant over the time, that means that the units have the same frequency.

Transient stability of the network applying disturbances $\varDelta P_i$ to the nodes has been then studied. This extra energy is taken from the kinetic energy of the rotators that after few time units restore normal operation. This type of perturbation constitutes a realistic model of an unbalanced power due to faults in transmission systems or problems with generators or heavy loads.

When a perturbation $\varDelta P_i$ is applied to node i equation (3.7) becomes:

$$\ddot{\tilde{\theta}}_i = -\alpha\dot{\tilde{\theta}}_i + P_i + \varDelta P_i + P^{MAX} \sum_{j \neq i} a_{j,i} \sin{(\tilde{\theta}_j - \tilde{\theta}_i)}, \qquad (3.8)$$

while the other dynamics remain unchanged.

As result of the application of the perturbation, two outcomes are possible:

1. the network is able to return to synchronism condition, despite the initial fluctuations that affect the transmitted power;

2. the network is not able to restore the synchronism and fluctuations in the phases difference persist over time. In this case the system loses its stability even when perturbations end.

To evaluate the perturbation response of each node, once synchronization between nodes has been established, increasing values of perturbations have been applied for 50 seconds. In this way a threshold $\tilde{P}_i$ has been defined for each node, representing the minimum value of node perturbation that causes loss of synchronization in the network:

$$\tilde{P}_i = (\varDelta P_i)_{MIN}. \tag{3.9}$$

The treshold distribution is shown in Fig. 3.3. The different threshold values indicate that not all nodes respond in the same way. An analysis to investigate the correspondence between threshold and topological properties of the node has been carried out. In Fig. 3.4 the trend of the threshold with nodes degree is shown. The value of the threshold tends to increase with increasing value of the degree. It is sufficient to apply a lower disturbance to nodes with few links to lose the network synchronism.

To fully investigate the response of the network, and the failure propagation, an high perturbation (20 pu) has been applied to each of the nodes.

Two different responses have been observed:

1. cascading failure: the perturbed node fails (loss of synchronism) and the failure involves first the nearby elements and then propagates to other (more for) nodes;

2. fast failure: all the nodes fail in short time.

These two kinds of response can be distinguished by comparing for each node the time $\tilde{t}$ defined as the time from the application of the perturbation to the complete loss of the network synchronism.

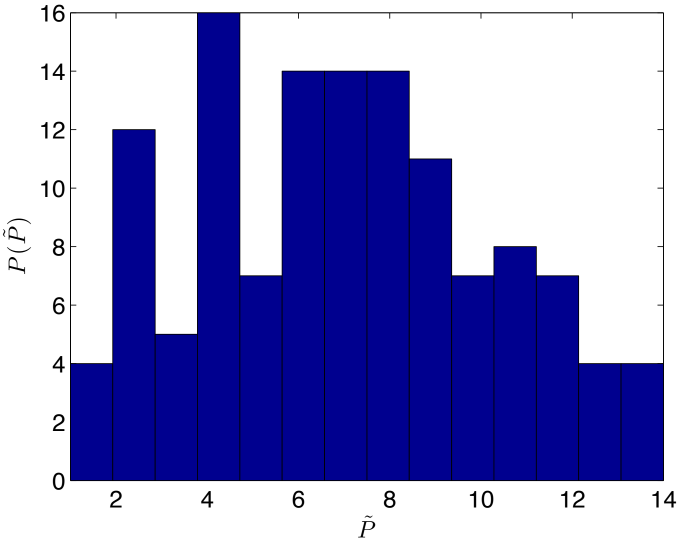

Fig. 3.3. Threshold distribution of the Italian high-voltage power grid.

Fig. 3.5 shows the behaviours of nodes 1 (in blue) and 68 (in red) that may be considered as examples of the two cases. In fact, these two nodes are characterized respectively by degree 1 and 7, betweenness 0 and 0.5385 and threshold values of 4 and 11, so node 1 is more peripheral than node 68. There is a graduality in the failure propagation of node 68 while an immediate propagation is obtained in node 1. The two graphs represent the trend of θ_1 and θ_{68} respectively showing the different propagation delay of perturbation. Time for complete desyncronization is respectively $\tilde{t_1} = 13.4947s$ and $\tilde{t_{68}} = 105.8578s$ for node 1 and node 68.

In Fig. 3.6 the parameter $\tilde{t}$ is shown for all the network nodes, while in Fig. 3.7 the parameter $\tilde{t}$ with respect to node degree is shown. The

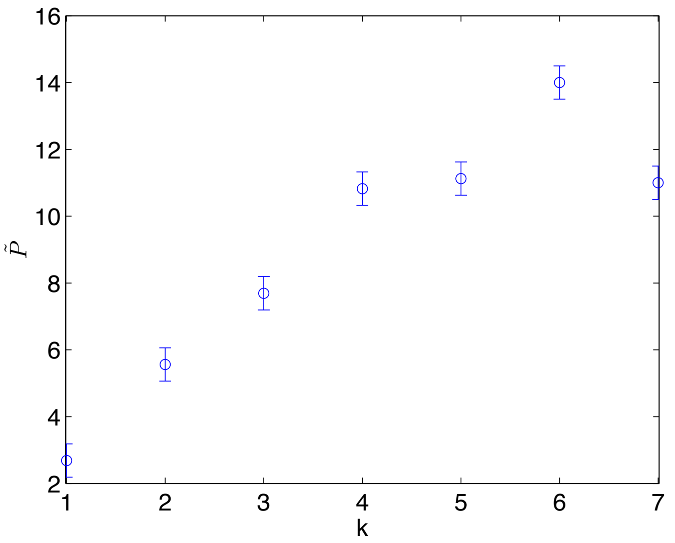

Fig. 3.4. Threshold $\tilde{P}$ with respect to node degree.

bigger is the degree of a node the bigger is the time interval $\tilde{t}$ to lose synchronization. Nodes with high degree tend to cascading failures.

3.4 Comparison with surrogate network

A comparison between the Italian high-voltage power grid and a surrogate random network in order to understand which features are peculiar of the Italian high-voltage power grid and which, on the contrary, are common features of these network is discussed in this Section. The surrogate data has been generated by considering the same number of nodes, the same number of links (and so the same degree) and a different arrangement of the links. In particular, in the surrogate data the links are randomly established. Therefore, an Erdös-Renyi network

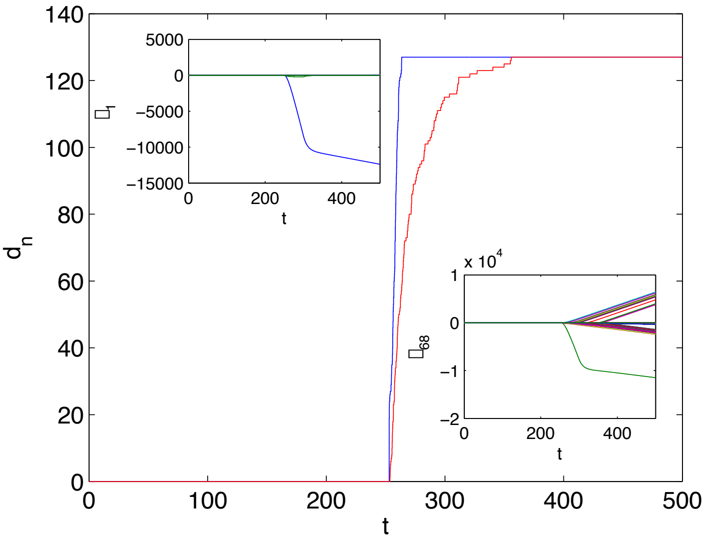

Fig. 3.5. Time to obtain complete loss of desynchronization (desynchronized nodes $d_n = 127$) for nodes 1 (blue) and 68 (red). The beahaviour of θ_1 and θ_{68} are showed respectively on the top and down of the picture.

with 127 nodes and 342 links has been built up. This network has then been used to perform a dynamical simulation with the Kuramoto-like model discussed in Section 3.2.

The average degree is $\langle k \rangle = 2.6772$; the clustering coefficient is $\langle c \rangle = 0.0198$ and the betweenness is $\langle b \rangle = 0.1981$. Compared with the values of the Italian high-voltage power grid, it can be observed that the clustering coefficient is lower. It should be also noted that this random network differs from the Italian high-voltage power grid for the fact that it does not take into account physical geographic constraints which, on the contrary, are a key factor of the Italian high-voltage power grid.

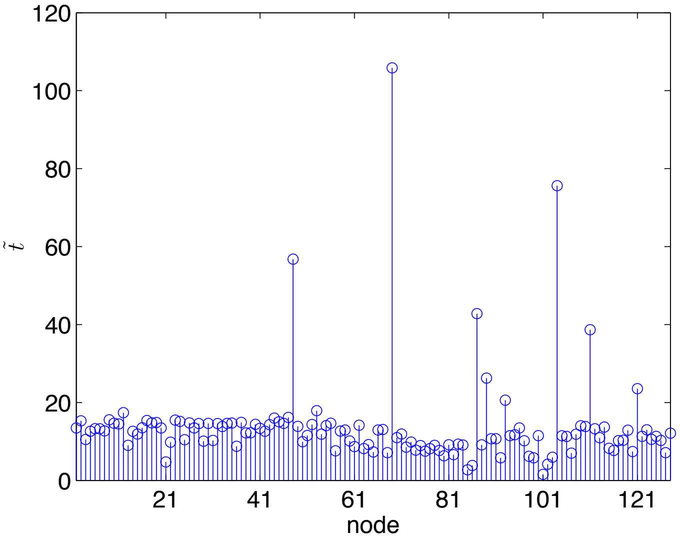

Fig. 3.6. Time for the complete loss of the synchronization for the Italian power grid when a perturbation $\Delta P = 20pu$ is applied to the node i.

The degree distribution and the betwenness distribution are reported in Figs. 3.8 and 3.9, respectively. No significant differences with the corresponding distributions observed in the Italian high-voltage power grid emerge.

The Kuramoto-like model in equation (3.7) has been then simulated on the surrogate network. The simulations were first devoted to derive the minimum value of P^{MAX} leading to synchronization. It has been obtained that $P^{MAX} = 13$ is needed to obtain complete synchronization. Interestingly, this value is significantly larger than the value $P^{MAX} = 5$ of the real network. This means that the surrogate network is more difficult to be synchronized. Then, the transient stability analysis of the surrogate network has been carried out. The threshold

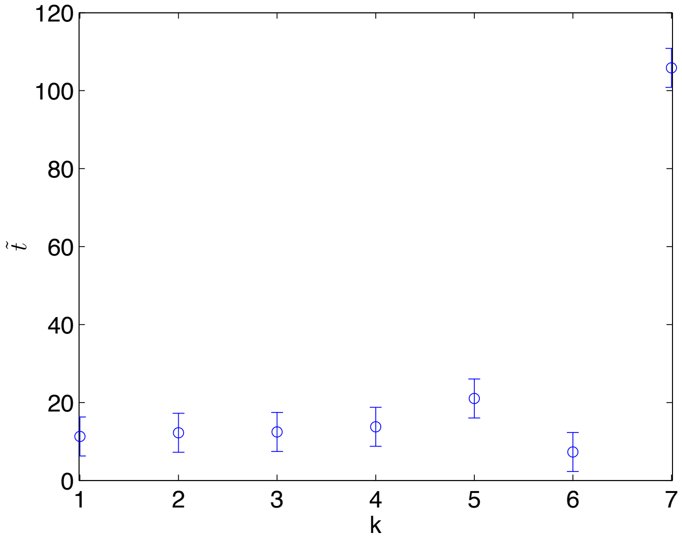

Fig. 3.7. $\tilde{t}$ with respect to node degree when a perturbation $\Delta P = 20pu$ is applied.

distribution obtained for the surrogate network is shown in Fig. 3.10. It can be observed that the threshold values are also on average larger than the corresponding values in the real network. The conclusion is that the surrogate network seems to be more robust.

The analysis of the threshold with respect to the node degree has been repeated for the surrogate network. The results are shown in Fig. 3.11, where the same tendency of the threshold to increase with the node degree can be observed.

As concerns the failure analysis, also in this case both cascading failures and fast failures have been observed. Also for the surrogate network cascading failures are associated with high degree nodes.

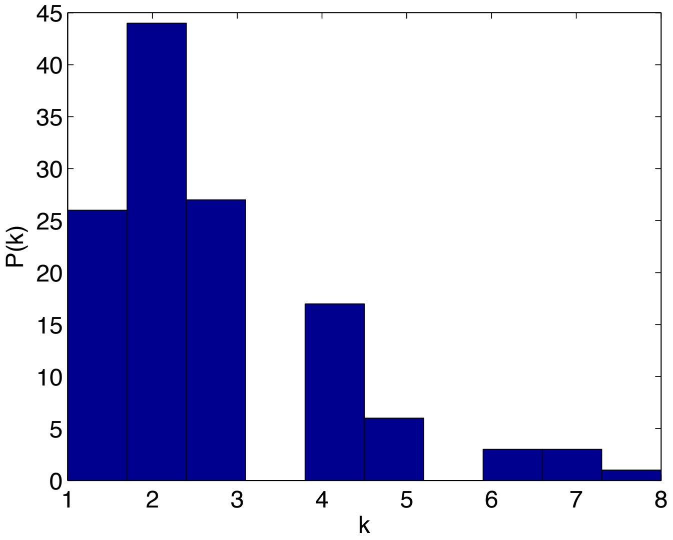

Fig. 3.8. Degree distribution of the surrogate network.

3.5 Conclusions

In this Chapter a study of the Italian high-voltage power grid has been proposed. A Kuramoto-like second-order model has been taken into account to model the node dynamics. It is interesting to note that the mapping between oscillators and power grid nodes can be made quantitative and under some approximations the class of Kuramoto-like models with bimodal distribution of the frequencies is the most appropriate choice. In fact in the power grid there are two kinds of oscillators: “sources” and “consumers”. Dynamical parameters such as the minimum value of perturbation leading to desynchronization and the time to reach the complete loss of synchronism have been introduced. A non-trivial relationship between dynamical and topological

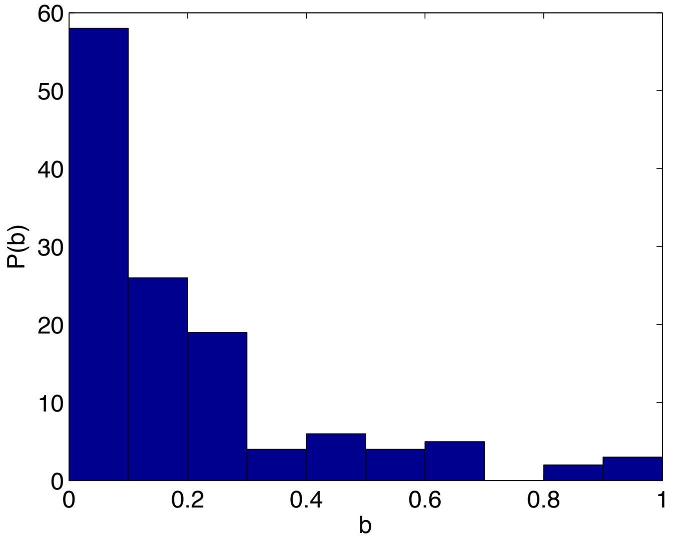

Fig. 3.9. Betweenness distribution of the surrogate network.

parameters of the network has been observed. In general, the higher is node degree the higher is the minimum absorbable perturbation and the bigger is the time interval to lose synchronization with cascading failure, but it can be concluded that the dynamical parameters studied are not a function of a single topological parameter.

The analysis has been then repeated for a surrogate network with the same number of nodes and links, but with random links in order to understand which specific features are related to the particular geographical shape underlying the Italian high-voltage power grid. The conclusions that can be drawn is that the surrogate network is more difficult to synchronize but also more robust, which can be explained with the particular geographic configuration of the Italian peninsula.

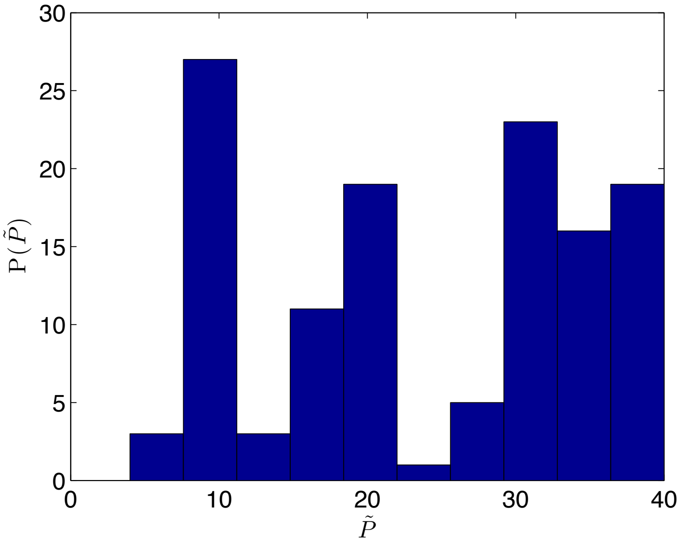

Fig. 3.10. Threshold distribution of the surrogate network.

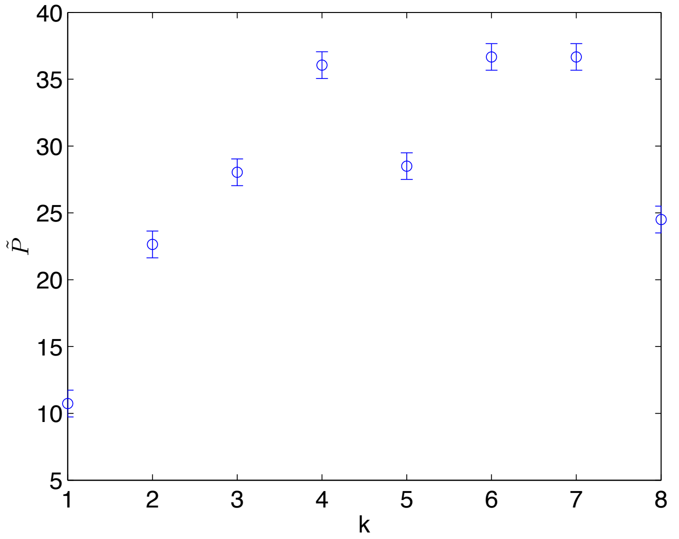

Fig. 3.11. Threshold $\tilde{P}$ with respect to node degree for the surrogate network.

4

Emulation of complex networks: the Wolfram Machine

Most of the tools for the study of complex systems are theoretical and/or software. In this Chapter, a new stand-alone complex system hardware emulator, called the *Wolfram Machine*, is presented. The system is a programmable hardware cellular automaton able to emulate and show the outcome of all elementary cellular automata, allowing for their experimental analysis. The system consists of an LED matrix and a board equipped with a microcontroller. This simple low-cost system can be programmed to reproduce the complex behavior of Wolfram's cellular automata, ranging from periodic patterns to Turing machines and Isles of Eden.

4.1 The Wolfram Cellular Automaton

Cellular automata are mathematical models for complex natural systems containing a large number of simple identical cells with local interactions. They were invented in the 1940s by the mathematicians John von Neuman and Stanislaw Ulam, to provide insight into the logical requirements for machine self-replication [44]. The idea was to construct a machine able to generate a new machine of identical complexity and capabilities. Cellular automata have been then applied to a wide range of different problems in mathematics, physics, biology, complexity, and modeling [45].

Cellular automata may be considered as an array of "colored" cells on a grid of specified shape where each cell may assume, at a given time, one of a finite set of possible values. The cell states evolve synchronously in discrete time steps according to identical local rules that take into account the previous states of the cell itself and of the neighboring ones.

Despite their simple construction, cellular automata are capable of complex behavior [46, 47]. According to the behavior exhibited by them, one-dimensional cellular automata have been classified into four classes by Wolfram [46].

From the perspective of nonlinear dynamical systems, cellular automata can be thought of as discrete dynamical systems with trajectories evolving in the configuration space that tend to some attractors or evolving around Isles of Eden [48], devoid of any basin of attraction. The attractor is a manifestation of "self-organizing" behavior, in which the dynamics evolves from a structure-less initial state toward an organized state, after a sufficiently long time.

Many researchers have studied in detail one-dimensional cellular automaton rules, showing that, even in this simple framework, they exhibit many of the complex behaviors of a continuous system [46, 47, 49].

These features make cellular automata and their generalization, such as Cellular Nonlinear Networks (CNNs), valuable tools for studying the behavior of complex systems.

One-dimensional cellular automata have been studied in particular by Stephen Wolfram. His research, started in the 1980s, culminated in the publication of his monumental book “A New Kind of Science”. In this remarkable book, considered a milestone of results in automata studies, Wolfram asserts that cellular automata operations underlie much of the real empirical world. He even asserts that the entire Universe itself is a big cellular-automaton computer [46].

Chua, then, reconsidered the Wolfram’s approach, which was based on empirical observations obtained with brute-force computer simulations, under the perspective of dynamical systems [50, 51] and geometrical approaches. He developed an analytical theory, valid for any elementary one-dimensional cellular automata, which provides a foundation for the emergence of behaviors shown by the automaton in terms of only six different classes of complexity [52].

A new low-cost stand-alone hardware device which constitutes a small self-contained implementation of the Wolfram cellular automaton has been developed.

4.2 Model of the Wolfram Cellular Automaton

A one-dimensional cellular automaton consists of a ring of coupled cells as shown in Fig. 4.1. Each cell evolves, synchronously with the others, combining its inputs through a local rule R (as shown in the block diagram of Fig. 4.2) that is the same for all cells. In the case of Wolfram cellular automata, only rules based on two neighboring cells are considered.

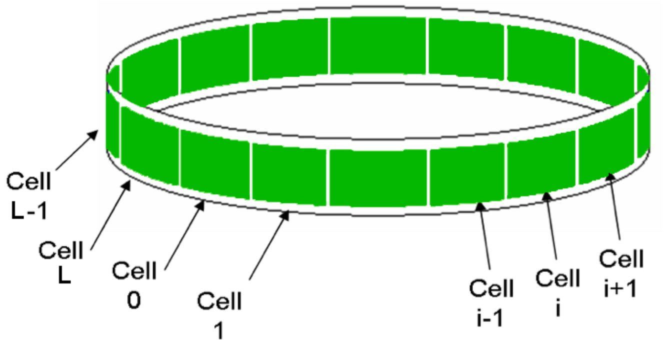

Fig. 4.1. Schematic representation of a one-dimensional cellular automaton, consisting of a ring of $L + 1$ identical cells.

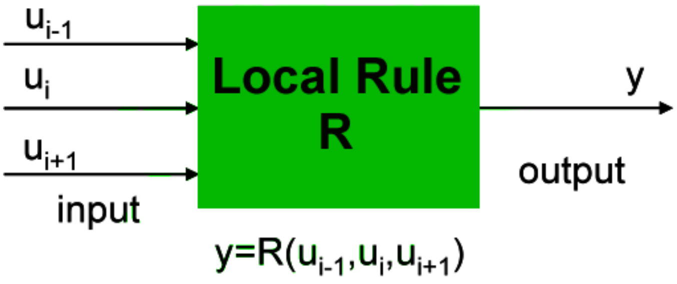

Fig. 4.2. Representation of inputs and output of a local rule of Wolfram cellular automaton cells.

The state of a cell and those of its two neighbors form a substring of three states (each one assuming one of two possible values 0 or 1 and coded blue or red respectively), so that there are $2^3 = 8$ possible input patterns for each cell. At every time step, the next value of a given cell is determined by a function of the states of the cell itself and its immediate left and right neighbors. The cells are updated synchronously taking into account the state values at the previous step. Under such hypotheses, there are $2^8 = 256$ possible rules [46].

A classification of all the 256 local rules is given in [53] in the framework of nonlinear dynamical system science. In this way, the Wolfram machine is seen as a complex class of cellular automata, with one spatial dimension, a binary state variable, and a neighborhood of radius one.

Every rule may be represented with a Boolean cube (as shown in Fig. 4.3) [47], where every vertex of the cube represents one of the eight possible states of the three-cells neighborhoods and has binary values, representing the output corresponding to the given input pattern.

According to the analysis reported in [49], each rule of the cellular automaton can be furthermore mapped into a nonlinear time-continuous dynamical system defined by the following state equation:

$$\begin{aligned} &\dot{x}_i = (-x_i + (|x_i + 1| - |x_i - 1|)) + \\ &+ \{z_2 + c_2|\,(z_1 + c_1|z_0 + b_1 u_{i-1} + b_2 u_i + b_3 u_{i+1}|)\,|\} \\ &x_i(0) = 0 \qquad\qquad\qquad\qquad i = 0, \cdots, L \end{aligned} \tag{4.1}$$

where b_1, b_2, b_3, c_1, c_2, z_0, z_1, z_2 are real numbers which characterize the given rules, u_i represents the binary state of the cellular automaton (assuming values -1 or 1), while x_i is the state of the equivalent continuous-time system to which the cellular automaton is mapped.

The parameters b_1, b_2, b_3, c_1, c_2, z_0, z_1, z_2 are such that system (4.1) converges to an equilibrium point $x_i(Q)$ for $i = 0, \cdots, L$. The output of the $i-th$ cell, defined as $y_i(t) = 0.5(|x_i(t)+1| - |x_i(t)-1|)$, converges to a Boolean value 1 or -1, given by the following formula:

$$y_i(Q) = sgn\left\{z_2 + c_2|\left(z_1 + c_1|z_0 + b_1 u_{i-1} + b_2 u_i + b_3 u_{i+1}|\right)|\right\}. \qquad (4.2)$$

The discrete-time evolution of the binary state of the cellular automaton cells is explicitly given by the following relationship:

$$u_i^{t+1} = sgn\left\{z_2 + c_2|\left(z_1 + c_1|z_0 + b_1 u_{i-1}^t + b_2 u_i^t + b_3 u_{i+1}^t|\right)|\right\}. \qquad (4.3)$$

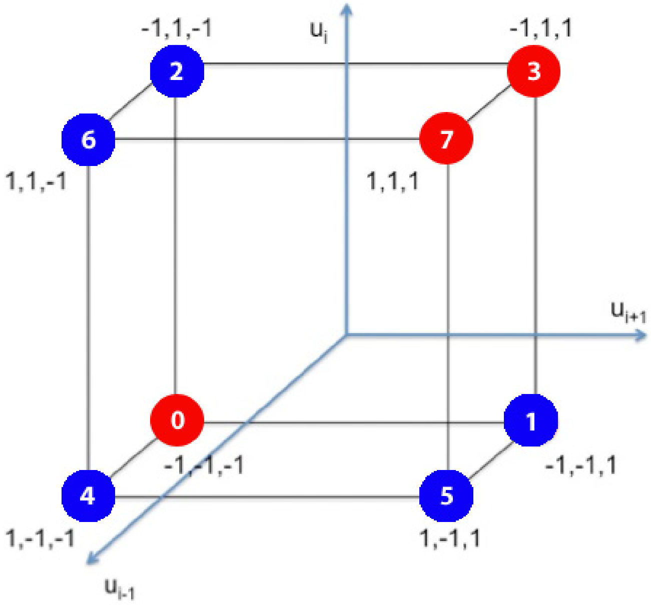

Fig. 4.3. A Boolean cube, representing rule 137, one-dimensional cellular automaton.

Using tools from nonlinear dynamics the degree of the nonlinearity of the Wolfram cellular automata can be quantified in terms of their index of complexity [47, 49, 53]. The complexity index κ is defined by the number of parallel planes necessary to segregate all blue vertices from the red vertices. Equivalently, the complexity index κ of each rule N is equal to $1+\alpha$, where $\alpha \in \{0, 1, 2\}$ is the number of absolute-value functions required in Eq. (4.3). In this way all 256 rules are classified by three possible values of the complexity index. There are 104 rules with complexity index one and they exhibit a period-1, period-2 or simple Bernoulli-shift patterns [54]. There are 126 rules with index two and they support mobile self-localizations, gliders, and non-trivially interacting propagating patterns. The remaining 26 rules, having complexity index three, have unpredictable complex behaviors. A rigorous classification of these rules according to the nature of space-time patterns they generate divides all rules into six groups [55, 56, 57]. Examples from all such groups will be discussed in Section 4.4.

4.3 The Wolfram Machine

The Wolfram Machine [58] consists of an LED Matrix, for visualization, i.e., a rectangular array of Light-Emitting-Diodes (LED), and a small board based on the ATmega168 microcontroller, for implementing equation (4.3) and controlling the display. The core of the system is thus the control board, in which the evolution of all the rules is computed. The whole system is shown in Fig. 4.4.

A 2416 (16 rows with 24 pixels each) Dot Matrix Red Display Information Board, manufactured by Sure Electronics, was used [59]. It is a memory mapping LED display board, driven by an HT1632 LED display controller. The device supports 16-gradation LEDs for each outline controlled in PWM (Pulse Width Modulation). In this way, the color intensity of each LED can be gradually varied (through the PWM control signal) from a maximum intensity to the off level. In our work, since the cells may only assume binary values, two levels (maximum and off level) have been only used. A serial interface is conveniently provided for the command mode and data mode. Only three or four signals are required for the interface between the host controller and the information board. These signals are: CS (Chip Select: it enables the information board); WR (Write Clock Input: it writes the clock input from the microcontroller); RD (Read Clock Input: it reads the clock input from the microcontroller; this signal is optional and has not been used in our work); DATA (Serial Data Input: it permits to send to the LED matrix the data to be visualized).

For each row i of the LED display, each pixel represents the state of a one-dimensional cellular automaton cell at a given time t. The next step is represented in row $i + 1$ (rows are numbered from top to bottom). In the basic configuration, therefore, 16 different time instants of the evolution of a cellular automaton with 24 cells can be visualized: an advantage of the system is that the display can be easily extended by cascading the information board for wider applications. Periodic boundary conditions are used.

Other characteristics of the display board are: compact dimensions, 2416 dot matrix on each board divided into 6 pieces of 0808 LED, operating voltage and current: 5 V, 350 mA (Max.), 200 mA (Avg.). The power can be supplied and command data can be transmitted by IDC sockets from microcontrollers.

The control board used is an Arduino Nano [60]. It is a complete, breadboard-friendly, small board based on the ATmega168 microcontroller. It needs only a DC power jack and works with a Mini-B USB cable used both for power and programming. It is also possible to use an external power-source connected directly to the proper pins. To provide the external power supply, two options have been incorporated: in the first case, an AC adapter for a mobile phone with Mini-B USB can be used; in the second case a 9 V battery can be employed to obtain a real portable stand-alone hardware system, as shown in Fig. 4.4.

The control board has 30 pins, 22 of which are dedicated to input and output operations. They are divided into analogic and digital pins. There are 14 digital pins and they can be used either as input or output. They operate at 5 V. Each pin can provide or receive a maximum of 40 mA and has an internal pull-up resistor (disconnected by default) of 20-50 $k\Omega$. There are 8 analogic pins and they can be used only for input and, by default, they measure from ground to 5 V, though it is possible to change the upper limit of their range. The remaining pins have specialized functions, i.e. for ground and external power.

The idea is to emulate a one-dimensional cellular automaton by connecting the LED Matrix to the Arduino board. By programming the board, the Wolfram Machine, a stand-alone emulation system, has been realized. The algorithm implemented allows anyone to reproduce

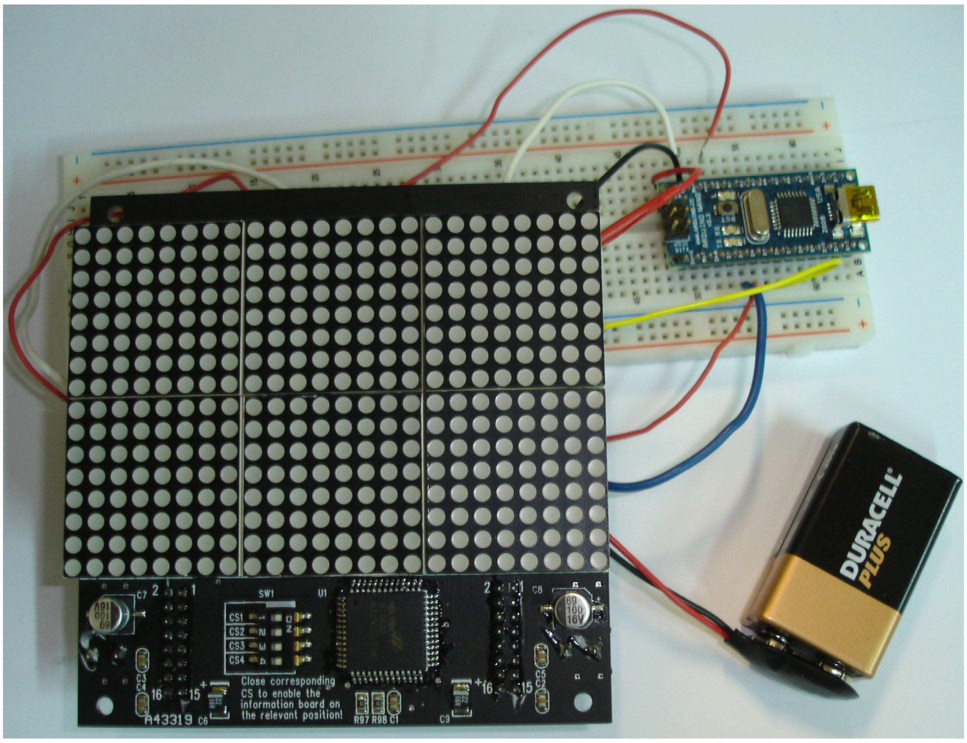
SW1
U1
CS1
CS2
CS3
CS4
Close corresponding CS to enable the information board on the relevant position!
A43319
R97 R98 C1
DURACELL
PLUS

Fig. 4.4. The Wolfram Machine, consisting of a microcontroller, an LED display, a breadboard and a 9V battery.

all 256 rules by changing the parameters appearing in equation (4.3). One possible set of parameters for each rule is listed in Table 4 of [49]. All parameters for the 256 rules have been already programmed and stored in the microcontroller, and the user only has to input the rule number to emulate any rule (this does not require the user to reprogram the microcontroller). Moreover, since the parameters listed in Table 4 of [49] represent only typical values, there is a large robust neighborhood of parameters that can emulate the same rule. The user may therefore input his own set of parameters by substituting the actual values with his own set and reprogramming the microcontroller, and verify they give the correct truth table. It is also possible to change the number of iterations for every rule to find eventual cycles, or to fix the string which codes the initial conditions to study the effect of the initial pattern on the cellular automaton behavior.

For example, to display the last 16 iterations after iterating 512 iterations, from some initial state, its enough to simply set to 512 the number of iterations. The microcontroller repeats the execution of the rule for 32 times and, after the first execution, the initial state of the first top row is the last row of the display. There is no limit for the number of possible iterations.

It is also possible to program the execution of several different rules in succession, in order to define a spatio-temporal algorithm, in analogy with CNNs. In this case, the user can program the number of iterations to be executed for each rule in the algorithm.

4.4 Experimental results

The results discussed in this Section refer to the emulation of different rules, according to their index of complexity $\kappa = 1, 2, 3$, as proposed in [47]. The time needed for the execution of a single rule is very small (order of magnitude of ms) so that, with this new system, it is possible to emulate all the 256 rules in a few minutes. In fact, in the algorithm a delay time has to be inserted in order to visualize the step-by-step evolution of the initial string. For each of the rules examined, a comparison between the computer simulation and a picture (taken with a digital photo camera) of the Wolfram Machine output is shown.

In Figs. 4.5 and 4.6 the evolution of two rules with complexity index $\kappa = 1$, rule 77 and 87 respectively, is shown. Each row represents the state of a cellular automaton with 24 cells, while time flows from top to bottom. A simple periodic behavior is obtained in these two cases. The images shown in Figs. 4.5 and 4.6, in particular, refer to the initial condition chosen by Wolfram in which only the central pixel of the array starts from a logic 1, while all the other cells starts from a logic 0. This pattern is the digital analog of the "unit impulse" used for testing continuous-time linear systems.

In Figs. 4.7 and 4.8 two rules with complexity index $\kappa = 2$, rule 73 and 82 respectively, are exhibited. In Figs. 4.9 and 4.10 an example of rules with complexity index $\kappa = 3$, rule 114 and 150 respectively, is shown.

Beyond the classification of the rules based on their complexity index, they can be grouped into six classes on the basis of the asymptotic behavior typically obtained with such rules starting from almost random initial conditions. According to this analysis [55, 56], out of 256 rules, only 88 rules can be considered as globally-independent from each other. All other rules are equivalent to one of these 88 rules in the sense that the remaining 168 rules can be derived from these 88 rules via one of the three global transformations from the *Vierergruppe* [53]; namely, the *Left-Right Transformation* $T^{\dagger}$, the *Global Complementation* $\overline{T}$, and the *Left-Right Complementation* T^{*}. These 88 independent rules are

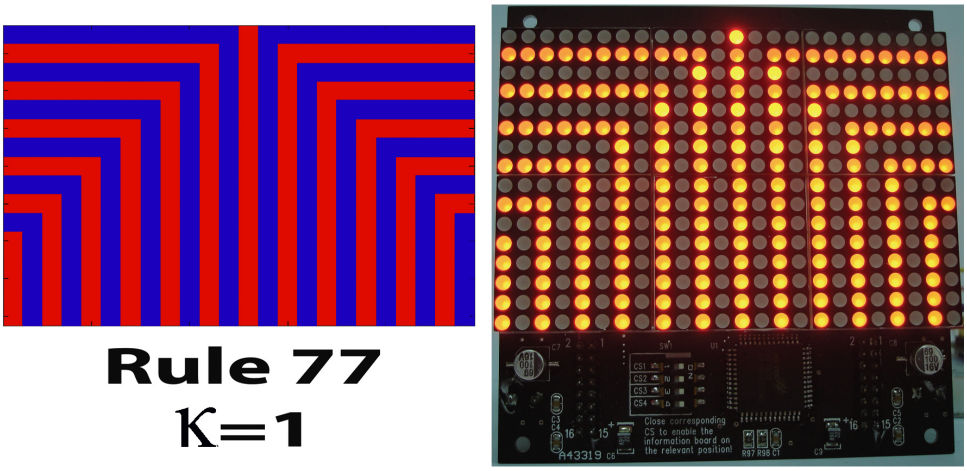

Fig. 4.5. Rule 77. Comparison between a PC-based numerical simulation (left) and the evolution of the Wolfram Machine (right) starting from the same "unit impulse" initial conditions.

classified into six groups, in a mathematically rigorous sense, unlike Wolfram's classification into four groups which is based on empirical simulations.

In the first group, indicated as $\mathscr{G} = 1$ (period-1 rules), there are 67 of the 256 rules and 25 of the 88 independent rules. In the second group (period-2 rules) there are 25 of the 256 rules and 13 of the 88 independent rules. In the third group (period-3 and period-6 rules) there are 6 of the 256 rules and 2 of the 88 independent rules. In the fourth group (Bernoulli σ_τ-shift rules) there are 108 of the 256 rules and 30 of the 88 independent rules. In the fifth group (complex Bernoulli rules) there are 18 of the 256 rules and 10 of the 88 independent rules. In the sixth group (hyper Bernoulli rules) there are 32 of the 256 rules and 8 of the 88 independent rules.

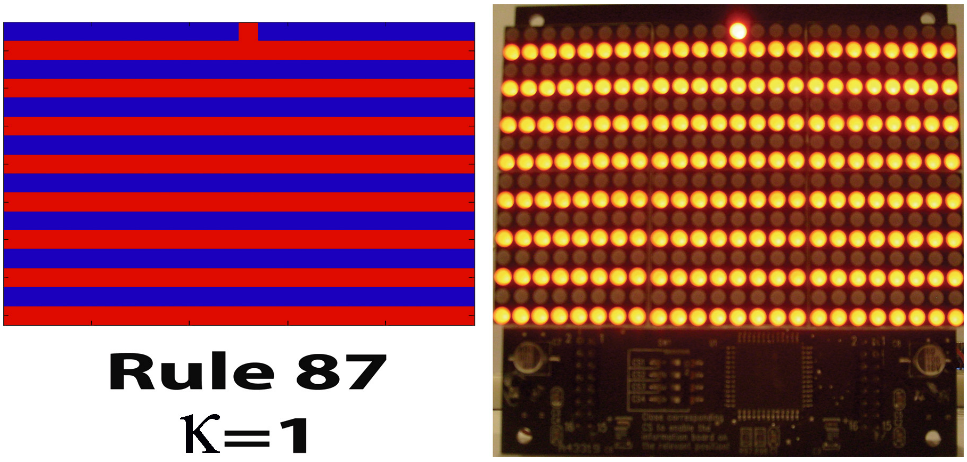

Fig. 4.6. Rule 87. Comparison between a PC-based numerical simulation (left) and the evolution of the Wolfram Machine (right) starting from the same "unit impulse" initial conditions.

The rules belonging to group 1 exhibit space-time patterns which mostly converge to a *period-1* orbit. These space-time patterns include single point attractors and period-1 Isle of Eden. An example of a rule of this group is shown in Fig. 4.11.

Group 2 includes rules characterized by the fact that almost all space-time patterns converge to a *period-2* orbit. An example of a rule of this group is shown in Fig. 4.12.

Almost all space-time patterns generated by rules of group 3 converge to a *period-3* orbit. An example of a rule of this group is shown in Fig. 4.13.

For group 4 rules, almost all space-time patterns converge to a *Bernoulli σ_τ-shift attractor*, or *Isle of Eden*, where $|\sigma| \in \{1, 2\}$ and $|\tau| \in \{1, 2\}$. An example of a rule of this group is shown in Fig. 4.14.

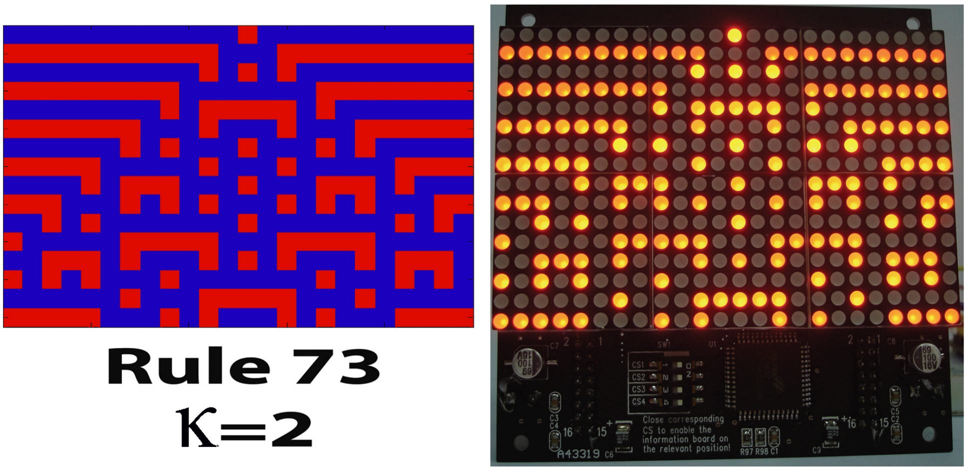

Fig. 4.7. Rule 73. Comparison between a PC-based numerical simulation (left) and the evolution of the Wolfram Machine (right) starting from the same "unit impulse" initial conditions.

Rules of groups 5 and 6 are characterized by space-time patterns which have very long transients and converge to period-T attractors with a very large period T. In these cases, the asymptotic behavior also depends on the length L and the initial configuration of the string. Group 5 includes bilateral rules, while group 6 non-bilateral ones. Two examples are reported in Figs. 4.15 and 4.21.

A complete gallery of the execution of all 256 rules is exhibited in Table 4.1.

Isles of Eden are particular behaviors exhibited by most (228 out of 256) of the rules of Wolfram cellular automata [61, 62]. They are period-n orbits which can be reached by the system, only if it starts from one of the n states visited by the orbit itself. No other initial conditions lead the cellular automaton to such Isles of Eden. The presence of Isles of

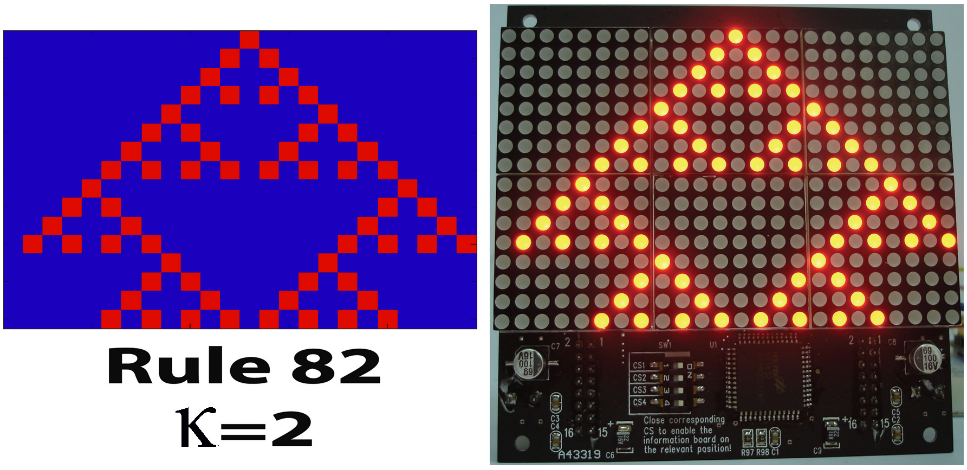

Fig. 4.8. Rule 82. Comparison between a PC-based numerical simulation (left) and the evolution of the Wolfram Machine (right) starting from the same "unit impulse" initial conditions.

Eden has been verified in three examples with different periods. Figure 4.17 refers to rule 97 exhibiting an Isle of Eden of period 3. Figure 4.18 refers to rule 14 exhibiting an Isle of Eden of period 6. Figure 4.19 refers to rule 84 exhibiting an Isle of Eden of period 8.

With the used LED matrix it is possible to obtain a bigger display by simply connecting more LED matrices in cascade to emulate and visualize bigger arrays or longer time evolutions. In Fig. 4.20 the emulation of rule 210 (having $\kappa = 2$) with two LED matrices in cascade is shown: the cellular automaton taken into consideration has therefore 48 cells.

The number of iterations can also be increased, as shown in Fig. 4.21, where rule 137 is emulated for 48 iterations. This is obtained by

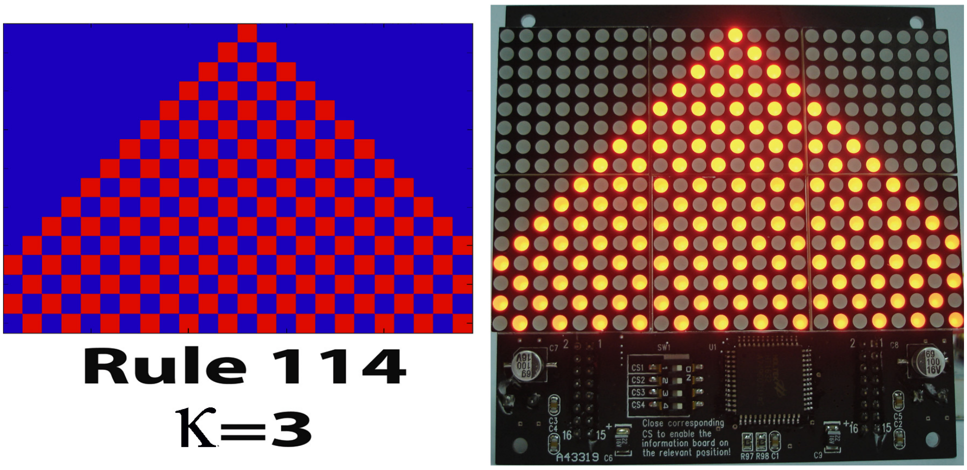

Fig. 4.9. Rule 114. Comparison between a PC-based numerical simulation (left) and the evolution of the Wolfram Machine (right) starting from the same "unit impulse" initial conditions.

repeating for three times the execution of the rule, by replacing (after the first execution) the initial state by the last row of the display.

4.5 Conclusions

A low-cost stand-alone portable system that constitutes a compact single-board implementation of a Wolfram Machine has been introduced. With this device it is possible to emulate and study all of the Wolfram's cellular automata without the need of a PC and to display their evolution on a LED matrix controlled by a microcontroller board. It is also possible to define spatio-temporal algorithms made of alternating rules and easily extending the basic configuration for emulating automata with a larger number of cells. In this sense, this system aims

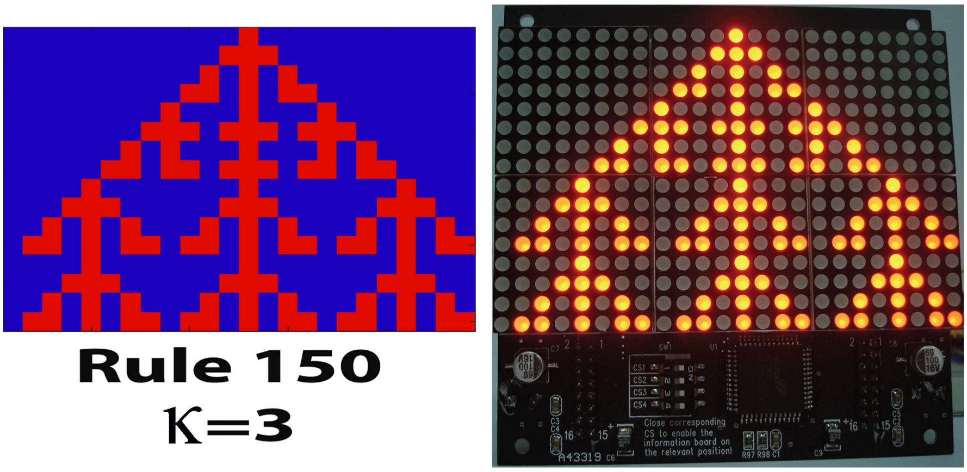

Fig. 4.10. Rule 150. Comparison between a PC-based numerical simulation (left) and the evolution of the Wolfram Machine (right) starting from the same "unit impulse" initial conditions.

to provide a new hardware tool for improving Wolfram's concept of New Kind of Science.

The Wolfram Machine introduced in this Chapter can be used both for educational aims and for developing stand-alone hardware tools for the control of LED screens. LED screens are recently gaining much interest for artistic installations and publicity [63]. An example is the OPEN WALL project in which a wall-mounted LED installation was set up in the city of Trondheim, Norway, with the aim of exploring the possibility of technology and interaction with technical people, researchers and public at large [63]. The installation has attracted a lot of interest, involving information and communication technology engineers, artists and a broad audience. By using the Wolfram Machine, an analogy with the artistic patterns, reproduced by using CNNs [64],

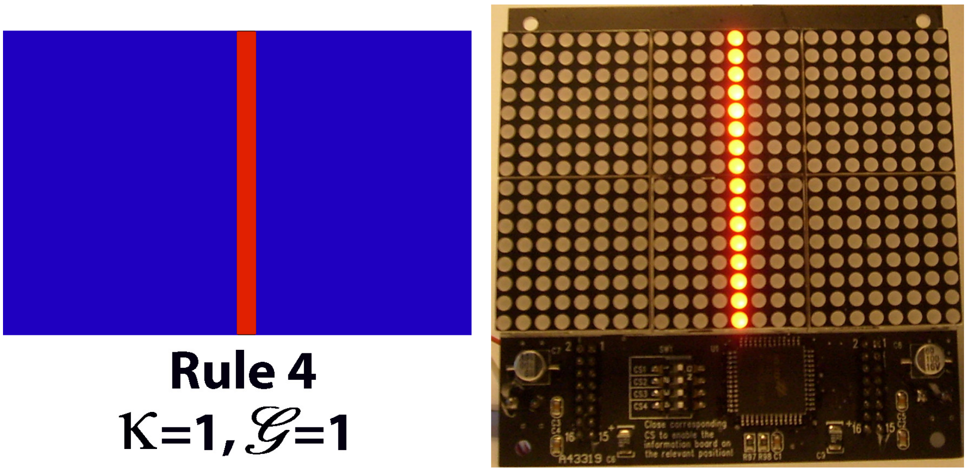

Fig. 4.11. Rule 4. Comparison between a PC-based numerical simulation (left) and the evolution of the Wolfram Machine (right) of a period-1 rule, starting from the same "unit impulse" initial conditions.

can be also established. For educational purposes the Wolfram Machine may be connected with a simple input interface, allowing students to explore the evolution of different Wolfram's rules and to experiment the effects of initial conditions in a hands-on low-cost laboratory of Wolfram's New Kind of Science. In the perspective of educational applications, it can also be useful to understand the advantages of microcontrollers to develop dedicated low-cost applications and to learn the basics on microcontroller programming with physically motivating examples.

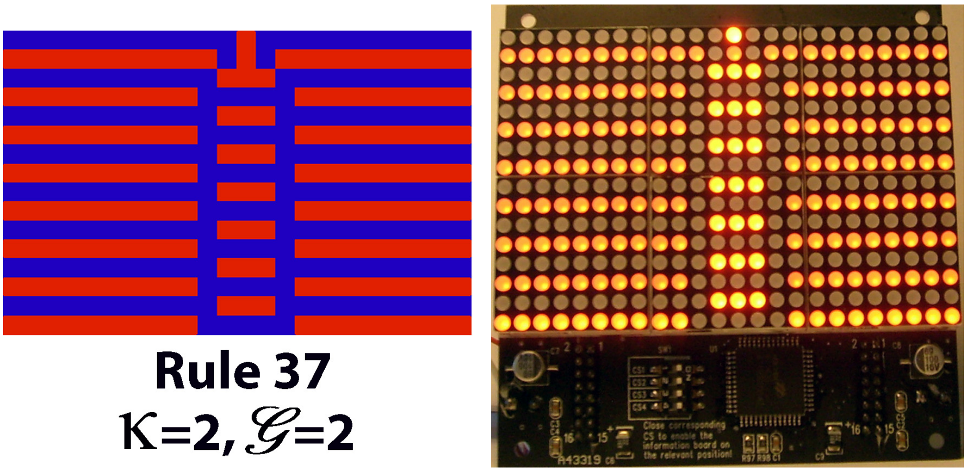

Fig. 4.12. Rule 37. Comparison between a PC-based numerical simulation (left) and the evolution of the Wolfram Machine (right) of a period-2 rule, starting from the same "unit impulse" initial conditions.

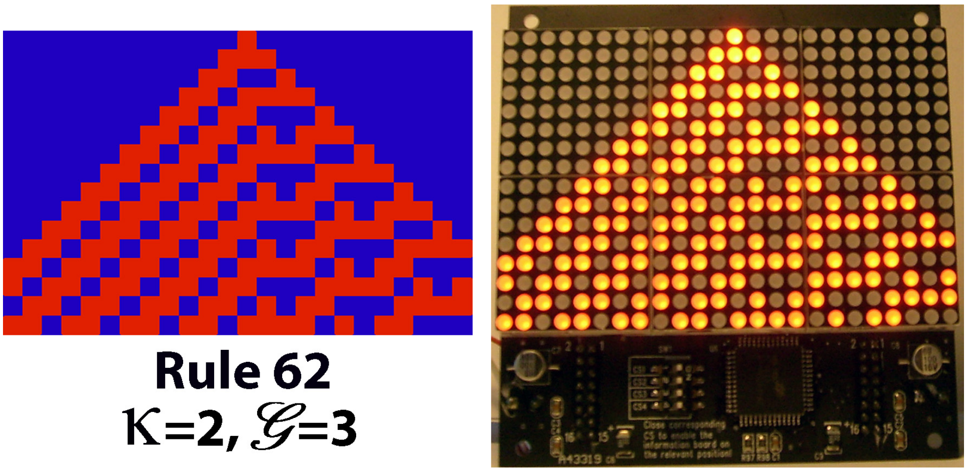

Fig. 4.13. Rule 62. Comparison between a PC-based numerical simulation (left) and the evolution of the Wolfram Machine (right) of a period-3 rule, starting from the same "unit impulse" initial conditions.

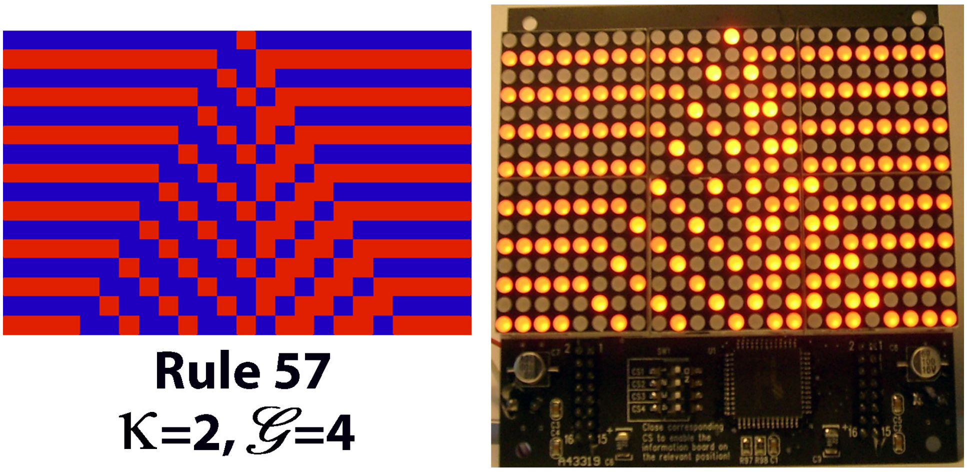

Fig. 4.14. Rule 57. Comparison between a PC-based numerical simulation (left) and the evolution of the Wolfram Machine (right) of a Bernoulli σ_τ-shift rule with $\sigma = 1$, and $\tau = 2$, starting from the same "unit impulse" initial conditions.

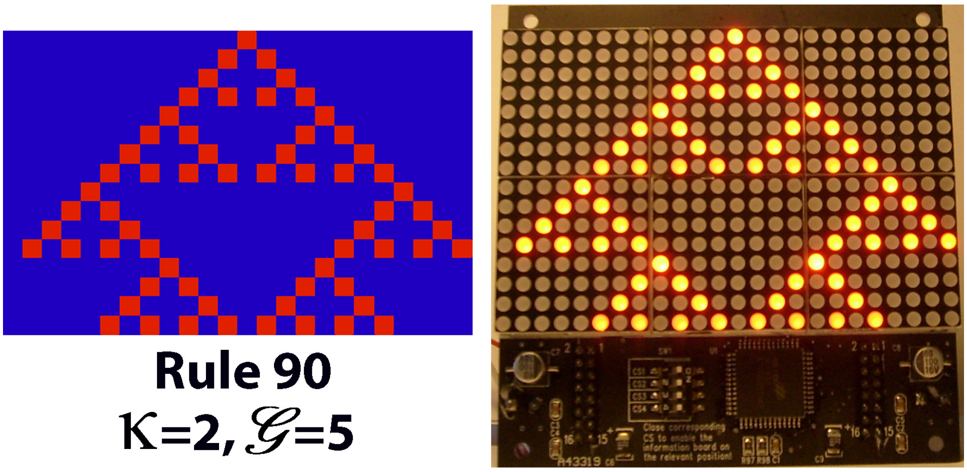

Fig. 4.15. Rule 90. Comparison between a PC-based numerical simulation (left) and the evolution of the Wolfram Machine (right) of a complex Bernoulli rule, starting from the same "unit impulse" initial conditions.

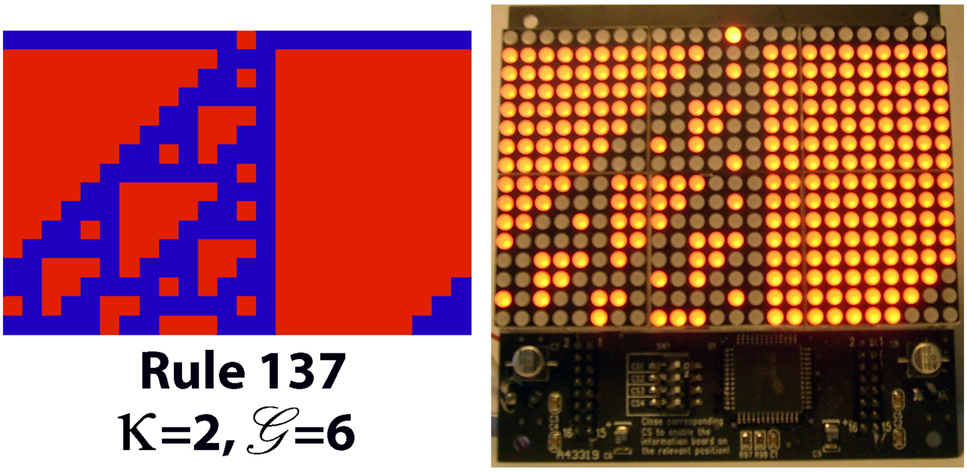

Fig. 4.16. Rule 137. Comparison between a PC-based numerical simulation (left) and the evolution of the Wolfram Machine (right) of a hyper Bernoulli rule, starting from the same "unit impulse" initial conditions.

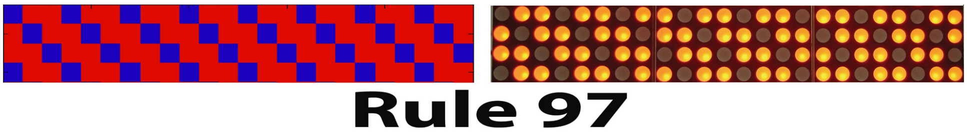

Fig. 4.17. Rule 97. Isle of Eden of period-3. Comparison between a PC-based numerical simulation (left) and the evolution of the Wolfram Machine (right).

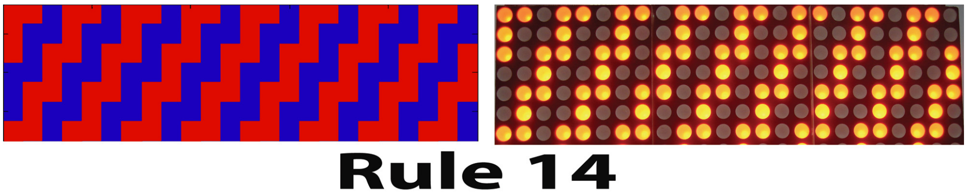

Fig. 4.18. Rule 14. Isle of Eden of period-6. Comparison between a PC-based numerical simulation (left) and the evolution of the Wolfram Machine (right).

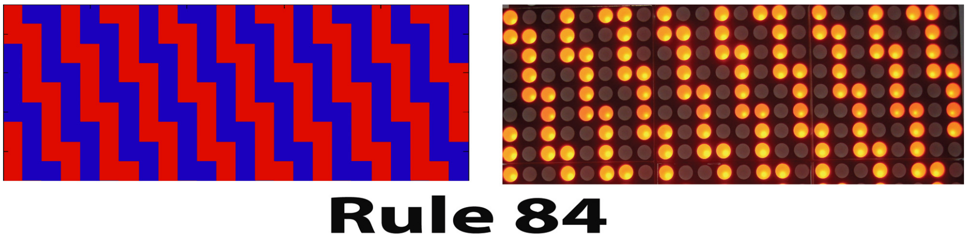

Fig. 4.19. Rule 84. Isle of Eden of period-8. Comparison between a PC-based numerical simulation (left) and the evolution of the Wolfram Machine (right).

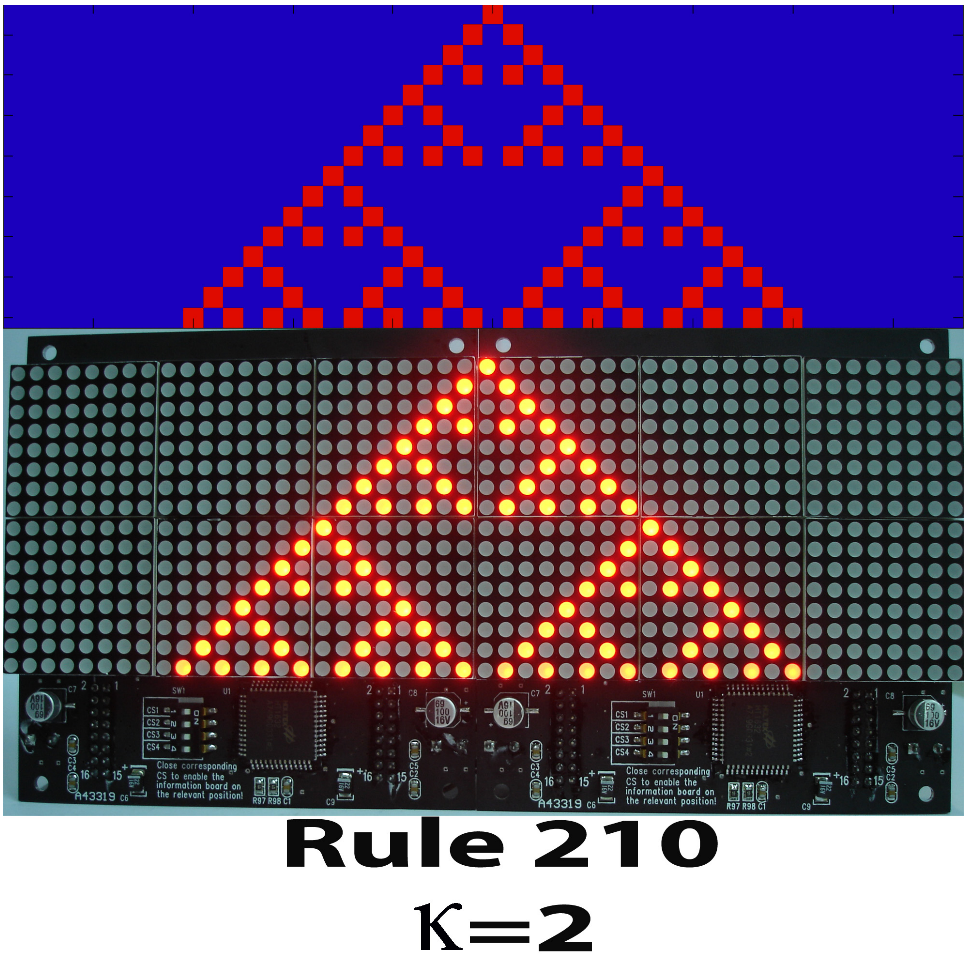

Fig. 4.20. Evolution of a cellular automaton with 48 cells obtained using two LED matrices in cascade. The rule emulated is rule 210. The comparison between a PC-based numerical simulation is also shown.

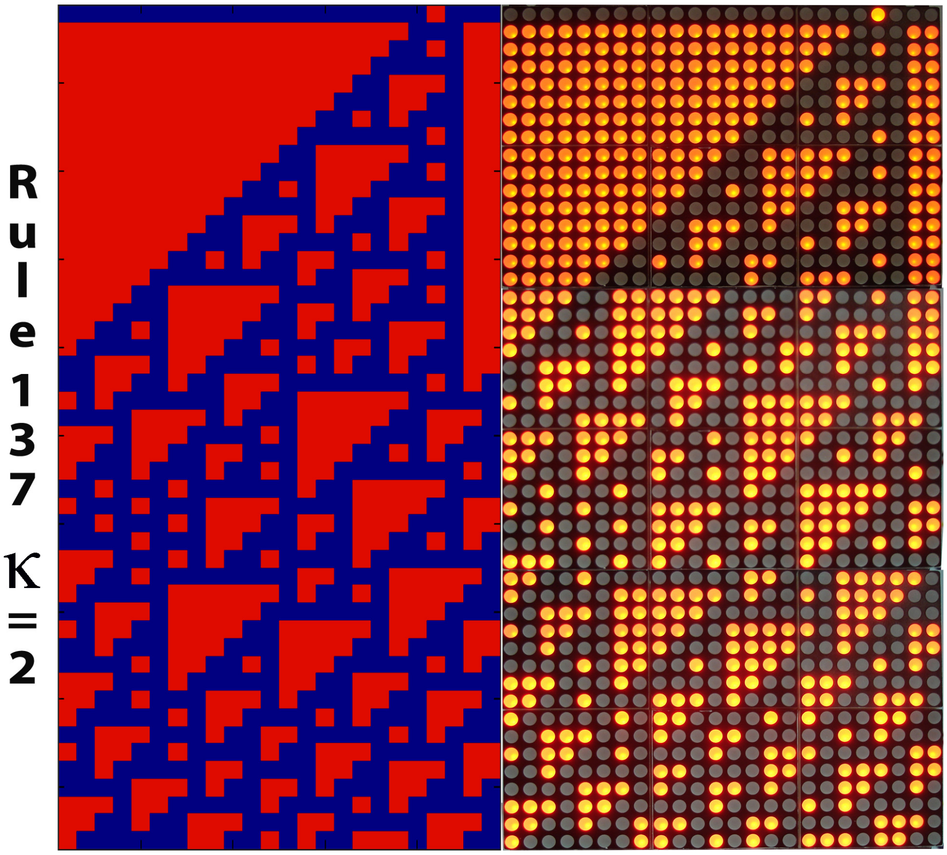

Fig. 4.21. Rule 137. This hyper Bernoulli rule is emulated for 48 iterations. A PC-based numerical simulation is shown for comparison.

Table 4.1: Rules emulated by the Wolfram Machine.

Rule 0, $\kappa=1$ $u_i^{t+1} = sgn\,[\, 0u_{i-1}^t + 0u_i^t + 0u_{i+1}^t - 1\,]$ 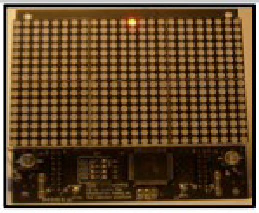	**Rule 1**, $\kappa=1$ $u_i^{t+1} = sgn\,[\, - u_{i-1}^t - u_i^t - u_{i+1}^t - 2\,]$ 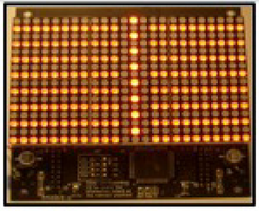	**Rule 2**, $\kappa=1$ $u_i^{t+1} = sgn\,[\, - u_{i-1}^t - u_i^t + u_{i+1}^t - 2\,]$ 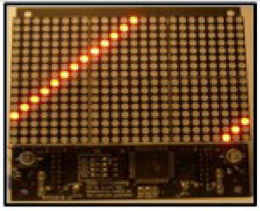
Rule 3, $\kappa=1$ $u_i^{t+1} = sgn\,[\, - u_{i-1}^t - u_i^t - 1\,]$ 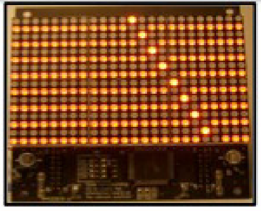	**Rule 4**, $\kappa=1$ $u_i^{t+1} = sgn\,[\, - u_{i-1}^t + u_i^t - u_{i+1}^t - 2\,]$ 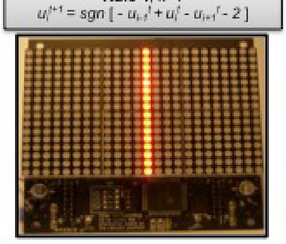	**Rule 5**, $\kappa=1$ $u_i^{t+1} = sgn\,[\, - u_{i-1}^t - u_{i+1}^t - 1\,]$ 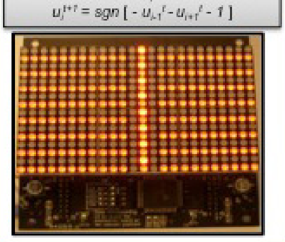
Rule 6, $\kappa=2$ $u_i^{t+1} = sgn\,[\, 1 - \|2u_{i-1}^t - u_i^t - u_{i+1}^t + 2\|\,]$ 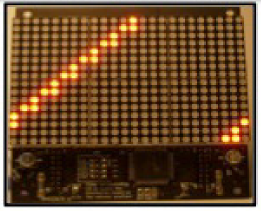	**Rule 7**, $\kappa=1$ $u_i^{t+1} = sgn\,[\, - 2u_{i-1}^t - u_i^t - u_{i+1}^t - 1\,]$ 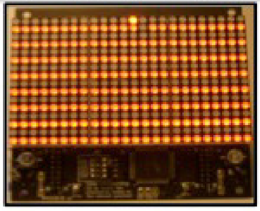	**Rule 8**, $\kappa=1$ $u_i^{t+1} = sgn\,[\, - u_{i-1}^t + u_i^t + u_{i+1}^t - 2\,]$ 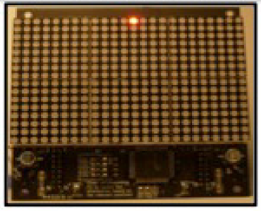
Rule 9, $\kappa=2$ $u_i^{t+1} = sgn\,[\, 1 - \|2u_{i-1}^t + u_i^t - u_{i+1}^t + 2\|\,]$ 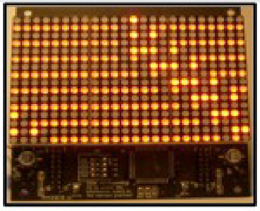	**Rule 10**, $\kappa=1$ $u_i^{t+1} = sgn\,[\, - u_{i-1}^t + u_{i+1}^t - 1\,]$ 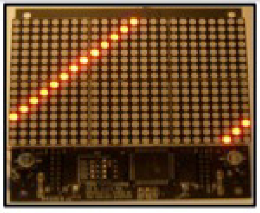	**Rule 11**, $\kappa=1$ $u_i^{t+1} = sgn\,[\, - 2u_{i-1}^t - u_i^t + u_{i+1}^t - 1\,]$ 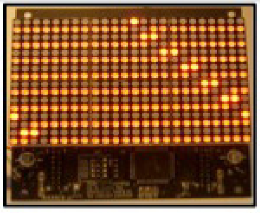

Table 4.1. *(Continued)*

Rule 12, $\kappa=1$ $u_i^{t+1} = sgn\,[\,-u_{i-1}^t + u_i^t - 1\,]$ 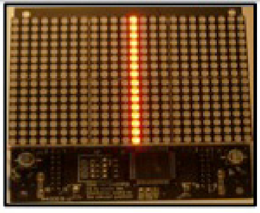	**Rule 13**, $\kappa=1$ $u_i^{t+1} = sgn\,[\,-2u_{i-1}^t + u_i^t - u_{i+1}^t - 1\,]$ 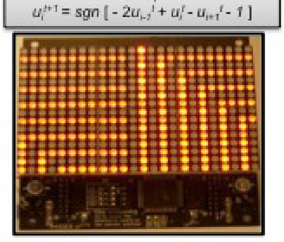	**Rule 14**, $\kappa=1$ $u_i^{t+1} = sgn\,[\,-2u_{i-1}^t + u_i^t + u_{i+1}^t - 1\,]$ 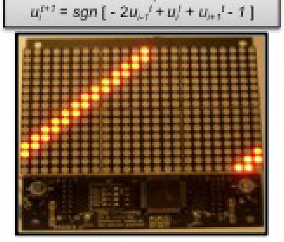
Rule 15, $\kappa=1$ $u_i^{t+1} = sgn\,[\,-u_{i-1}^t]$ 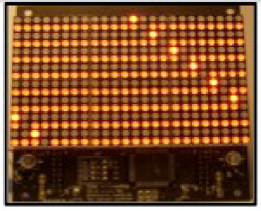	**Rule 16**, $\kappa=1$ $u_i^{t+1} = sgn\,[\,u_{i-1}^t - u_i^t - u_{i+1}^t - 2\,]$ 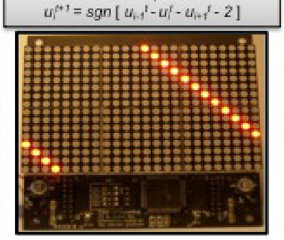	**Rule 17**, $\kappa=1$ $u_i^{t+1} = sgn\,[\,-u_i^t - u_{i+1}^t - 1\,]$ 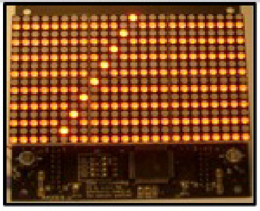
Rule 18, $\kappa=2$ $u_i^{t+1} = sgn\,[\,1 - \lvert u_{i-1}^t + 2u_i^t + u_{i+1}^t + 2\rvert\,]$ 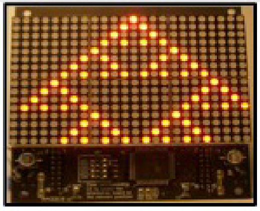	**Rule 19**, $\kappa=1$ $u_i^{t+1} = sgn\,[\,-u_{i-1}^t - 2u_i^t - u_{i+1}^t - 1\,]$ 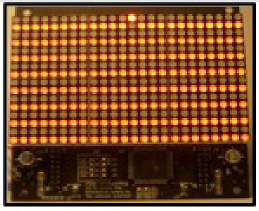	**Rule 20**, $\kappa=2$ $u_i^{t+1} = sgn\,[\,1 - \lvert -2u_{i-1}^t - 2u_i^t + u_{i+1}^t + 1\rvert\,]$ 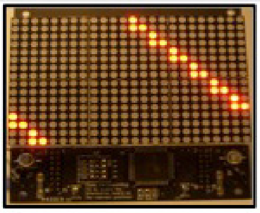
Rule 21, $\kappa=1$ $u_i^{t+1} = sgn\,[\,-u_{i-1}^t - u_i^t - 2u_{i+1}^t - 1\,]$ 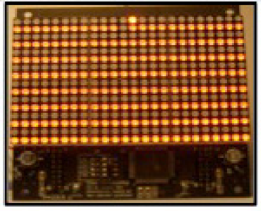	**Rule 22**, $\kappa=2$ $u_i^{t+1} = sgn\,[\,1 - \lvert u_{i-1}^t + u_i^t + u_{i+1}^t + 1\rvert\,]$ 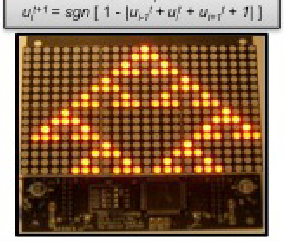	**Rule 23**, $\kappa=1$ $u_i^{t+1} = sgn\,[\,-u_{i-1}^t - u_i^t - u_{i+1}^t]$ 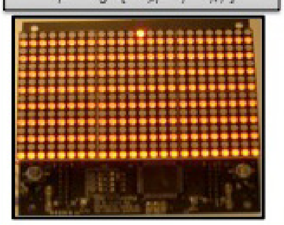

Table 4.1. *(Continued)*

Rule 24, κ=2 $u_i^{t+1} = sgn\,[\,-2 + \lvert u_{i-1}^t - u_i^t - u_{i+1}^t\rvert\,]$ 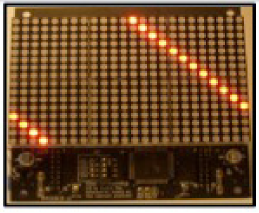	**Rule 25**, κ=2 $u_i^{t+1} = sgn\,[\,3 - \lvert u_{i-1}^t - 2u_i^t + 4u_{i+1}^t + 1\rvert\,]$ 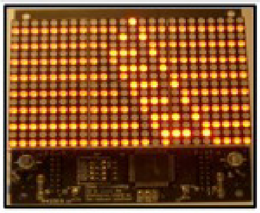	**Rule 26**, κ=2 $u_i^{t+1} = sgn\,[\,3 - \lvert 2u_{i-1}^t - u_i^t + 4u_{i+1}^t - 1\rvert\,]$ 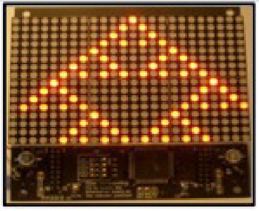
Rule 27, κ=3 $u_i^{t+1} = sgn[2 - \lvert 3 + \lvert 2u_{i-1}^t - 4u_i^t + u_{i+1}^t - 3$ 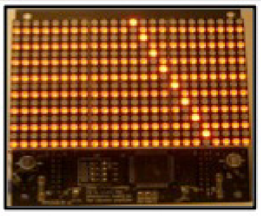	**Rule 28**, κ=2 $u_i^{t+1} = sgn\,[\,3 - \lvert 2u_{i-1}^t + 4u_i^t - u_{i+1}^t - 1\rvert\,]$ 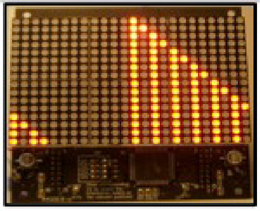	**Rule 29**, κ=3 $u_i^{t+1} = sgn[2 - \lvert 3 - \lvert 2u_{i-1}^t + u_i^t - 4u_{i+1}^t - 3$ 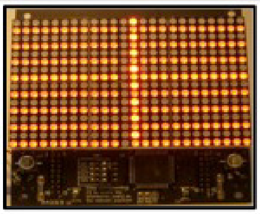
Rule 30, κ=2 $u_i^{t+1} = sgn\,[\,2 - \lvert -2u_{i-1}^t - u_i^t - u_{i+1}^t - 1\rvert\,]$ 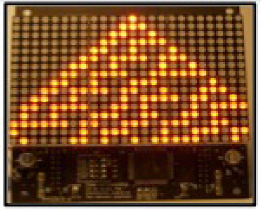	**Rule 31**, κ=1 $u_i^{t+1} = sgn\,[\,-3\,u_{i-1}^t - u_i^t - u_{i+1}^t + 2\,]$ 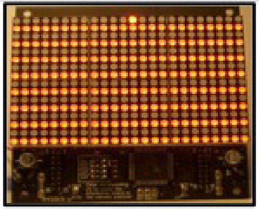	**Rule 32**, κ=1 $u_i^{t+1} = sgn\,[\,u_{i-1}^t - u_i^t + u_{i+1}^t - 2\,]$ 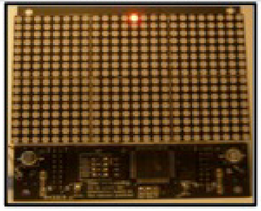
Rule 33, κ=2 $u_i^{t+1} = sgn\,[\,1 - \lvert -2u_{i-1}^t + u_i^t + 2u_{i+1}^t + 1\rvert\,]$ 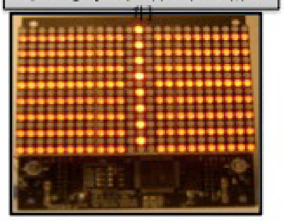	**Rule 34**, κ=1 $u_i^{t+1} = sgn\,[\,-u_i^t + u_{i+1}^t - 1\,]$ 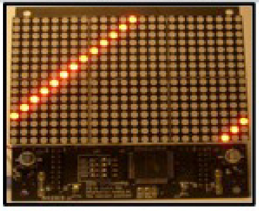	**Rule 35**, κ=1 $u_i^{t+1} = sgn\,[\,-u_{i-1}^t - 2u_i^t + u_{i+1}^t - 1\,]$ 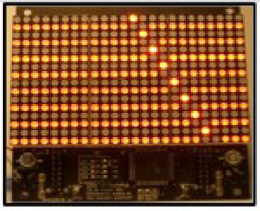

Table 4.1. *(Continued)*

Rule 36, $\kappa=2$ $u_i^{t+1} = sgn\,[\,-2 + \vert u_{i-1}^t - u_i^t + u_{i+1}^t\vert\,]$ 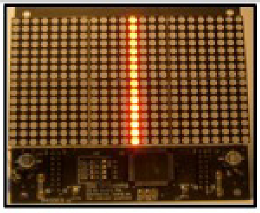	**Rule 37**, $\kappa=2$ $u_i^{t+1} = sgn\,[\,3 - \vert 2u_{i-1}^t - u_i^t - 4u_{i+1}^t - 1\vert\,]$ 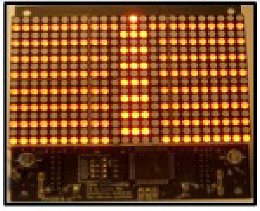	**Rule 38**, $\kappa=2$ $u_i^{t+1} = sgn\,[\,3 - \vert -u_{i-1}^t + 2u_i^t + 4u_{i+1}^t - 1\vert\,]$ 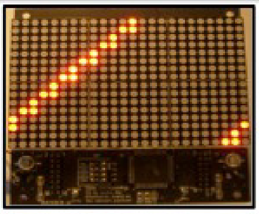
Rule 39, $\kappa=3$ $u_i^{t+1} = sgn[2-\vert -3+\vert -4u_{i-1}^t - 3u_i^t + u_{i+1}^t - 3\vert\vert]$ 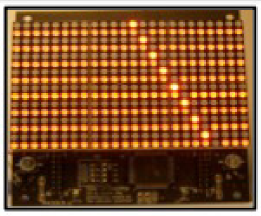	**Rule 40**, $\kappa=2$ $u_i^{t+1} = sgn\,[\,1 - \vert -2u_{i-1}^t - 2u_i^t + u_{i+1}^t - 1\vert\,]$ 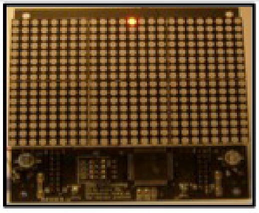	**Rule 41**, $\kappa=2$ $u_i^{t+1} = sgn\,[\,1 - \vert -u_{i-1}^t - u_i^t + u_{i+1}^t - 1\vert\,]$ 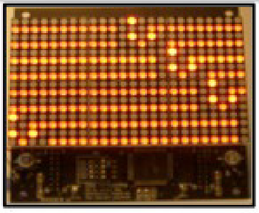
Rule 42, $\kappa=1$ $u_i^{t+1} = sgn\,[\,-u_{i-1}^t - u_i^t + 2u_{i+1}^t - 1\,]$ 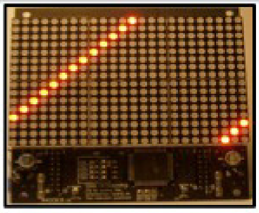	**Rule 43**, $\kappa=1$ $u_i^{t+1} = sgn\,[\,-u_{i-1}^t - u_i^t + u_{i+1}^t\,]$ 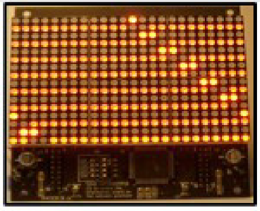	**Rule 44**, $\kappa=2$ $u_i^{t+1} = sgn\,[\,3 - \vert -4u_{i-1}^t - 2u_i^t + u_{i+1}^t - 1\vert\,]$ 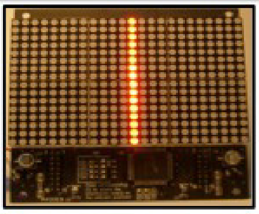
Rule 45, $\kappa=2$ $u_i^{t+1} = sgn\,[\,2 - \vert -2u_{i-1}^t - u_i^t + u_{i+1}^t - 1\vert\,]$ 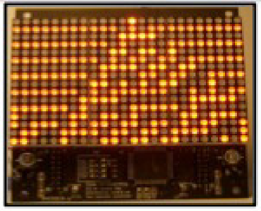	**Rule 46**, $\kappa=3$ $u_i^{t+1} = sgn\,[\,2 - \vert 3 - \vert u_{i-1}^t - 2u_i^t - 3u_{i+1}^t + 4\vert\vert\,]$ 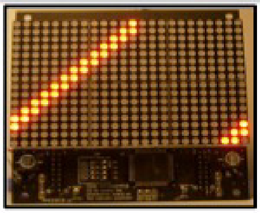	**Rule 47**, $\kappa=1$ $u_i^{t+1} = sgn\,[\,-3u_{i-1}^t - u_i^t + u_{i+1}^t + 2\,]$ 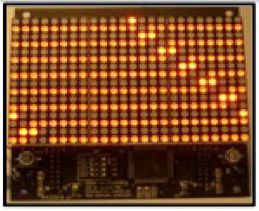

Table 4.1. *(Continued)*

Rule 48, $\kappa=1$ $u_i^{t+1} = sgn\,[\,u_{i-1}^t - u_i^t - 1\,]$ 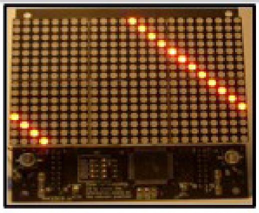	**Rule 49**, $\kappa=1$ $u_i^{t+1} = sgn\,[\,u_{i-1}^t - 2u_i^t - u_{i+1}^t - 1\,]$ 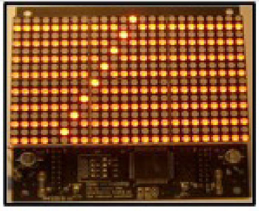	**Rule 50**, $\kappa=1$ $u_i^{t+1} = sgn\,[\,u_{i-1}^t - 2u_i^t + u_{i+1}^t - 1\,]$ 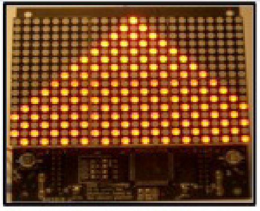
Rule 51, $\kappa=1$ $u_i^{t+1} = sgn\,[\,-u_i^t\,]$ 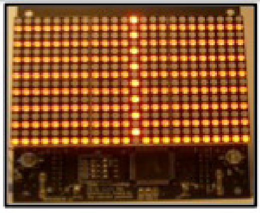	**Rule 52**, $\kappa=2$ $u_i^{t+1} = sgn\,[\,3 - \lvert -2u_{i-1}^t - 4u_i^t - u_{i+1}^t - 1 \rvert\,]$ 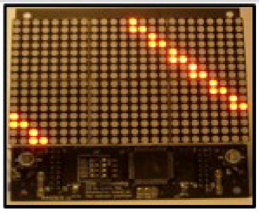	**Rule 53**, $\kappa=3$ $u_i^{t+1} = sgn[2 - \lvert 3 + \lvert 4u_{i-1}^t + u_i^t - 3u_{i+1}^t - 2 \rvert \rvert]$ 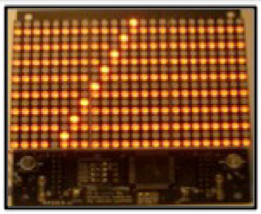
Rule 54, $\kappa=2$ $u_i^{t+1} = sgn\,[\,2 - \lvert -u_{i-1}^t - 2u_i^t - u_{i+1}^t - 1 \rvert\,]$ 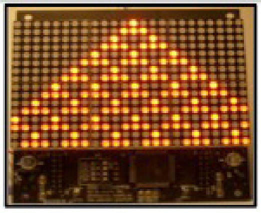	**Rule 55**, $\kappa=1$ $u_i^{t+1} = sgn\,[\,-u_{i-1}^t - 3u_i^t - u_{i+1}^t + 2\,]$ 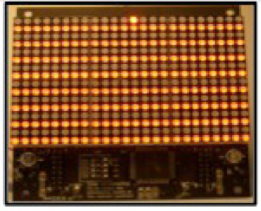	**Rule 56**, $\kappa=2$ $u_i^{t+1} = sgn\,[\,3 - \lvert 2u_{i-1}^t + 4u_i^t - u_{i+1}^t + 1 \rvert\,]$ 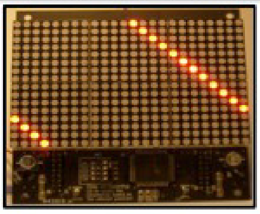
Rule 57, $\kappa=2$ $u_i^{t+1} = sgn\,[\,2 - \lvert -u_{i-1}^t - 2u_i^t + u_{i+1}^t - 1 \rvert\,]$ 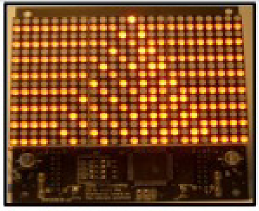	**Rule 58**, $\kappa=3$ $u_i^{t+1} = sgn[2 - \lvert 3 - \lvert u_{i-1}^t + 2u_i^t - 4u_{i+1}^t + 3 \rvert \rvert]$ 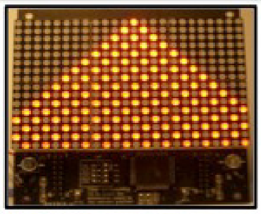	**Rule 59**, $\kappa=1$ $u_i^{t+1} = sgn\,[\,-u_{i-1}^t - 3u_i^t + u_{i+1}^t + 2\,]$ 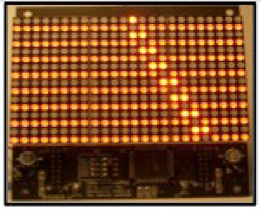

Table 4.1. *(Continued)*

Rule 60, $\kappa=2$ $u_i^{t+1} = sgn\,[\,1 - \lvert u_{i-1}^t - u_i^t \rvert\,]$ 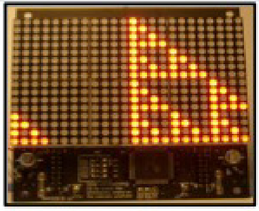	**Rule 61**, $\kappa=2$ $u_i^{t+1} = sgn\,[\,3 - \lvert -2u_{i-1}^t - 2u_i^t + u_{i+1}^t - 1 \rvert\,]$ 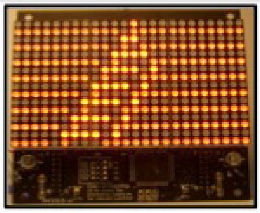	**Rule 62**, $\kappa=2$ $u_i^{t+1} = sgn\,[\,3 - \lvert -2u_{i-1}^t - 2u_i^t - u_{i+1}^t - 1 \rvert\,]$ 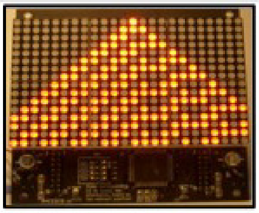
Rule 63, $\kappa=1$ $u_i^{t+1} = sgn[6 - \lvert 3 - \lvert 5u_{i-1}^t + 8u_i^t + 3u_{i+1}^t + 5$ 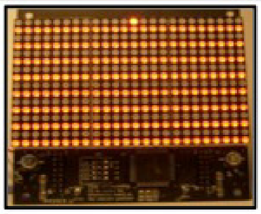	**Rule 64**, $\kappa=1$ $u_i^{t+1} = sgn\,[\,u_{i-1}^t + u_i^t - u_{i+1}^t - 2\,]$ 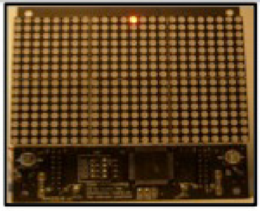	**Rule 65**, $\kappa=2$ $u_i^{t+1} = sgn\,[\,1 - \lvert 2u_{i-1}^t - 2u_i^t + u_{i+1}^t + 1 \rvert\,]$ 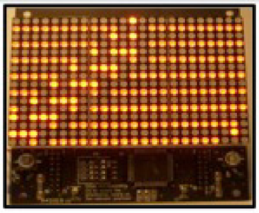
Rule 66, $\kappa=2$ $u_i^{t+1} = sgn\,[\,-2 + \lvert -u_{i-1}^t - u_i^t + u_{i+1}^t \rvert\,]$ 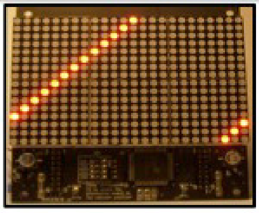	**Rule 67**, $\kappa=2$ $u_i^{t+1} = sgn\,[\,3 - \lvert 2u_{i-1}^t - 4u_i^t - u_{i+1}^t - 1 \rvert\,]$ 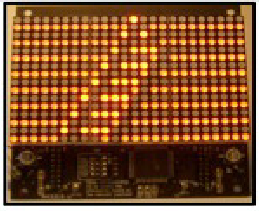	**Rule 68**, $\kappa=1$ $u_i^{t+1} = sgn\,[\,u_i^t - u_{i+1}^t - 1\,]$ 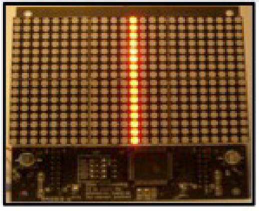
Rule 69, $\kappa=1$ $u_i^{t+1} = sgn\,[\,-u_{i-1}^t + u_i^t - 2u_{i+1}^t - 1\,]$ 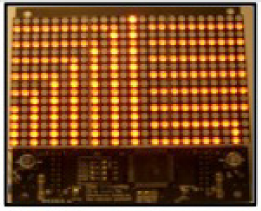	**Rule 70**, $\kappa=2$ $u_i^{t+1} = sgn\,[\,3 - \lvert -u_{i-1}^t + 4u_i^t + 2u_{i+1}^t - 1 \rvert\,]$ 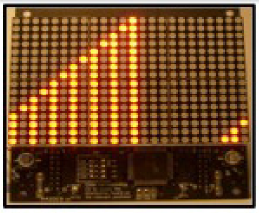	**Rule 71**, $\kappa=3$ $u_i^{t+1} = sgn[2 - \lvert 3 - \lvert 4u_{i-1}^t + u_i^t - 2u_{i+1}^t - 3$ 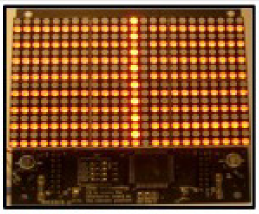

Table 4.1. *(Continued)*

Rule 72, $\kappa=2$ $u_i^{t+1} = sgn\,[\,1 - \lvert -2u_{i-1}^t + u_i^t - 2u_{i+1}^t - 1\rvert\,]$ 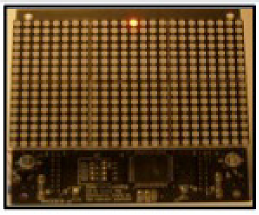	**Rule 73**, $\kappa=2$ $u_i^{t+1} = sgn\,[\,1 - \lvert u_{i-1}^t - u_i^t + u_{i+1}^t + 1\rvert\,]$ 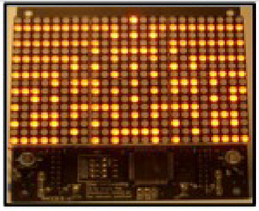	**Rule 74**, $\kappa=2$ $u_i^{t+1} = sgn\,[\,3 - \lvert 2u_{i-1}^t + u_i^t + 4u_{i+1}^t - 1\rvert\,]$ 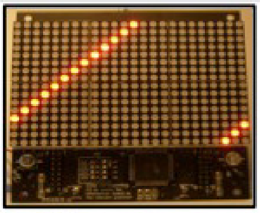
Rule 75, $\kappa=2$ $u_i^{t+1} = sgn\,[\,2 - \lvert 2u_{i-1}^t - u_i^t + u_{i+1}^t + 1\rvert\,]$ 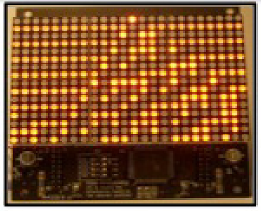	**Rule 76**, $\kappa=1$ $u_i^{t+1} = sgn\,[\,-u_{i-1}^t + 2u_i^t - u_{i+1}^t - 1\,]$ 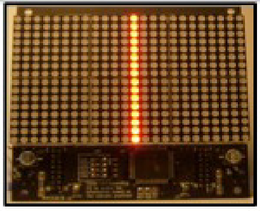	**Rule 77**, $\kappa=1$ $u_i^{t+1} = sgn\,[\,-u_{i-1}^t + u_i^t - u_{i+1}^t\,]$ 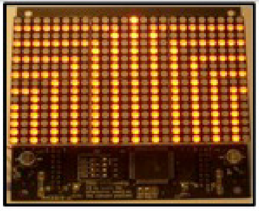
Rule 78, $\kappa=3$ $u_i^{t+1} = sgn[2 - \lvert 3 + \lvert 3u_{i-1}^t - u_i^t + 2u_{i+1}^t + 4\rvert\rvert]$ 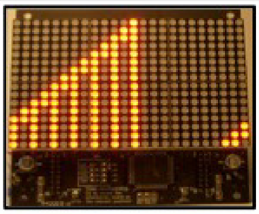	**Rule 79**, $\kappa=1$ $u_i^{t+1} = sgn\,[\,-3u_{i-1}^t + u_i^t - u_{i+1}^t + 2\,]$ 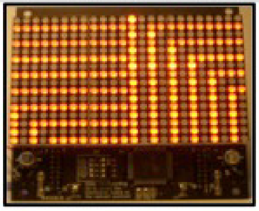	**Rule 80**, $\kappa=1$ $u_i^{t+1} = sgn\,[\,u_{i-1}^t - u_{i+1}^t - 1\,]$ 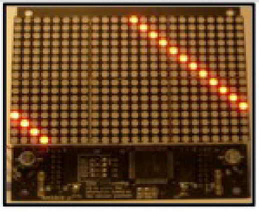
Rule 81, $\kappa=1$ $u_i^{t+1} = sgn\,[\,u_{i-1}^t - u_i^t - 2u_{i+1}^t - 1\,]$ 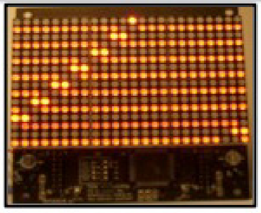	**Rule 82**, $\kappa=2$ $u_i^{t+1} = sgn\,[\,3 - \lvert -2u_{i-1}^t - u_i^t - 4u_{i+1}^t - 1\rvert\,]$ 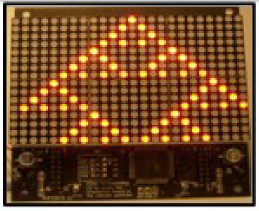	**Rule 83**, $\kappa=3$ $u_i^{t+1} = sgn[2 - \lvert 3 - \lvert 3u_{i-1}^t + 4u_i^t - 3u_{i+1}^t + 1\rvert\rvert]$ 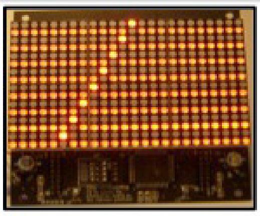

Table 4.1. *(Continued)*

Rule 84, $\kappa=1$ $u_i^{t+1} = sgn\,[\,u_{i-1}^t + u_i^t - 2u_{i+1}^t - 1\,]$ 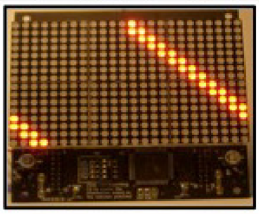	**Rule 85**, $\kappa=1$ $u_i^{t+1} = sgn\,[\,-u_{i+1}^t\,]$ 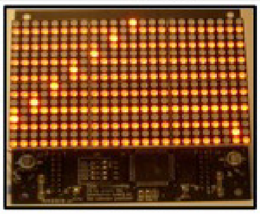	**Rule 86**, $\kappa=2$ $u_i^{t+1} = sgn\,[\,2 - \lvert -u_{i-1}^t - u_i^t - 2u_{i+1}^t - 1\rvert\,]$ 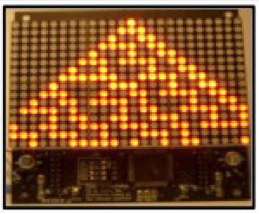
Rule 87, $\kappa=1$ $u_i^{t+1} = sgn\,[\,-u_{i-1}^t - u_i^t - 3u_{i+1}^t + 2\,]$ 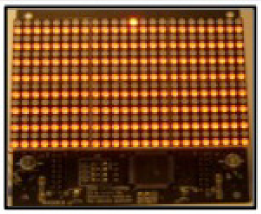	**Rule 88**, $\kappa=2$ $u_i^{t+1} = sgn\,[\,3 - \lvert -4u_{i-1}^t - u_i^t - 2u_{i+1}^t + 1\rvert\,]$ 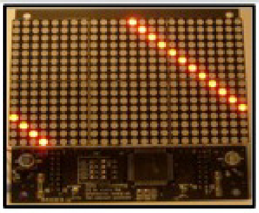	**Rule 89**, $\kappa=2$ $u_i^{t+1} = sgn\,[\,2 - \lvert u_{i-1}^t - u_i^t + 2u_{i+1}^t + 1\rvert\,]$ 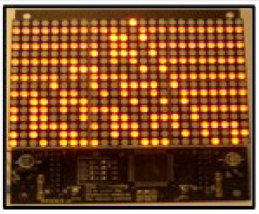
Rule 90, $\kappa=2$ $u_i^{t+1} = sgn\,[\,1 - \lvert u_{i-1}^t + u_{i+1}^t\rvert\,]$ 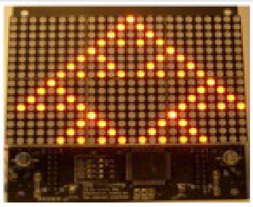	**Rule 91**, $\kappa=2$ $u_i^{t+1} = sgn\,[\,3 - \lvert -2u_{i-1}^t + u_i^t - 2u_{i+1}^t - 1\rvert\,]$ 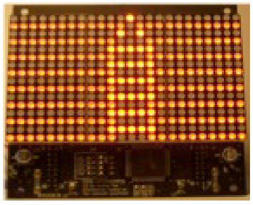	**Rule 92**, $\kappa=3$ $u_i^{t+1} = sgn[2 - \lvert 3 - \lvert u_{i-1}^t - 2u_i^t + 4u_{i+1}^t + 3\rvert\rvert]$ 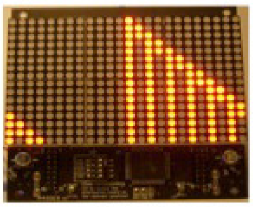
Rule 93, $\kappa=1$ $u_i^{t+1} = sgn\,[\,-u_{i-1}^t + u_i^t - 3u_{i+1}^t + 2\,]$ 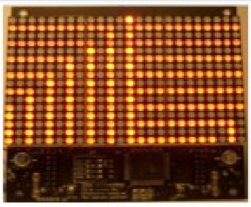	**Rule 94**, $\kappa=2$ $u_i^{t+1} = sgn\,[\,3 - \lvert -2u_{i-1}^t - u_i^t - 2u_{i+1}^t - 1\rvert\,]$ 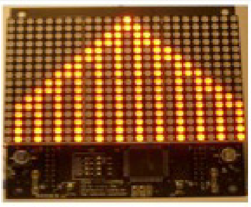	**Rule 95**, $\kappa=1$ $u_i^{t+1} = sgn\,[\,-u_{i-1}^t - u_{i+1}^t + 1\,]$ 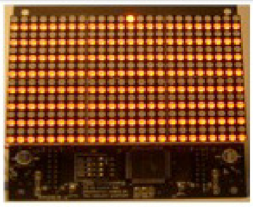

Table 4.1. *(Continued)*

Rule 96, κ=2 $u_i^{t+1} = sgn\,[\,1 - \lvert -2u_{i-1}^t + u_i^t + u_{i+1}^t + 2\rvert\,]$ 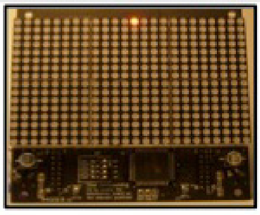	**Rule 97**, κ=2 $u_i^{t+1} = sgn\,[\,1 - \lvert -u_{i-1}^t + u_i^t + u_{i+1}^t + 1\rvert\,]$ 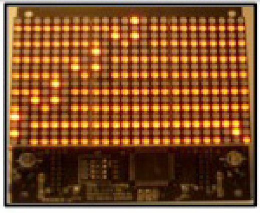	**Rule 98**, κ=2 $u_i^{t+1} = sgn\,[\,3 - \lvert -u_{i-1}^t - 2u_i^t - 4u_{i+1}^t + 1\rvert\,]$ 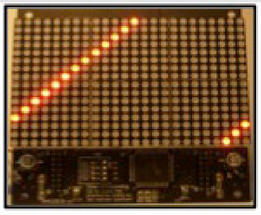
Rule 99, κ=2 $u_i^{t+1} = sgn\,[\,2 - \lvert -u_{i-1}^t + 2u_i^t + u_{i+1}^t + 1\rvert\,]$ 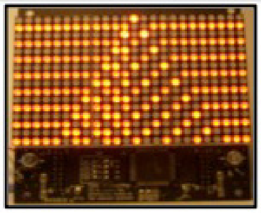	**Rule 100**, κ=2 $u_i^{t+1} = sgn\,[\,3 - \lvert -u_{i-1}^t - 4u_i^t - 2u_{i+1}^t + 1\rvert\,]$ 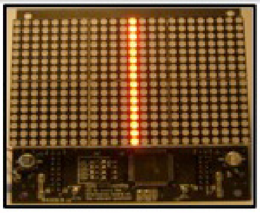	**Rule 101**, κ=2 $u_i^{t+1} = sgn[3 - \lvert 6 - \lvert 2u_{i-1}^t - 3u_i^t + 3u_{i+1}^t - 1\rvert\rvert]$ 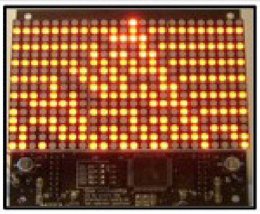
Rule 102, κ=2 $u_i^{t+1} = sgn\,[\,1 - \lvert u_i^t + u_{i+1}^t\rvert\,]$ 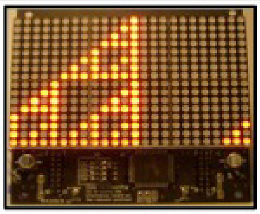	**Rule 103**, κ=2 $u_i^{t+1} = sgn\,[\,3 - \lvert -u_{i-1}^t + 2u_i^t + 2u_{i+1}^t + 1\rvert\,]$ 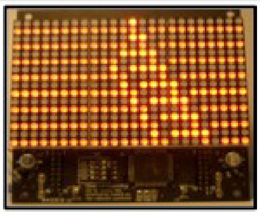	**Rule 104**, κ=2 $u_i^{t+1} = sgn\,[\,1 - \lvert -u_{i-1}^t - u_i^t - u_{i+1}^t + 1\rvert\,]$ 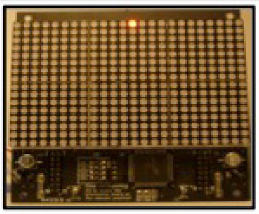
Rule 105, κ=3 $u_i^{t+1} = sgn\,[\,1 - \lvert 2 - \lvert -u_{i-1}^t + u_i^t - u_{i+1}^t + 1\rvert\rvert\,]$ 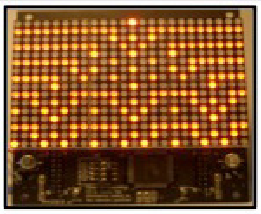	**Rule 106**, κ=2 $u_i^{t+1} = sgn\,[\,2 - \lvert u_{i-1}^t + u_i^t + 2u_{i+1}^t - 1\rvert\,]$ 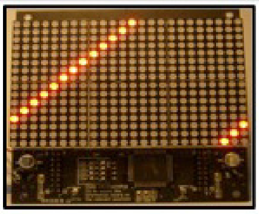	**Rule 107**, κ=2 $u_i^{t+1} = sgn\,[\,-1 + \lvert -u_{i-1}^t - u_i^t + u_{i+1}^t + 1\rvert\,]$ 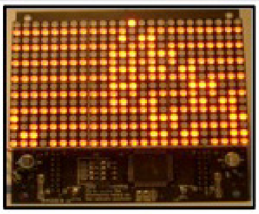

Table 4.1. *(Continued)*

Rule 108, κ=2 $u_i^{t+1} = sgn\,[\,2 - |-u_{i-1}^t - 2u_i^t - u_{i+1}^t + 1|\,]$ 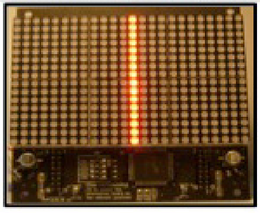	**Rule 109**, κ=2 $u_i^{t+1} = sgn\,[\,-1 + |-u_{i-1}^t + u_i^t - u_{i+1}^t + 1|\,]$ 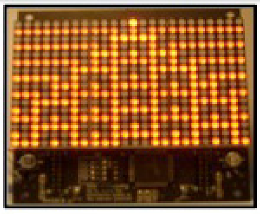	**Rule 110**, κ=2 $u_i^{t+1} = sgn\,[\,-2 + |u_{i-1}^t + 2u_i^t - 3u_{i+1}^t - 1|\,]$ 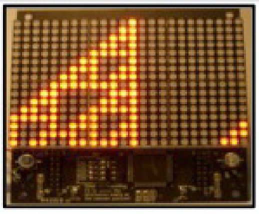
Rule 111, κ=2 $u_i^{t+1} = sgn\,[\,-1 + |u_{i-1}^t - 2u_i^t + 2u_{i+1}^t - 1|\,]$ 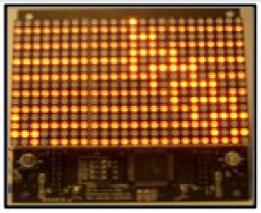	**Rule 112**, κ=1 $u_i^{t+1} = sgn\,[\,2u_{i-1}^t - u_i^t - u_{i+1}^t - 1\,]$ 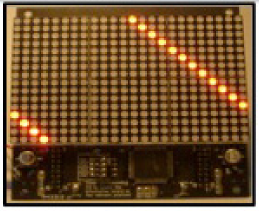	**Rule 113**, κ=1 $u_i^{t+1} = sgn\,[\,u_{i-1}^t - u_i^t - u_{i+1}^t\,]$ 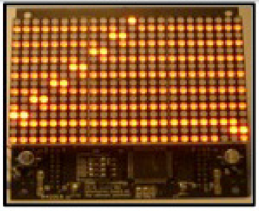
Rule 114, κ=3 $u_i^{t+1} = sgn(2-|3-|4u_{i-1}^t + 2u_i^t - u_{i+1}^t + 3||)$ 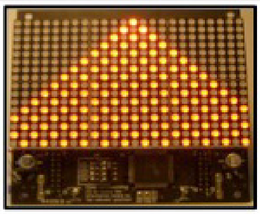	**Rule 115**, κ=1 $u_i^{t+1} = sgn\,[\,u_{i-1}^t - 3u_i^t - u_{i+1}^t + 2\,]$ 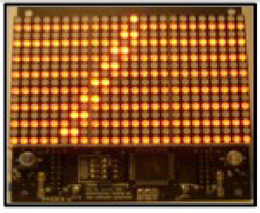	**Rule 116**, κ=3 $u_i^{t+1} = sgn(2-|3-|4u_{i-1}^t - u_i^t + 2u_{i+1}^t + 3||)$ 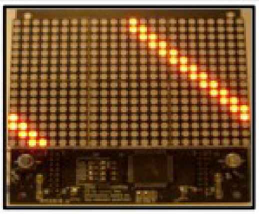
Rule 117, κ=3 $u_i^{t+1} = sgn\,[\,u_{i-1}^t - u_i^t - 3u_{i+1}^t + 2\,]$ 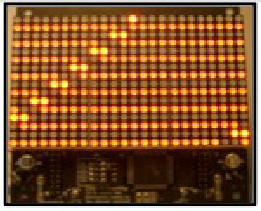	**Rule 118**, κ=2 $u_i^{t+1} = sgn\,[\,3 - |-u_{i-1}^t - 2u_i^t - 2u_{i+1}^t - 1|\,]$ 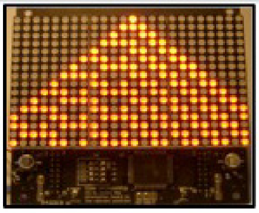	**Rule 119**, κ=1 $u_i^{t+1} = sgn\,[\,-u_i^t - u_{i+1}^t + 1\,]$ 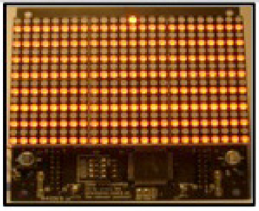

Table 4.1. *(Continued)*

Rule 120, κ=2 $u_i^{t+1} = sgn\,[\,2 - \lvert 2u_{i-1}^t + u_i^t + u_{i+1}^t - 1\rvert\,]$ 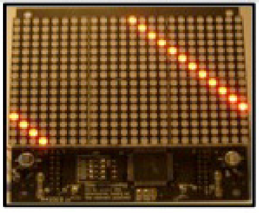	**Rule 121**, κ=2 $u_i^{t+1} = sgn\,[\,-1 + \lvert -u_{i-1}^t + u_i^t + u_{i+1}^t - 1\rvert\,]$ 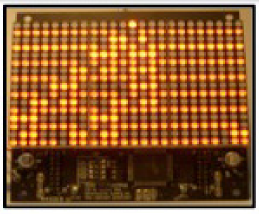	**Rule 122**, κ=2 $u_i^{t+1} = sgn\,[\,3 - \lvert -2u_{i-1}^t - u_i^t - 2u_{i+1}^t + 1\rvert\,]$ 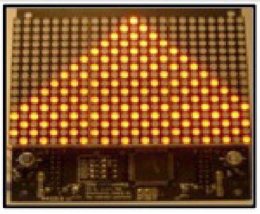
Rule 123, κ=2 $u_i^{t+1} = sgn\,[\,-1 + \lvert 2u_{i-1}^t + u_i^t - 2u_{i+1}^t - 1\rvert\,]$ 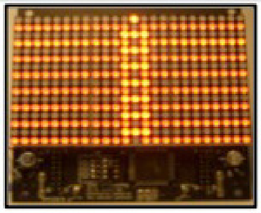	**Rule 124**, κ=2 $u_i^{t+1} = sgn\,[\,3 - \lvert 2u_{i-1}^t + 2u_i^t + u_{i+1}^t - 1\rvert\,]$ 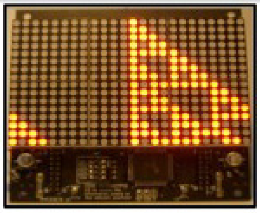	**Rule 125**, κ=2 $u_i^{t+1} = sgn\,[\,-1 + \lvert -u_{i-1}^t + 2u_i^t + 2u_{i+1}^t - 2\rvert\,]$ 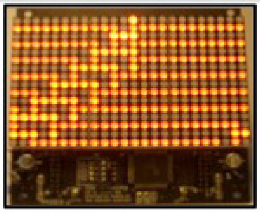
Rule 126, κ=2 $u_i^{t+1} = sgn\,[\,2 - \lvert -u_{i-1}^t - u_i^t - u_{i+1}^t\rvert\,]$ 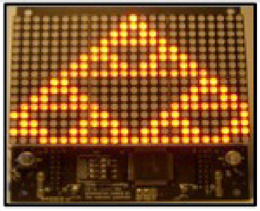	**Rule 127**, κ=1 $u_i^{t+1} = sgn\,[\,-u_{i-1}^t - u_i^t - u_{i+1}^t + 2\,]$ 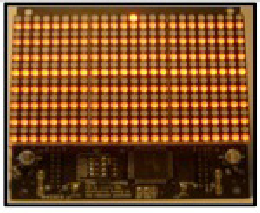	**Rule 128**, κ=1 $u_i^{t+1} = sgn\,[\,u_{i-1}^t + u_i^t + u_{i+1}^t - 2\,]$ 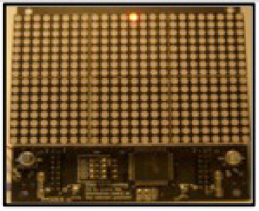
Rule 129, κ=2 $u_i^{t+1} = sgn\,[\,-2 + \lvert u_{i-1}^t + u_i^t + u_{i+1}^t\rvert\,]$ 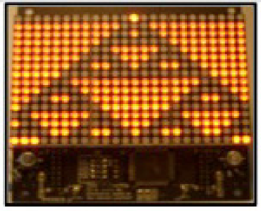	**Rule 130**, κ=2 $u_i^{t+1} = sgn\,[\,1 - \lvert -u_{i-1}^t + u_i^t - 2u_{i+1}^t + 2\rvert\,]$ 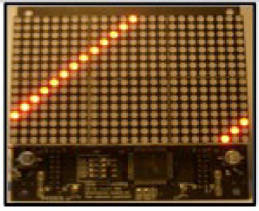	**Rule 131**, κ=2 $u_i^{t+1} = sgn\,[\,3 - \lvert 4u_{i-1}^t - 2u_i^t - u_{i+1}^t + 1\rvert\,]$ 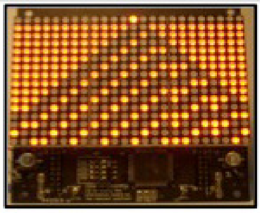

Table 4.1. *(Continued)*

Rule 132, κ=2 $u_i^{t+1} = sgn\ [1 - \vert 2u_{i-1}^t - u_i^t - 2u_{i+1}^t + 1\vert\ ]$ 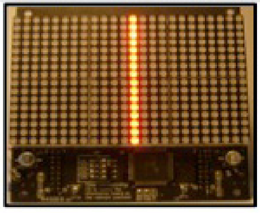	**Rule 133**, κ=2 $u_i^{t+1} = sgn\ [\ 3 - \vert -2u_{i-1}^t - u_i^t + 4u_{i+1}^t + 1\vert\ ]$ 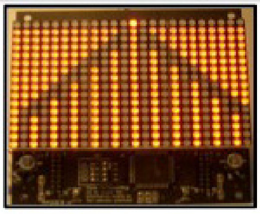	**Rule 134**, κ=2 $u_i^{t+1} = sgn\ [\ 1 - \vert u_{i-1}^t - u_i^t - u_{i+1}^t + 1\vert\ ]$ 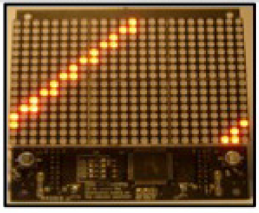
Rule 135, κ=2 $u_i^{t+1} = sgn\ [\ 2 - \vert 2u_{i-1}^t - u_i^t - u_{i+1}^t + 1\vert\ ]$ 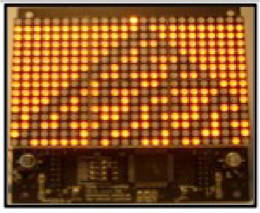	**Rule 136**, κ=1 $u_i^{t+1} = sgn\ [\ u_i^t + u_{i+1}^t - 1\ ]$ 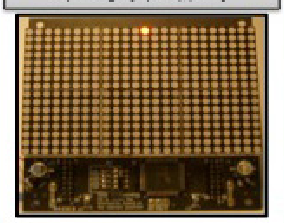	**Rule 137**, κ=2 $u_i^{t+1} = sgn\ [\ 3 - \vert -u_{i-1}^t - 2u_i^t + 4u_{i+1}^t - 1\vert\ ]$ 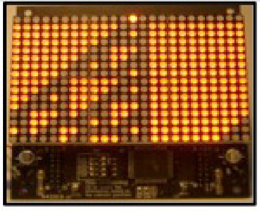
Rule 138, κ=1 $u_i^{t+1} = sgn\ [\ - u_{i-1}^t + u_i^t + 2u_{i+1}^t - 1\ ]$ 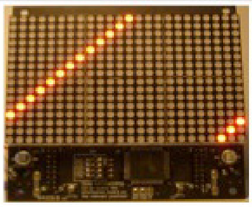	**Rule 139**, κ=3 $u_i^{t+1} = sgn[2 - \vert 3 + \vert u_{i-1}^t - 2u_i^t + 3u_{i+1}^t - 4\vert\vert]$ 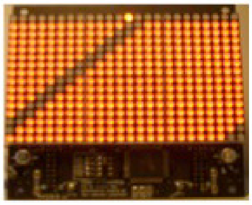	**Rule 140**, κ=1 $u_i^{t+1} = sgn\ [\ - u_{i-1}^t + 2u_i^t + u_{i+1}^t - 1\ ]$ 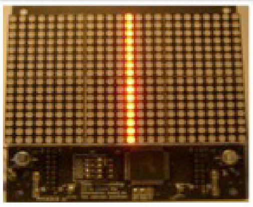
Rule 141, κ=3 $u_i^{t+1} = sgn[2 - \vert 3 - \vert 2u_{i-1}^t - 4u_i^t + 3u_{i+1}^t + 1\vert\vert]$ 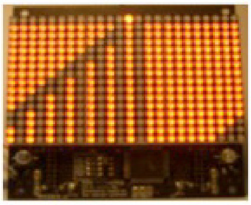	**Rule 142**, κ=1 $u_i^{t+1} = sgn\ [\ - u_{i-1}^t + u_i^t + u_{i+1}^t\ ]$ 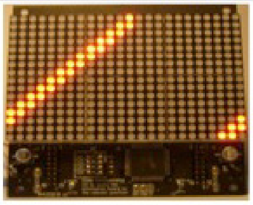	**Rule 143**, κ=1 $u_i^{t+1} = sgn\ [\ - 3u_{i-1}^t + u_i^t + u_{i+1}^t + 2\ ]$ 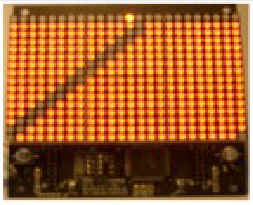

Table 4.1. *(Continued)*

Rule 144, κ=2 $u_i^{t+1} = sgn\,[\,1 - \lvert -2u_{i-1}^t + u_i^t - u_{i+1}^t + 2\rvert\,]$ 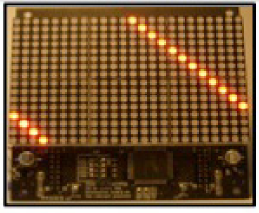	**Rule 145**, κ=2 $u_i^{t+1} = sgn\,[\,3 - \lvert -u_{i-1}^t - 2u_i^t + 4u_{i+1}^t + 1\rvert\,]$ 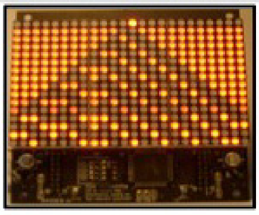	**Rule 146**, κ=2 $u_i^{t+1} = sgn\,[\,1 - \lvert u_{i-1}^t - u_i^t + u_{i+1}^t - 1\rvert\,]$ 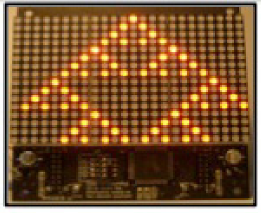
Rule 147, κ=2 $u_i^{t+1} = sgn\,[\,2 - \lvert u_{i-1}^t - 2u_{i-1}^t + u_{i+1}^t - 1\rvert\,]$ 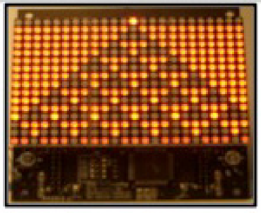	**Rule 148**, κ=2 $u_i^{t+1} = sgn\,[\,1 - \lvert -u_{i-1}^t - u_i^t + u_{i+1}^t + 1\rvert\,]$ 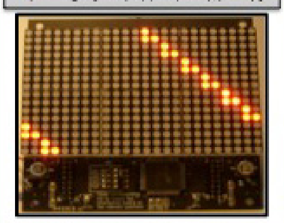	**Rule 149**, κ=2 $u_i^{t+1} = sgn\,[\,2 - \lvert -u_{i-1}^t - u_i^t + 2u_{i+1}^t + 1\rvert\,]$ 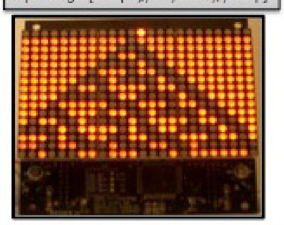
Rule 150, κ=3 $u_i^{t+1} = sgn[3 - \lvert 7 - \lvert 4u_{i-1}^t - 3u_i^t + 4u_{i+1}^t - 3\rvert$ 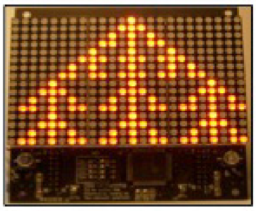	**Rule 151**, κ=2 $u_i^{t+1} = sgn\,[\,-1 + \lvert -u_{i-1}^t - u_i^t - u_{i+1}^t + 1\rvert\,]$ 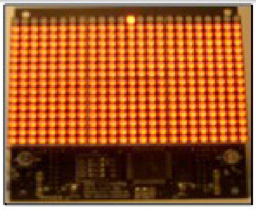	**Rule 152**, κ=2 $u_i^{t+1} = sgn\,[\,3 - \lvert u_{i-1}^t + 4u_i^t - 2u_{i+1}^t - 1\rvert\,]$ 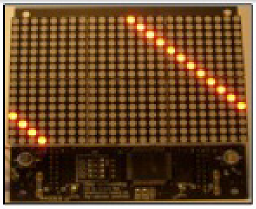
Rule 153, κ=2 $u_i^{t+1} = sgn\,[\,1 - \lvert - u_i^t + u_{i+1}^t\rvert\,]$ 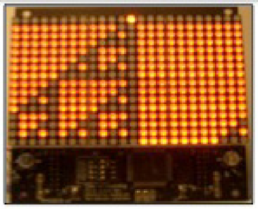	**Rule 154**, κ=2 $u_i^{t+1} = sgn\,[\,2 - \lvert u_{i-1}^t - u_i^t + 2u_{i+1}^t - 1\rvert\,]$ 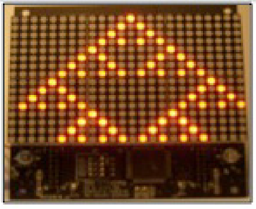	**Rule 155**, κ=2 $u_i^{t+1} = sgn\,[\,3 - \lvert -u_{i-1}^t + 2u_i^t - 2u_{i+1}^t + 1\rvert\,]$ 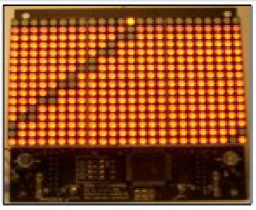

Table 4.1. *(Continued)*

Rule 156, κ=2 $u_i^{t+1} = sgn\,[\,2 - \lvert u_{i-1}^t + 2u_i^t - u_{i+1}^t - 1\rvert\,]$ 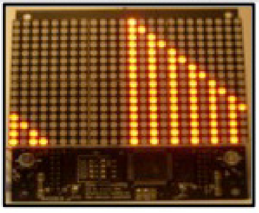	**Rule 157**, κ=2 $u_i^{t+1} = sgn\,[\,3 - \lvert u_{i-1}^t + 2u_i^t - 2u_{i+1}^t - 1\rvert\,]$ 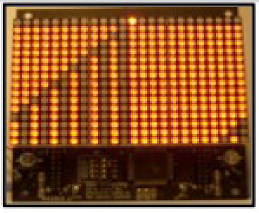	**Rule 158**, κ=2 $u_i^{t+1} = sgn\,[\,-1 + \lvert u_{i-1}^t - u_i^t - u_{i+1}^t - 1\rvert\,]$ 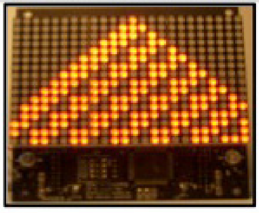
Rule 159, κ=2 $u_i^{t+1} = sgn\,[\,-1 + \lvert -2u_{i-1}^t + u_i^t + u_{i+1}^t + 2\rvert\,]$ 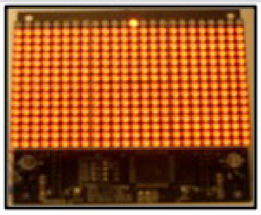	**Rule 160**, κ=1 $u_i^{t+1} = sgn\,[\,u_{i-1}^t + u_{i+1}^t - 1\,]$ 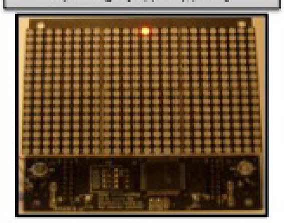	**Rule 161**, κ=2 $u_i^{t+1} = sgn\,[\,3 - \lvert 2u_{i-1}^t + u_i^t - 4u_{i+1}^t + 1\rvert\,]$ 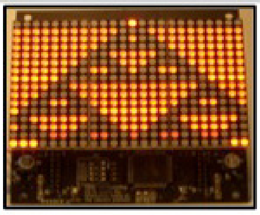
Rule 162, κ=1 $u_i^{t+1} = sgn\,[\,u_{i-1}^t - u_i^t + 2u_{i+1}^t - 1\,]$ 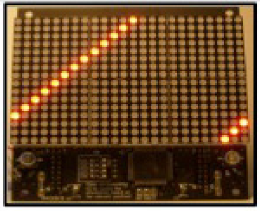	**Rule 163**, κ=3 $u_i^{t+1} = sgn[2 - \lvert 3 - \lvert 3u_{i-1}^t - 4u_i^t - 3u_{i+1}^t - 1$ 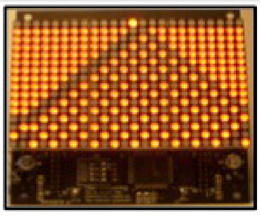	**Rule 164**, κ=2 $u_i^{t+1} = sgn\,[\,-3 + \lvert -2u_{i-1}^t + u_i^t - 2u_{i+1}^t - 1\rvert\,]$ 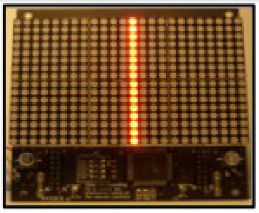
Rule 165, κ=2 $u_i^{t+1} = sgn\,[\,1 - \lvert -u_{i-1}^t + u_{i+1}^t\rvert\,]$ 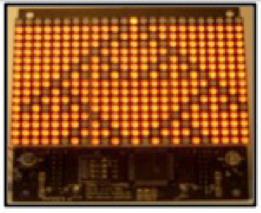	**Rule 166**, κ=2 $u_i^{t+1} = sgn\,[\,2 - \lvert u_{i-1}^t - u_i^t - 2u_{i+1}^t + 1\rvert\,]$ 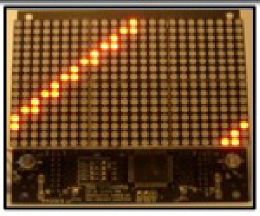	**Rule 167**, κ=2 $u_i^{t+1} = sgn\,[\,3 - \lvert -2u_{i-1}^t + u_i^t + 2u_{i+1}^t - 1\rvert\,]$ 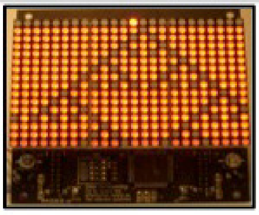

Table 4.1. *(Continued)*

Rule 168, $\kappa=1$ $u_i^{t+1} = sgn\,[\,u_{i-1}^t + u_i^t + 2u_{i+1}^t - 1\,]$ 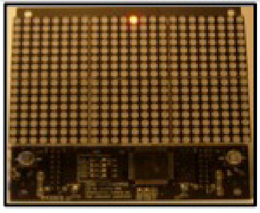	**Rule 169**, $\kappa=2$ $u_i^{t+1} = sgn\,[\,2 - \lvert u_{i-1}^t + u_i^t - 2u_{i+1}^t + 1\rvert\,]$ 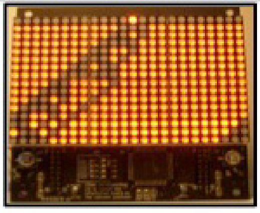	**Rule 170**, $\kappa=1$ $u_i^{t+1} = sgn\,[\,u_{i+1}^t\,]$ 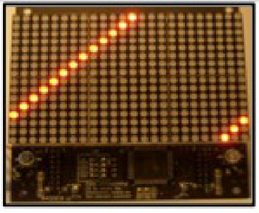
Rule 171, $\kappa=1$ $u_i^{t+1} = sgn\,[\,-u_{i-1}^t - u_i^t + 2u_{i+1}^t + 1\,]$ 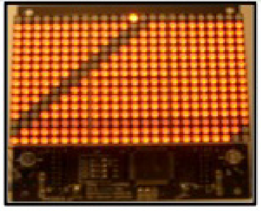	**Rule 172**, $\kappa=3$ $u_i^{t+1} = sgn[2-\lvert 3-\lvert -3u_{i-1}^t - 4u_i^t + 2u_{i+1}^t + 1\rvert\rvert]$ 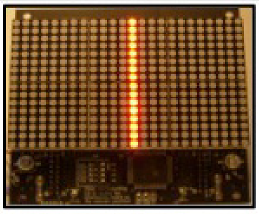	**Rule 173**, $\kappa=2$ $u_i^{t+1} = sgn\,[\,3 - \lvert -2u_{i-1}^t - u_i^t + 2u_{i+1}^t - 1\rvert\,]$ 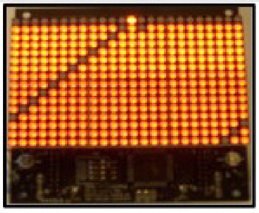
Rule 174, $\kappa=1$ $u_i^{t+1} = sgn\,[\,-u_{i-1}^t + u_i^t + 2u_{i+1}^t + 1\,]$ 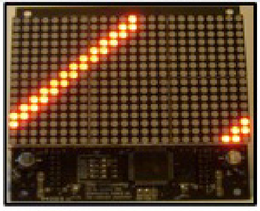	**Rule 175**, $\kappa=1$ $u_i^{t+1} = sgn\,[\,-u_{i-1}^t + u_{i+1}^t + 1\,]$ 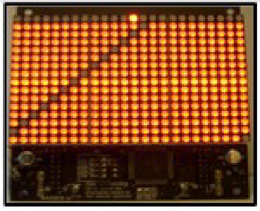	**Rule 176**, $\kappa=1$ $u_i^{t+1} = sgn\,[\,2u_{i-1}^t - u_i^t + u_{i+1}^t - 1\,]$ 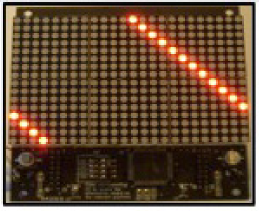
Rule 177, $\kappa=3$ $u_i^{t+1} = sgn[2-\lvert -3+\lvert 4u_{i-1}^t - 2u_i^t - u_{i+1}^t - 3\rvert\rvert]$ 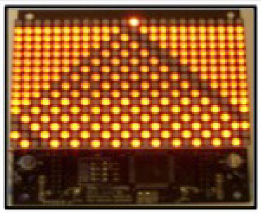	**Rule 178**, $\kappa=1$ $u_i^{t+1} = sgn\,[\,u_{i-1}^t - u_i^t + u_{i+1}^t\,]$ 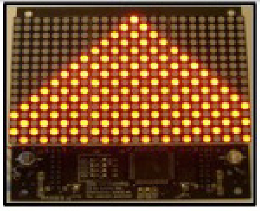	**Rule 179**, $\kappa=1$ $u_i^{t+1} = sgn\,[\,u_{i-1}^t - 3u_i^t + u_{i+1}^t + 2\,]$ 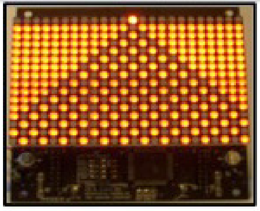

Table 4.1. *(Continued)*

Rule 180, κ=2 $u_i^{t+1} = sgn\,[\,2 - \lvert -2u_{i-1}^t - u_i^t + u_{i+1}^t + 1\rvert\,]$ 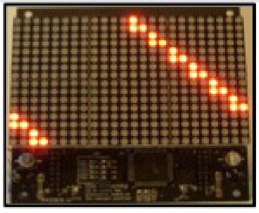	**Rule 181**, κ=2 $u_i^{t+1} = sgn\,[\,3 - \lvert 2u_{i-1}^t + u_i^t - 2u_{i+1}^t - 1\rvert\,]$ 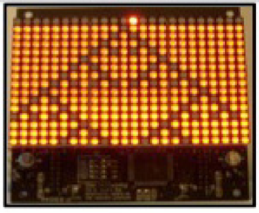	**Rule 182**, κ=2 $u_i^{t+1} = sgn\,[\,-1 + \lvert -u_{i-1}^t + u_i^t - u_{i+1}^t - 1\rvert\,]$ 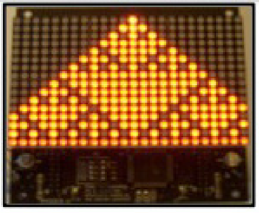
Rule 183, κ=2 $u_i^{t+1} = sgn\,[\,-1 + \lvert u_{i-1}^t - 2u_i^t + u_{i+1}^t + 2\rvert\,]$ 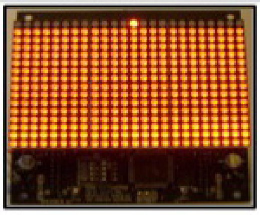	**Rule 184**, κ=3 $u_i^{t+1} = sgn(2 - \lvert 3 + \lvert u_{i-1}^t - 2u_i^t + 3u_{i+1}^t - 4\rvert$ 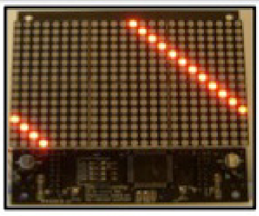	**Rule 185**, κ=2 $u_i^{t+1} = sgn\,[\,3 - \lvert -u_{i-1}^t - 2u_i^t + 2u_{i+1}^t - 1\rvert\,]$ 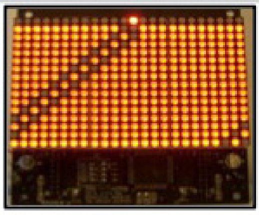
Rule 186, κ=1 $u_i^{t+1} = sgn\,[\,u_{i-1}^t - u_i^t + 2u_{i+1}^t + 1\,]$ 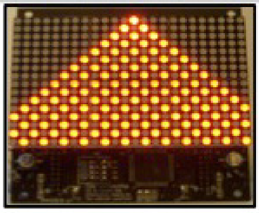	**Rule 187**, κ=1 $u_i^{t+1} = sgn\,[\,-u_i^t + u_{i+1}^t + 1\,]$ 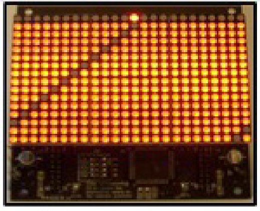	**Rule 188**, κ=2 $u_i^{t+1} = sgn\,[\,3 - \lvert 2u_{i-1}^t + 2u_i^t - u_{i+1}^t - 1\rvert\,]$ 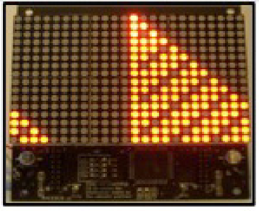
Rule 189, κ=2 $u_i^{t+1} = sgn\,[\,2 - \lvert u_{i-1}^t + u_i^t - u_{i+1}^t\rvert\,]$ 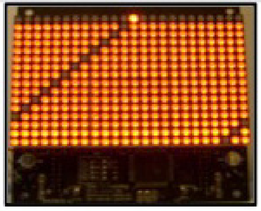	**Rule 190**, κ=2 $u_i^{t+1} = sgn\,[\,-1 + \lvert -2u_{i-1}^t + 2u_i^t + u_{i+1}^t + 1\rvert\,]$ 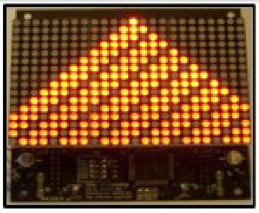	**Rule 191**, κ=1 $u_i^{t+1} = sgn\,[\,-u_{i-1}^t - u_i^t + u_{i+1}^t + 2\,]$ 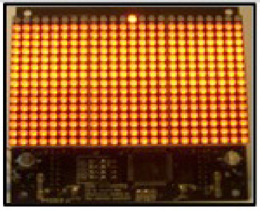

Table 4.1. *(Continued)*

Rule 192, κ=1 $u_i^{t+1} = sgn\,[\, u_{i-1}^t + u_i^t - 1\,]$ 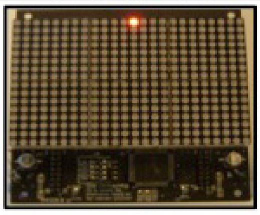	**Rule 193**, κ=2 $u_i^{t+1} = sgn\,[\,3 - \lvert 4u_{i-1}^t - 2u_{i-1}^t - u_{i+1}^t - 1\rvert\,]$ 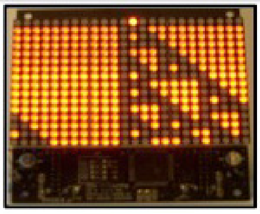	**Rule 194**, κ=2 $u_i^{t+1} = sgn\,[\,3 - \lvert -2u_{i-1}^t + 4u_i^t + u_{i+1}^t - 1\rvert\,]$ 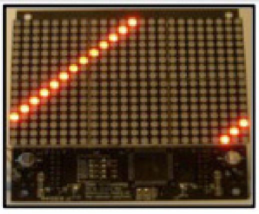
Rule 195, κ=2 $u_i^{t+1} = sgn\,[\,1 - \lvert -u_{i-1}^t + u_i^t\rvert\,]$ 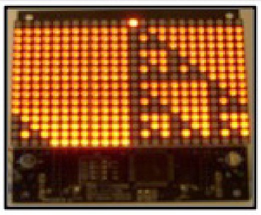	**Rule 196**, κ=1 $u_i^{t+1} = sgn\,[\, u_{i-1}^t + 2u_i^t - u_{i+1}^t - 1\,]$ 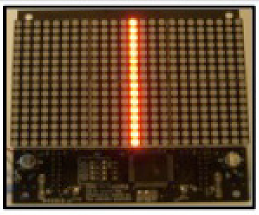	**Rule 197**, κ=3 $u_i^{t+1} = sgn[2 - \lvert 3 - \lvert 3u_{i-1}^t + 4u_i^t + 2u_{i+1}^t - 1\rvert\rvert]$ 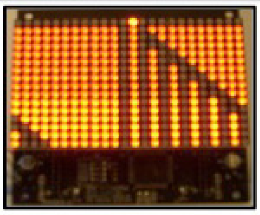
Rule 198, κ=2 $u_i^{t+1} = sgn\,[\,2 - \lvert u_{i-1}^t - 2u_i^t - u_{i+1}^t + 1\rvert\,]$ 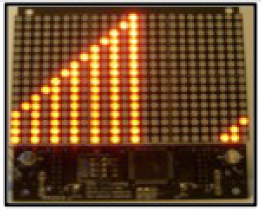	**Rule 199**, κ=2 $u_i^{t+1} = sgn\,[\,3 - \lvert 2u_{i-1}^t - 2u_i^t - u_{i+1}^t + 1\rvert\,]$ 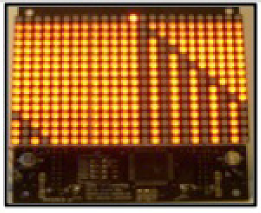	**Rule 200**, κ=1 $u_i^{t+1} = sgn\,[\, u_{i-1}^t + 2u_i^t + u_{i+1}^t - 1\,]$ 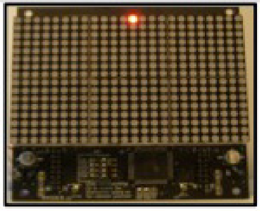
Rule 201, κ=2 $u_i^{t+1} = sgn\,[\,2 - \lvert u_{i-1}^t - 2u_i^t + u_{i+1}^t + 1\rvert\,]$ 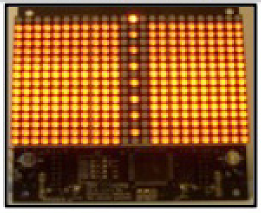	**Rule 202**, κ=3 $u_i^{t+1} = sgn[2 - \lvert 3 - \lvert 3u_{i-1}^t - 4u_i^t + 2u_{i+1}^t + 1\rvert\rvert]$ 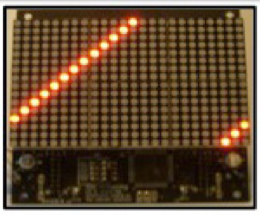	**Rule 203**, κ=2 $u_i^{t+1} = sgn\,[\,3 - \lvert -2u_{i-1}^t + 2u_i^t - u_{i+1}^t - 1\rvert\,]$ 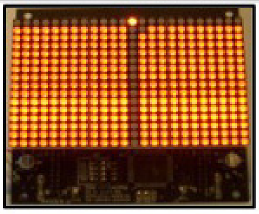

Table 4.1. *(Continued)*

Rule 204, $\kappa=1$ $u_i^{t+1} = sgn\,[\,u_i^t\,]$ 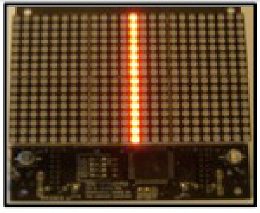	**Rule 205**, $\kappa=1$ $u_i^{t+1} = sgn\,[\,-u_{i-1}^t + 2u_i^t - u_{i+1}^t + 1\,]$ 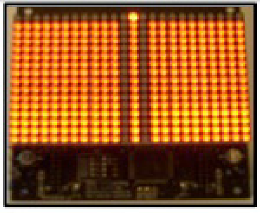	**Rule 206**, $\kappa=1$ $u_i^{t+1} = sgn\,[\,-u_{i-1}^t + 2u_i^t + u_{i+1}^t + 1\,]$ 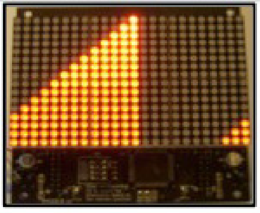
Rule 207, $\kappa=1$ $u_i^{t+1} = sgn\,[\,-u_{i-1}^t + u_i^t + 1\,]$ 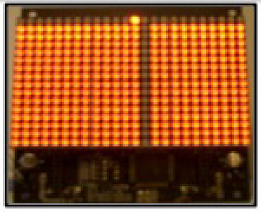	**Rule 208**, $\kappa=1$ $u_i^{t+1} = sgn\,[\,2u_{i-1}^t + u_i^t - u_{i+1}^t - 1\,]$ 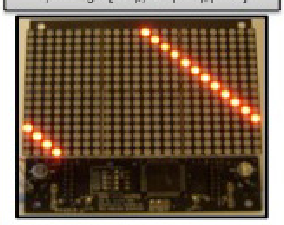	**Rule 209**, $\kappa=3$ $u_i^{t+1} = sgn[2 - \|3 - \|2u_{i-1}^t + u_i^t - 4u_{i+1}^t\| - 3\|]$ 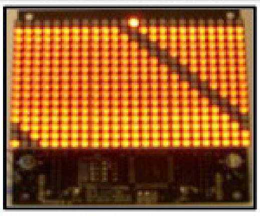
Rule 210, $\kappa=2$ $u_i^{t+1} = sgn\,[\,2 - \|-2u_{i-1}^t + u_i^t - u_{i+1}^t + 1\|\,]$ 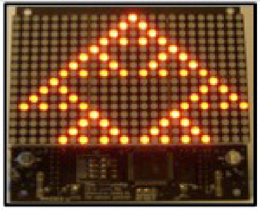	**Rule 211**, $\kappa=2$ $u_i^{t+1} = sgn\,[\,3 - \|-2u_{i-1}^t + 2u_i^t - u_{i+1}^t + 1\|\,]$ 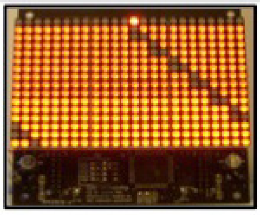	**Rule 212**, $\kappa=1$ $u_i^{t+1} = sgn\,[\,u_{i-1}^t + u_i^t - u_{i+1}^t\,]$ 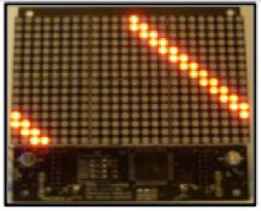
Rule 213, $\kappa=1$ $u_i^{t+1} = sgn\,[\,u_{i-1}^t + u_i^t - 3u_{i+1}^t + 2\,]$ 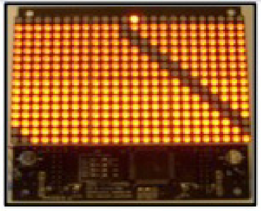	**Rule 214**, $\kappa=2$ $u_i^{t+1} = sgn\,[\,-1 + \|u_{i-1}^t + u_i^t - u_{i+1}^t + 1\|\,]$ 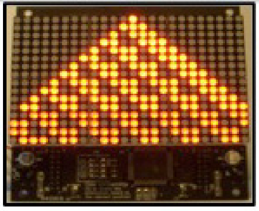	**Rule 215**, $\kappa=2$ $u_i^{t+1} = sgn\,[\,-1 + \|2u_{i-1}^t + 2u_i^t + u_{i+1}^t - 1\|\,]$ 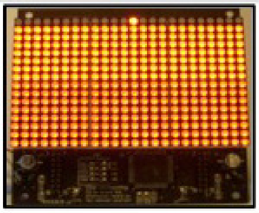

Table 4.1. *(Continued)*

Rule 216, $\kappa=3$ $u_i^{t+1} = sgn(2 - \|-3 + \|-3u_{i-1}^t + u_i^t - 4u_{i+1}^t + 2\|$ 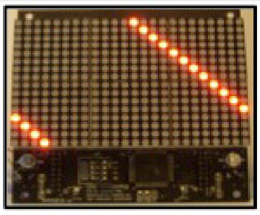	**Rule 217**, $\kappa=2$ $u_i^{t+1} = sgn\,[\,3 - \|-u_{i-1}^t + 2u_i^t - 2u_{i+1}^t - 1\|\,]$ 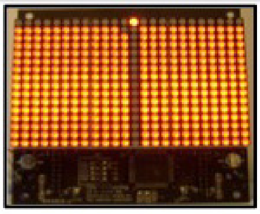	**Rule 218**, $\kappa=2$ $u_i^{t+1} = sgn\,[\,3 - \|2u_{i-1}^t - u_i^t + 2u_{i+1}^t - 1\|\,]$ 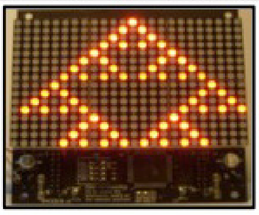
Rule 219, $\kappa=2$ $u_i^{t+1} = sgn\,[\,2 - \|-u_{i-1}^t + u_i^t - u_{i+1}^t\|\,]$ 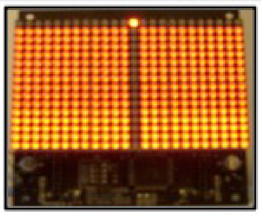	**Rule 220**, $\kappa=1$ $u_i^{t+1} = sgn\,[\,u_{i-1}^t + 2u_i^t - u_{i+1}^t + 1\,]$ 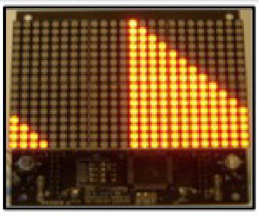	**Rule 221**, $\kappa=1$ $u_i^{t+1} = sgn\,[\,u_i^t - u_{i+1}^t + 1\,]$ 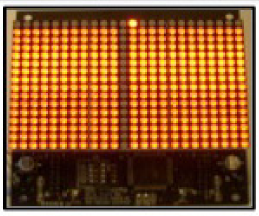
Rule 222, $\kappa=2$ $u_i^{t+1} = sgn\,[\,-1 + \|-u_{i-1}^t - 2u_i^t + u_{i+1}^t - 2\|\,]$ 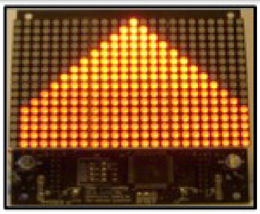	**Rule 223**, $\kappa=1$ $u_i^{t+1} = sgn\,[\,-u_{i-1}^t + u_i^t - u_{i+1}^t + 2\,]$ 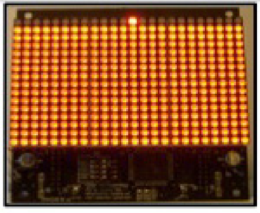	**Rule 224**, $\kappa=1$ $u_i^{t+1} = sgn\,[\,2u_{i-1}^t + u_i^t + u_{i+1}^t - 1\,]$ 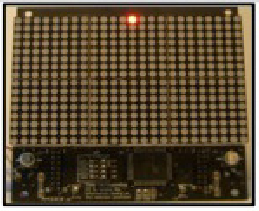
Rule 225, $\kappa=2$ $u_i^{t+1} = sgn\,[\,2 - \|-2u_{i-1}^t + u_i^t + u_{i+1}^t + 1\|\,]$ 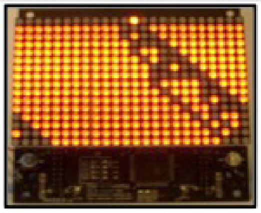	**Rule 226**, $\kappa=3$ $u_i^{t+1} = sgn(2 - \|3 - \|2u_{i-1}^t - u_i^t - 4u_{i+1}^t + 3\|$ 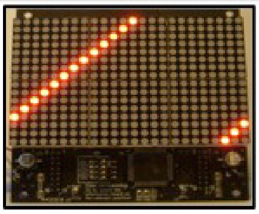	**Rule 227**, $\kappa=2$ $u_i^{t+1} = sgn\,[\,3 - \|2u_{i-1}^t - 2u_i^t - u_{i+1}^t - 1\|\,]$ 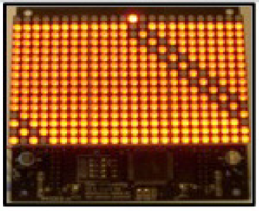

Table 4.1. *(Continued)*

Rule 228, *κ=3* $u_i^{t+1} = sgn[2 - \lvert 3 - \lvert 2u_{i-1}^t + 4u_i^t + u_{i+1}^t - 3\rvert\rvert]$ 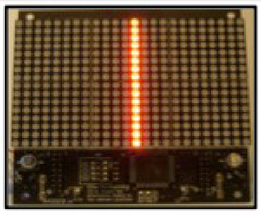	**Rule 229**, *κ=2* $u_i^{t+1} = sgn[\,3 - \lvert -2u_{i-1}^t + u_i^t + 2u_{i+1}^t + 1\rvert\,]$ 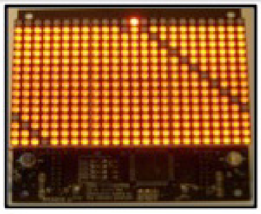	**Rule 230**, *κ=2* $u_i^{t+1} = sgn[\,3 - \lvert -u_{i-1}^t + 2u_i^t + 2u_{i+1}^t - 1\rvert\,]$ 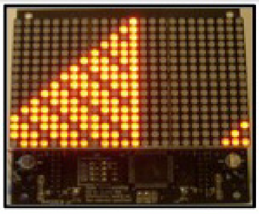
Rule 231, *κ=2* $u_i^{t+1} = sgn[\,2 - \lvert u_{i-1}^t - u_i^t - u_{i+1}^t\rvert\,]$ 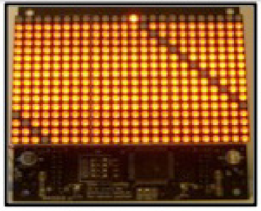	**Rule 232**, *κ=1* $u_i^{t+1} = sgn[\,u_{i-1}^t + u_i^t + u_{i+1}^t\,]$ 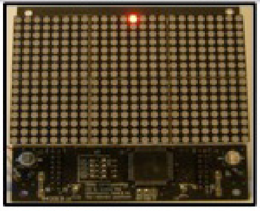	**Rule 233**, *κ=2* $u_i^{t+1} = sgn[\,-1 + \lvert u_{i-1}^t + u_i^t + u_{i+1}^t + 1\rvert\,]$ 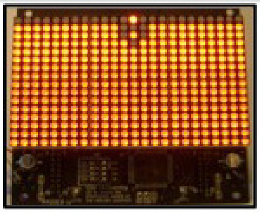
Rule 234, *κ=1* $u_i^{t+1} = sgn[\,u_{i-1}^t + u_i^t + 2u_{i+1}^t + 1\,]$ 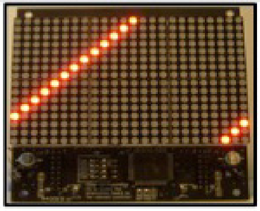	**Rule 235**, *κ=2* $u_i^{t+1} = sgn[\,-1 + \lvert 2u_{i-1}^t + 2u_i^t + u_{i+1}^t + 1\rvert\,]$ 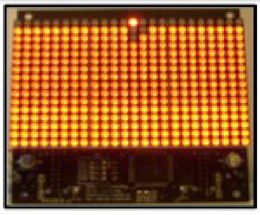	**Rule 236**, *κ=1* $u_i^{t+1} = sgn[\,u_{i-1}^t + 2u_i^t + u_{i+1}^t + 1\,]$ 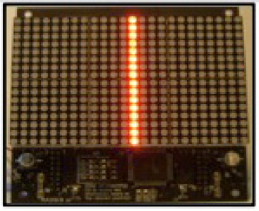
Rule 237, *κ=2* $u_i^{t+1} = sgn[\,-1 + \lvert 2u_{i-1}^t - u_i^t + 2u_{i+1}^t - 1\rvert\,]$ 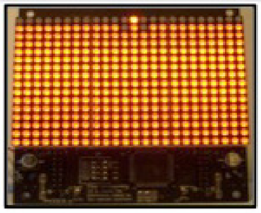	**Rule 238**, *κ=1* $u_i^{t+1} = sgn[\,u_i^t + u_{i+1}^t + 1\,]$ 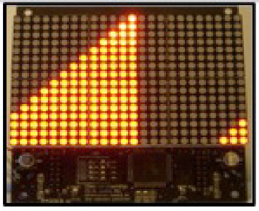	**Rule 239**, *κ=1* $u_i^{t+1} = sgn[\,-u_{i-1}^t + u_i^t + u_{i+1}^t + 2\,]$ 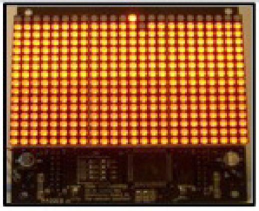

Table 4.1. *(Continued)*

Rule 240, $\kappa=1$ $u_i^{t+1} = sgn\,[\,u_{i-1}^t\,]$ 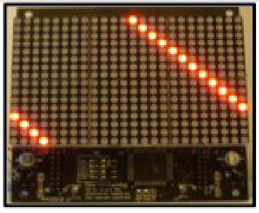	**Rule 241**, $\kappa=1$ $u_i^{t+1} = sgn\,[\,2u_{i-1}^t - u_i^t - u_{i+1}^t + 1\,]$ 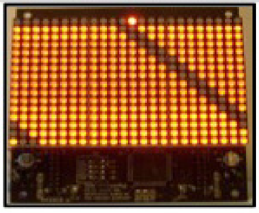	**Rule 242**, $\kappa=1$ $u_i^{t+1} = sgn\,[\,2u_{i-1}^t - u_i^t + u_{i+1}^t + 1\,]$ 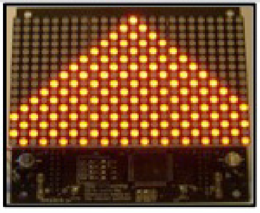
Rule 243, $\kappa=1$ $u_i^{t+1} = sgn\,[\,u_{i-1}^t - u_i^t + 1\,]$ 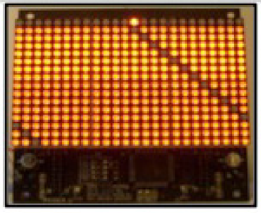	**Rule 244**, $\kappa=1$ $u_i^{t+1} = sgn\,[\,2u_{i-1}^t + u_i^t - u_{i+1}^t + 1\,]$ 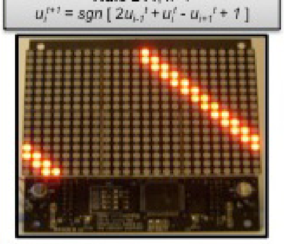	**Rule 245**, $\kappa=1$ $u_i^{t+1} = sgn\,[\,u_{i-1}^t - u_{i+1}^t + 1\,]$ 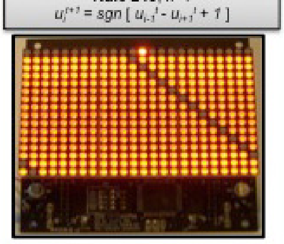
Rule 246, $\kappa=2$ $u_i^{t+1} = sgn\,[\,-1 + \lvert -u_{i-1}^t + 2u_i^t - 2u_{i+1}^t - 1\rvert\,]$ 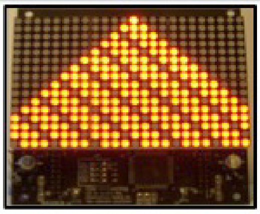	**Rule 247**, $\kappa=1$ $u_i^{t+1} = sgn\,[\,u_{i-1}^t - u_i^t - u_{i+1}^t + 2]$ 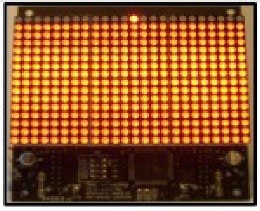	**Rule 248**, $\kappa=1$ $u_i^{t+1} = sgn\,[\,2u_{i-1}^t + u_i^t + u_{i+1}^t + 1\,]$ 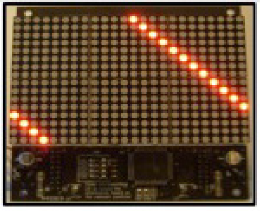
Rule 249, $\kappa=2$ $u_i^{t+1} = sgn\,[\,-1 + \lvert 2u_{i-1}^t - u_i^t - u_{i+1}^t + 2\rvert\,]$ 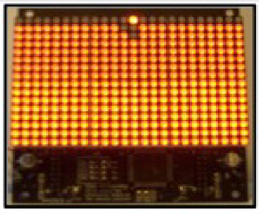	**Rule 250**, $\kappa=1$ $u_i^{t+1} = sgn\,[\,u_{i-1}^t + u_{i+1}^t + 1\,]$ 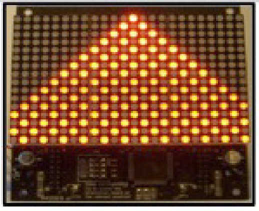	**Rule 251**, $\kappa=1$ $u_i^{t+1} = sgn\,[\,u_{i-1}^t - u_i^t + u_{i+1}^t + 2]$ 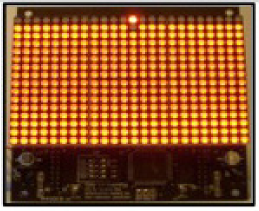

Table 4.1. *(Continued)*

Rule 252, $\kappa=1$ $u_i^{t+1} = sgn\,[\,u_{i-1}^t + u_i^t + 1\,]$ 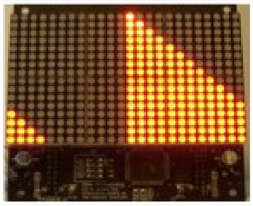	**Rule 253**, $\kappa=1$ $u_i^{t+1} = sgn\,[\,u_{i-1}^t + u_i^t - u_{i+1}^t + 2]$ 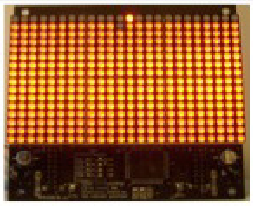	**Rule 254**, $\kappa=1$ $u_i^{t+1} = sgn\,[\,u_{i-1}^t + u_i^t + u_{i+1}^t + 2\,]$ 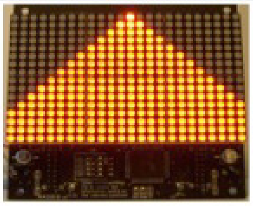
Rule 255, $\kappa=1$ $u_i^{t+1} = sgn\,[\,1\,]$ 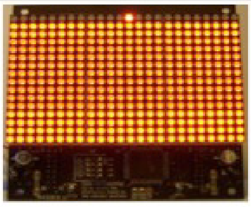		

5

Concluding remarks

Complex networks are today pervading our world with implications and applications in engineering, physics, biology, ecology and social systems.

We are members of and we use many social systems, often providing us a plenty of new data which give new insights on the structure and properties of the system itself and of complex systems in general. Modeling is always a primary tool for studying such systems. In this Thesis real social networks, in particular extracted from the popular on-line social network Facebook, have been deeply analyzed to understand their peculiar characteristics as high levels of clustering, low values of the characteristic path length and node betweenness, division into communities and heterogeneous degree distribution. These results have been confirmed by recent works on social networks. With the aim to reproduce these characteristics, a new model for growing social networks has been proposed. It is based on the idea that communities play a fundamental role in social networks and may be involved also in the growing process of the network itself.

On-line social networks are interesting not only as a collection of complex networks, but every node may be interpreted as a time-series generator. In fact, with this consideration, an analysis on the number of on-line friends using a Facebook account has been carried out. In this way, a social time series has been extracted observing the on-line friends number. The application of the Kaplan test to the time series obtained has showed the presence of a deterministic component.

Focusing on applications of complex networks, a very interesting case study is the analysis of power grids. In this Thesis an analysis of the Italian high-voltage (380 kV) power grid under the point of view of dynamical nodes has been proposed. The mapping between oscillators and power grid nodes, divided into “sources” and “consumer”, has been made using Kuramoto-like models with bimodal distribution of the frequencies. Synchronization, representing the normal working operating regime, in this network has been analyzed and the effect of perturbations has been studied with the aim to investigate the dynamical robustness of the network to faults. Dynamical parameters such as the minimum value of perturbation leading to desynchronization and the time to reach the complete loss of synchronism have been defined. A non-trivial relationship between dynamical and topological parameters of the network has been discussed.

The study of complex networks is mostly based on data analysis, models, theoretical and software tools. In this Thesis, focusing on a simple topology, we have investigated the possibility of designing and implementing a hardware tool for complex network emulation with possible applications in the field of artistic installations and publicity. In particular, the emulation of one-dimensional cellular automata has been investigated. A new hardware tool for implementing Wolfram's concept of New Kind of Science has been developed.

With this device, a low-cost stand-alone portable system, it is possible to emulate and study all of the Wolfram's cellular automata without the need of a PC and to display their evolution on a LED matrix controlled by a microcontroller board. It is also possible to define spatio-temporal algorithms made of alternating rules and easily extending the basic configuration for emulating automata with a larger number of cells.

6

Acknowledgements

During these three years I had the daily possibility to live cultural and human experiences in a really great adventure.

I want to thank prof. Luigi Fortuna, coordinator of this PhD course and my tutor, but most of all a great engineer and researcher, for the opportunities that he offered me.

I thank two real friends: Eng. Mattia Frasca and Eng. Arturo Buscarino, because whenever I had problems they were always there to give me suggestions.

I will never forget the possibility I had to collaborate with prof. Leon O. Chua, the ‘father’ of nonlinear circuit theory, an example of scientific rigour and devotion. Thanks to prof. Vito Latora for his useful help and to prof. Stanislaw Jankowski for the period I stayed in Poland and for his friendship.

I want to thank all the friends at “Centro Orientamento e Formazione” and in particular prof. Vincenzo Perciavalle and dr. Carmelo Pappalardo.

Thanks to all the guys at the Lab, because happiness is needed to produce good results, and to all the students that worked with me in these years.

Last, but not least, a special thanks goes to my family and to my girlfriend for their constant support, love and for being always on my side.

References

1. L. O. Chua, *CNN: A vision of complexity*, International Journal of Bifurcation and Chaos, Vol. 7(1), pp. 22192426 (1997).
2. S. Boccaletti, V. Latora, Y. Moreno, M. Chavez, D. U. Hwang, *Complex networks: Structure and dynamics*, Physics Reports, Vol. 424, pp. 175-308 (2006).
3. I. Pool, M. Kochen, *Contacts and influence*, Social Networks, Vol. 1, pp 5-51 (1978).
4. P. Erdös, A. Rényi, *On Random Graphs I*, Publicationes Mathematicae, Vol. 6, pp. 290-297 (1959).
5. S. Milgram, *The small world problem*, Psychology Today, Vol. 2 (1967).
6. D. J. Watts, S. H. Strogatz, *Collective dynamics of 'small world' networks*, Nature, Vol. 393, pp. 440-442 (1998).
7. A. L. Barabàsi, R. Albert, *Emergence of scaling in random networks*, Science, Vol. 286, pp. 509-512 (1999).
8. L. da F. Costa, F. A. Rodrigues, G. Travieso, P. R. Villas Boas, *Characterization of complex networks: A survey of measurements*, Advances in Physics, Vol. 56(1), pp. 167–242 (2007).
9. X. F. Wang, G. Chen, *Complex Networks: Small-World, Scale-Free and Beyond*, Circuits and Systems Magazine, Vol. 3(1), pp. 6–20 (2003).
10. M. E. J. Newman, D. J. Watts, *Renormalization group analysis of the small-world network model*, Phys. Lett. A, Vol. 263, pp. 341-346 (1999).
11. R. Albert, A. L. Barabási, *Statistical mechanics of complex networks*, Rev. Mod. Phys., Vol. 74, pp. 47-97 (2002).
12. S. N. Dorogovtsev, J. F. F. Mendes, A.N. Samukhin, *Structure of Growing Networks with Preferential Linking*, Phys. Rev. Lett., Vol. 85, (2000).

13. P. L. Krapivsky, S. Redner, F. Leyvraz, *Connectivity of Growing Random Networks*, Phys. Rev. Lett., Vol. 85 (2000).
14. S. N. Dorogovtsev, J. F. F. Mendes, *Effect of the accelerating growth of communications networks on their structure*, Phys. Rev. E, Vol. 63 (2001).
15. J. Gómez-Gardenes, Y. Moreno, *Local versus global knowledge in the Barabási-Albert scale-free network model*, Phys. Rev. E, Vol. 69, (2004).
16. A. Capocci, V. D. P. Servedio, F. Colaiori, L. S. Buriol, D. Donato, S. Leonardi, G. Caldarelli, *Preferential attachment in the growth of social networks: The internet encyclopedia Wikipedia*, Phys. Rev. E, Vol. 74 (2006).
17. L.C. Freeman, *Some Antecedents of Social Network Analysis*, Connections, Vol. 19, pp. 39-42 (1996).
18. *https://www.facebook.com/press/info.php?statistics*
19. M. Girvan, M. E. J. Newman, *Community structure in social and biological networks*, Proceedings of the National Academy of Sciences (PNAS), Vol. 99, pp. 7821-7826 (2002).
20. M. A. Porter, J. P. Onnela, P. J. Mucha, *Communities in Networks*, Notices of the American Mathematical Society, Vol. 56, pp. 1082-1097 (2009).
21. A. Khadivi, A. A. Rad, M. Hasler, *Network community-detection enhancement by proper weighting*, Physical Review E, Vol. 83, 046104 (2011).
22. Y. Pan, D. H. Li, J. G. Liu, J. Z. Liang, *Detecting community structure in complex networks via node similarity*, Physica A, Vol. 389(14), pp. 2849–2857 (2010).
23. F. Wu, B.A. Huberman, *Finding communities in linear time: a physics approach*, Eur. Phys. J. B, Vol. 38, pp. 331-338 (2004).
24. A. Buscarino, L. Fortuna, M. Frasca, A. Sarra Fiore, *A New Model for Growing Social Networks*, Complexity in Engineering, pp. 103–105 (2010).
25. J. Ugander, B. Karrer, L. Backstrom, C. Marlow, *The Anatomy of the Facebook Social Graph*, arXiv:1111.4503v1 (2011).
26. L. Backstrom, P. Boldi, M. Rosa, J. Ugander, S. Vigna, *Four Degrees of Separation*, arXiv:1111.4570v1 (2011).
27. P. E. Greenwood, M.S. Nikulin, *A guide to chi-squared testing*, Wiley, New York (1996).
28. V. D. Blondel, J.L. Guillaume, R. Lambiotte, E. Lefebvre, *Fast unfolding of communities in large networks*, J. Stat. Mech. (2008).

29. L. Fortuna, M. Frasca, L. V. Gambuzza, A. Sarra Fiore, S. A. Ramzy, T. R. Mofeed, *Analysis of the determinism of time-series extracted from social and biological systems*, Iraq Journal of Electrical and Electronic Engineering, Vol. 6, (2010).
30. D. T. Kaplan, L. Glass, *Coarse grained embeddings of time series:random walks, Gaussian random processes, and deterministic chaos*, Physica D: Nonlinear Phenomena, Vol. 64(4), pp. 431–454 (1993).
31. P. Crucitti, V. Latora, M. Marchiori, *Model for cascading failures in complex networks*, Physical Review E, Vol. 69, 045104 (2004).
32. P. Crucitti, V. Latora, M. Marchiori, *Locating critical lines in high-voltage electrical power grids*, Fluctuation and Noise Letters, Vol. 5, pp. 201–208 (2005).
33. R. V. Solé, M. Rosas-Casals, B. Corominas Muntra, S. Valverde, *Robustness of the European power grids under intentional attack*, Physical Review E, Vol. 77, 026102 (2008).
34. M. Rosas-Casals, *Power grids as complex networks: topology and fragility*, Physical Review E, Vol. 88, 026102 (2010).
35. V. Rosato, S. Bologna, F. Tiriticco, *Topological properties of high-voltage electrical transmission networks*, Electric Power Systems Research, Vol. 77, pp. 99–105 (2007).
36. G. Filatrella, A. H. Nielsen, N. F. Pedersen, *Analysis of a power grid using a Kuramoto-like model*, Eur. Phys. J. B, Vol. 61, pp. 485–491 (2008).
37. F. Dörfler, F. Bullo, *Synchronization and Transient Stability in Power Networks and Non-Uniform Kuramoto Oscillators*, American Control Conference (ACC), pp. 930–937 (2010).
38. V. Fioriti, S. Ruzzante, E. Castorini, E. Marchei, V. Rosato, *Stability of a distributed generation network using the Kuramoto models*, Critical Information Infrastructure Security, ser. Lecture Notes in Computer Science. Springer, pp. 14–23 (2009).
39. J. A. Acebrón, L. L. Bonilla, P. Vicente, J. Conrad, F. Ritort, R. Spigler, *The Kuramoto model: a simple paradigm for synchronization phenomena*, Reviews of Modern Physics, Vol. 77, pp. 137–185 (2005).
40. L. Buzna, S. Lozano, A. Díaz-Guilera, *Synchronization in symmetric bipolar population networks*, Physical Review E, Vol. 80, 066120 (2009).
41. Union for the Co-Ordination of Transport of Electricity (UCTE), *https://www.entsoe.eu/resources/grid-map/*.

42. P. Crucitti, V. Latora, M. Marchiori, *A topological analysis of the Italian electric power grid*, Physica A, Vol. 338, pp. 92–97 (2004).

43. L. Fortuna, M. Frasca, A. Sarra Fiore, V. Latora, V. *Analysis of the italian power grid based on Kuramoto-like model*, Physchon 2011, Leon, Spain (2011).

44. A. Ilachinski, *Cellular Automata: A discrete universe*, World Scientific Publishing Co. Pte. Ltd (2001).

45. M. Caratozzolo, S. Carnazza, L. Fortuna, M. Frasca, S. Guglielmino, G. Gurrieri, G. Marletta, *Self-organizing models of bacterial aggregation states*, Mathematical Biosciences and Engineering, Vol. 5, pp. 75–83 (2008).

46. S. Wolfram, *A New Kind of Science*, Wolfram Media Inc., Champaign Illinois, USA (2002).

47. L. O. Chua, S. Yoon, R. Dogaru, *A nonlinear dynamics perspective of Wolframs new kind of science. Part I: Threshold of complexity*, International Journal of Bifurcation and Chaos, Vol. 12, pp. 2655–2766 (2002).

48. L. O. Chua, *A nonlinear dynamics perspective of Wolframs new kind of science, volume III*, World Scientific Publishing Co. Pte. Ltd (2009).

49. L. O. Chua, V. I. Sbitnev, S. Yoon, *A nonlinear dynamics perspective of Wolframs new kind of science. Part II: Universal neuron*, International Journal of Bifurcation and Chaos, Vol. 13, pp. 2377–2491 (2003).

50. L. O. Chua, V. I. Sbitnev, S. Yoon, *A nonlinear dynamics perspective of Wolframs new kind of science. Part V: Fractals everywhere*, International Journal of Bifurcation and Chaos, Vol. 15, pp. 3701-3849 (2005).

51. L. O. Chua, V. I. Sbitnev, S. Yoon, *A nonlinear dynamics perspective of Wolframs new kind of science. Part VI: From time-reversible attractors to the arrow of time*, International Journal of Bifurcation and Chaos, Vol. 16, pp. 1097-1373 (2006).

52. L. O. Chua, G. E. Pazienza, *A nonlinear dynamics perspective of Wolframs new kind of science. Part XII: Period-3, period-6, and permutive rules*, International Journal of Bifurcation and Chaos, Vol. 19, pp. 3887–4038 (2009).

53. L. O. Chua, V. I. Sbitnev, S. Yoon, *A nonlinear dynamics perspective of Wolframs new kind of science. Part III: Predicting the unpredictable*, International Journal of Bifurcation and Chaos, Vol. 14, pp. 3689–3820 (2004).

54. L. O. Chua, V. I. Sbitnev, S. Yoon, *A nonlinear dynamics perspective of Wolframs new kind of science. Part IV: From Bernoulli shift to 1/f spectrum*, International Journal of Bifurcation and Chaos, Vol. 15, pp. 1045-1183 (2005).

55. L. O. Chua, G. E. Pazienza, L. Orzo, V. I. Sbitnev, J. Shin, *A nonlinear dynamics perspective of Wolframs new kind of science. Part IX: Quasi-ergodicity*, International Journal of Bifurcation and Chaos, Vol. 18, pp. 2487–2642 (2008).

56. L. O. Chua, G. E. Pazienza, J. Shin, *A nonlinear dynamics perspective of Wolframs new kind of science. Part X: Period-1 rules*, International Journal of Bifurcation and Chaos, Vol. 19, pp. 1425–1654 (2009).

57. L. O. Chua, G. E. Pazienza, *A nonlinear dynamics perspective of Wolframs new kind of science. Part XI: Period-2 rules*, International Journal of Bifurcation and Chaos, Vol. 19, pp. 1751–1930 (2009).

58. L. Fortuna, M. Frasca, A. Sarra Fiore, L. O. Chua, *The Wolfram Machine*, International Journal of Bifurcation and Chaos, Vol. 20, pp. 3863-3917 (2010).

59. Sure Electronics Inc[Copyright 2004-2008] *2416 Dot Matrix Display Information Board Users Guide* ,Copyright 2004-2008 Sure Electronics Inc (2004-2008).

60. M. Banzi, *Getting started with Arduino*, OReilly Media Inc (2008).

61. L. O. Chua, J. Guan, V. I. Sbitnev, S. Yoon, *A nonlinear dynamics perspective of Wolframs new kind of science. Part VII: Isles of Eden*, International Journal of Bifurcation and Chaos, Vol. 17, pp. 2839–3012 (2007).

62. L. O. Chua, K. Karacs, V. I. Sbitnev, J. Guan, J. Shin, *A nonlinear dynamics perspective of Wolframs new kind of science. Part VIII: More isles of Eden*, International Journal of Bifurcation and Chaos, Vol. 17, pp. 3741–3894 (2007).

63. S. U. Ahmed, C. Camerano, L. Fortuna, M. Frasca, L. Jaccheri, *Information technology and art: Concepts and state of the practice*, Handbook of Multimedia for Digital Entertainment and Arts, pp. 567–592 (2009).

64. M. Bucolo, A. Buscarino, L. Fortuna, M. Frasca, M. G. Xibilia, *From Dynamical Emerging Patterns to Patterns in Visual Art*, International Journal of Bifurcation and Chaos, Vol. 18, pp. 51–81 (2008).

List of Figures